UNDERSTANDING THE EFFECTS OF CYCLIC STRAIN ON ANGIOGENESIS

by

Jacob Ceccarelli

**A dissertation submitted in partial fulfillment
of the requirements for the degree of
Doctor of Philosophy
(Biomedical Engineering)
in the University of Michigan
2013**

Doctoral Committee:

**Associate Professor Andrew James Putnam, Chair
Professor Joseph L. Bull
Assistant Professor Darnell Kaigler
Associate Professor Jan Phillip Stegemann**

Acknowledgements

First and foremost I would like to thank my advisor, Professor Andrew Putnam, for accepting me into the lab amid stiff competition and guiding me through six years of toil to reach this point. His enthusiasm for science and patience during my setbacks were instrumental in keeping me motivated and productive. I would also like to thank him for taking me to Michigan, which I viewed as an adventure and opportunity.

I would also like to thank the other members of my dissertation committee, Professors Jan Stegemann, Darnell Kaigler Jr., and Joseph Bull. Their collaborative efforts and insights have helped to improve as a scientist since the establishment of the committee.

Several funding sources were critical to the success of my project. NIH R01-HL085339 and R01HL-085339-S1, the University of Michigan first year BME fellowship, Rackham Graduate School travel and research awards, and two 1-year graduate student fellowships from UC Irvine allowed me to focus solely on research throughout graduate school.

Next I would like to thank those who contributed to my scientific

success: my colleagues in the lab and collaborators in others. In Irvine, Peter Kim welcomed me into the lab and taught me the basics, which I have used throughout my dissertation work. Suraj Kachgal was an excellent source of information and discussion with respect to molecular biology techniques, and most notably his insights contributed my proficiency with Western blotting. In addition, Suraj, Bita Carrion, and Isaac Janson moved with me from Irvine and made the transition to new state and school very smooth. I would also like to thank Albert Cheng, an undergraduate student who I worked closely with, for his hard work on my project. Of special note are Ram Rao, Stephanie Grainger, Marina Vigen, Yan Peng Kong, David Lai, and Rahul Singh, who allowed me to collaborate with them on their respective projects, solved key problems by providing useful data or techniques, or both. I am extremely grateful to them for including me in their work and helping me with mine.

The friends I made in Ann Arbor were extremely important for my mental health over the years, and I am eternally grateful for their company. I am glad to have been able to distract myself with them when I needed a break, train and compete with excellent teammates, and celebrate milestones in our lives and careers.

No one has been more supportive during my time here than my

parents, Gary and Laurie Ceccarelli. Without their discipline and guidance I would not have been able to accomplish anything. They have generously given me countless gifts, plane tickets home, visits, and updates about family and friends that have made me feel like I have a place to come back to after I finished here.

Finally, I would like to thank my patient and understanding girlfriend and best friend, Ita Nagy, who has endured having a country between us for four years.

Table of Contents

List of Figures

List of Appendices

List of Abbreviations

ECM – extracellular matrix

tPa – tissue-type plasminogen activator

uPa – urokinase-type plasminogen activator

uPar - urokinase-type plasminogen activator receptor

VEGF – vascular endothelial growth factor

TGF-β – transforming growth factor-beta

ROCK – Rho kinase

MLCK – myosin light chain kinase

BDM – butanedione monoxime

EC – endothelial cell

HUVECs – human umbilical vein endothelial cells

HMVECs – human microvascular endothelial cells

HASMCs – human aortic smooth muscle cells

PDMS – polydimethylsiloxane

DPBS – Dulbecco’s phosphate-buffered saline

EGM-2 – Endothelial Growth Medium-2

Abstract

The size of engineered tissues is currently limited by oxygen diffusion. Vascularization of these constructs could alleviate this problem if the cues that control blood vessel organization can be manipulated. Our laboratory has adapted a method for generating bona fide capillaries in fibrin gels to study how mechanical strain affects the growth and organization of engineered blood vessel networks and remodeling of the extracellular matrix. A PDMS multi-well platform was designed to allow cell culture in a mechanically labile environment that also allowed visualization of the extracellular matrix under strain. The platform was calibrated using a custom microscope stage mount composed of two clamps attached to a micrometer for strain application. Strains from 0 – 12% were applied to fibrin hydrogels and the corresponding principle strains were calculated, revealing a linear relationship between the two. Cell culture experiments were performed using a custom, automated linear stage able to apply cyclic or static strains to the PDMS platform under standard mammalian cell culture conditions. These experiments revealed that human umbilical vein endothelial cells, in the presence of supportive human aortic smooth muscle cells, formed vasculature parallel to the applied strain and that the alignment was reversible upon halting the strain. Examination of the fibrin matrix revealed no cell-mediated directional matrix remodeling and only modest alignment of the matrix at 10% strain, the maximum used in these studies. Contact guidance was thus ruled out as a primary source of capillary alignment, prompting an investigation of intracellular mechanotransduction as a mediator of the directional sprouting. The use of multiple genetic constructs to modulate RhoA activity and the application of drugs to inhibit Rho-associated kinase, myosin light chain kinase, and myosin ATPase showed that perturbation of this mechanosensitive pathway led to decreased capillary network lengths without diminishing the ability of the capillaries to align parallel to the direction of applied strain. These findings demonstrate that mechanical inputs can be used to control angiogenic patterning in engineered tissues and suggest that an alternative mechanosensitive pathway may be responsible for directional angiogenesis in response to strain.

Chapter 1

Introduction

1.1 Tissue Engineering

Organ and vascular malfunction play roles in six of the ten leading causes of death in the United States [1], contributing to over one million deaths in 2011 alone, and driving the need for organ transplantation. In the United Kingdom [2] and the United States [3], the number of patients waiting for most organs vastly exceeds the number of available donors (Figure 1-1). The field of tissue engineering aims to change that. By building functional replacement organs and substitute tissues in the laboratory, tissue engineers hope to improve the length and quality of life for millions of people. Although crude methods of tissue engineering have existed for hundreds or thousands of years, modern tissue engineering is attempting to truly recapitulate, and repair, living organs. To fully realize its potential, engineers must overcome challenges with respect to tissue

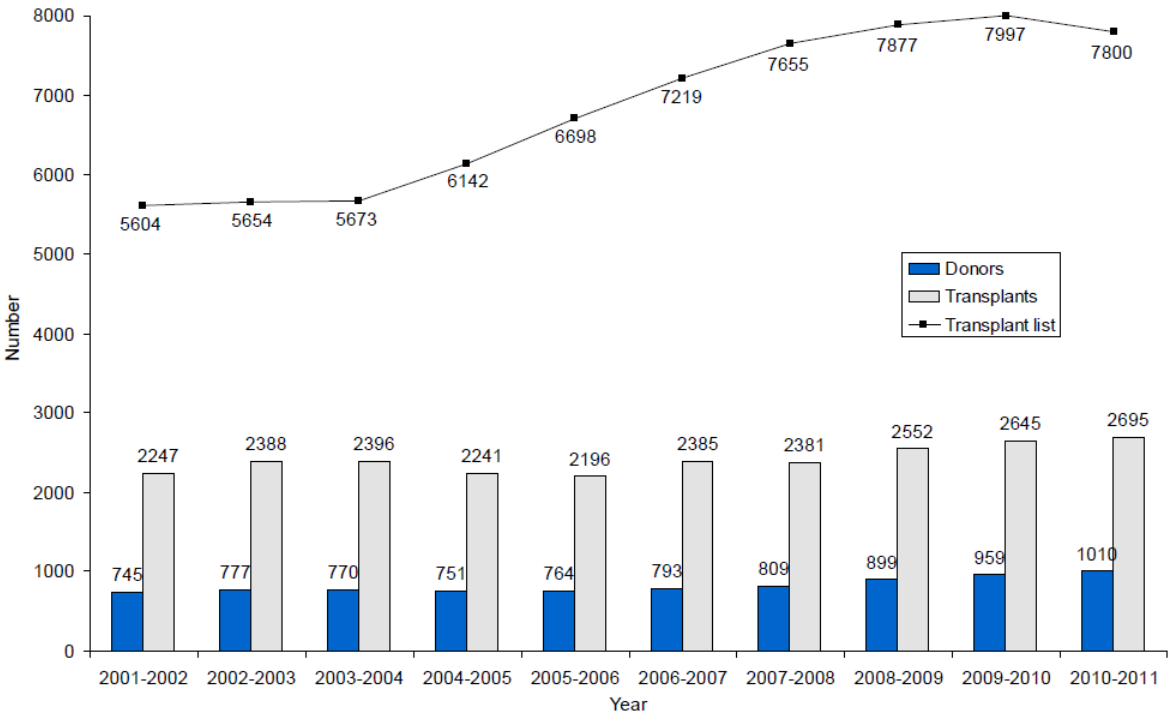

Figure 1-1 The number of people waiting for transplants exceeds the number of available organs.[2]

organization, strength, biological functionality, and vascularization.

Modern tissue engineering began in the late 1980s and early 1990s [4-6] and has already generated several therapies and products. Epidermal replacements using cultured keratinocytes and fibroblasts [7], tissue-engineered bladders using autologous cells seeded onto collagen or collagen-polyglycolic acid scaffolds [8], and an engineered arterial graft generated using autologous tissues [9, 10] are examples of how far the field has come in such a short time. These successes also highlight two important challenges in tissue engineering. First, the arterial grafts required a conditioning phase where they were exposed to increasing

pulsatile strain to strengthen the tissue. While this is relatively straightforward in a thin, tubular construct, it remains difficult to create thicker tissues with the necessary mechanical properties to withstand implantation and normal activity. Optimization of the conditioning phase with various mechanical inputs such as shear flow and cyclic strain will likely yield improvements to the mechanical properties of engineered tissues in the near future. Second, clinically successful engineered tissues, such as skin and cartilage, are thin or relatively avascular. In the case of successful bladder engineering, the hollow, thin tissue was in several cases wrapped in a vascularized omentum, facilitating nutrient exchange [8]. Thin tissues are better capable of functioning without a vascular supply of their own and rely on diffusion to provide oxygen and remove waste. The maximum thickness of a tissue without its own vasculature has been estimated to be 100-200 μm [11-13], and unsurprisingly, attempts to engineer tissues larger than this have met with less success.

1.2 Angiogenesis and Vascularization of Engineered Tissues

There are two forms of angiogenesis: intussusceptive and sprouting. Intussusceptive angiogenesis is the splitting of an existing vessel into two via the production of trans-capillary “pillars” that fuse to form a septum

between the two new capillaries, eventually splitting into a true capillary branch-point [14]. This form of angiogenesis has only recently begun to receive attention, and it is currently believed that its most important role is in vascular remodeling [15]. Vascular expansion is believed to be primarily driven by sprouting angiogenesis. Upon induction by pro-angiogenic cues, quiescent endothelial cells making up the capillary walls begin to degrade the underlying basement membrane and release their cell-cell contacts. Relying in part on Notch-Dll4 signaling to segregate into so-called “tip” and “stalk” cells [16, 17], the now active endothelial cells begin to form a new sprout. Tip cells lead the newly forming capillary up growth factor gradients [18], finally anastomosing, or joining, with another capillary to complete the vascular circuit [19, 20]. Stalk cells migrate behind the tip cell and form the body of the capillary. These cells proliferate to allow lengthening of the growing sprout and will also form the lumen by fusion of intracellular vesicles [21].

Healthy angiogenesis only appears in adults under limited circumstances: wound healing, menstruation, and mammary gland development during pregnancy [22]; pathological angiogenesis manifests in diseases such as macular degeneration, where aberrant blood vessel formation in the eye can lead to blindness, and in many cancers, where the

blood supply is usurped to feed growing tumors. This work is primarily about understanding angiogenesis in the context of engineered tissues. Discussions of pathological angiogenesis are reviewed extensively elsewhere [22, 23].

Strategies to create vascularized engineered tissues rely on isolated endothelial cells self-assembling into capillary-like structures, a phenomenon first described in vitro by Folkman and Haudenschild in 1980 [24]. Prior to this, methods of studying angiogenesis were limited to in vivo models that are much less amenable to manipulation than in vitro systems. Folkman and Haudenschild's advance was quickly adapted to study angiogenesis in 3D protein hydrogels [25], enabling the study of the effects of particular growth factors on angiogenesis [26, 27]. As the field of tissue engineering emerged in the early 1990s the need for implantable vascularized tissues became clear. Proof-of-concept for the implantation of such tissues was achieved when it was shown that endothelial cells encapsulated in collagen-fibronectin gels could be implanted into mice and form a network that carried blood after anastomosis with the host's circulation [28]. Vascularized tissues are now routinely created for in vitro and in vivo angiogenesis assays [29]. Although multiple clinical trials have emerged to attempt to treat ischemic conditions, none have yet led to

commercial products. However, many in vitro angiogenesis models have been developed to improve understanding of how vascular networks are formed [30] and under what conditions they are most functional [31, 32].

One of the most important issues confounding the production of implantable, vascularized tissues is that they inosculate with the host vasculature slowly. Therapies involving the injection of living cells, even if they are contained within a scaffold, will inevitably suffer from considerable cell death due to the lack of immediate perfusion of the tissue. Pre-vascularization of implantable tissue scaffolds appears to be one means by which this problem can be ameliorated. Such tissues inosculate with the host blood supply, as evidenced by the presence of erythrocytes, much earlier than non-pre-vascularized tissues [33, 34]. However, because the process generally takes days rather than hours to complete, there is a risk of ischemic loss of delivered cells in the interior of the implant even in this case. One potential mechanism to improve the rate of inosculation is to create a highly organized vascular bed, rather than randomly-oriented vessels. This may allow an implant to be oriented in such a way as to maximize the rate of inosculation and spare the lives of implanted cells, or allow the creation of a larger vascular tree connected to larger vessels that can be surgically connected directly to the host vasculature.

1.3 Control of Vascular Patterning via Mechanotransduction

Tissue architecture is often extremely intricate, containing multiple cell types closely juxtaposed in complex arrangements, and the supporting vascular bed must ensure all cells within are in close proximity to the blood supply. Therefore, understanding how the growing vasculature forms patterns that allow it to follow tissue architecture are critical to tissue engineering. How endothelial cells organize into the highly ordered arrangement of capillaries that saturate most tissues remains an open question. The field of tissue engineering poses another unique challenge: to generate an engineered tissue, cells are removed from their developmental context and placed in an extracellular matrix (ECM) scaffold that imperfectly replicates the in vivo environment, then asked to assemble into a functional vascular network and recapitulate a particular architecture. Although this strategy works surprisingly well for creating vascularized implants, researchers can currently assert almost no control over the orientation of the vessels within them.

One cue emerging as an important regulator of pattern morphogenesis is mechanotransduction via cell-cell and cell-ECM contacts. Cell-cell contacts are especially important during development, and it has

been hypothesized that mechanical cues are critical determinants of cell fate during this process [35-37]. However, the issue remains unsettled due to the difficulty of measuring mechanical forces under developmental conditions. Outside of development it is clear that cells are influenced by a variety of mechanical stimuli including the rigidity of their substrate [38, 39], tension generated by neighboring cells [40], shear stresses from flow [41], and tensile stresses propagated through the ECM [42]. All of these factors must be understood to engineer functional tissues, but tensile stresses are particularly important because they represent a simple way by which engineers can stimulate cells within tissue constructs to simulate their native environment and to induce favorable morphogenetic processes. In the body, endothelial and smooth muscle cells constantly experience stress and strain: a basal level of stress from the blood pressure itself, and cyclic strain from the heartbeat. Even capillaries, shielded from the high pressures in larger vessels, experience stresses and strains during wound healing and muscle contraction during exercise. Improved understanding of the mechanical microenvironment may elucidate methods that allow better control over the architecture of the vascular tree in engineered tissues.

The effects of strain on endothelial, smooth muscle, and other cell

types relevant to angiogenesis have been studied extensively in 2D. Application of cyclic strain has been found to regulate pro-angiogenic growth factor expression in cardiomyocytes [43] and smooth muscle cells [44], indicating that mechanical forces may play a role in recruiting nascent vasculature to the wound site. Smooth muscle cells, which help to regulate vascular tone, show marked changes in cytoskeletal architecture and decreased membrane localization of the small GTPases RhoA and Rac when exposed to static strain [45]. Endothelial cells are also directly affected by cyclic strain, up-regulating expression of the pro-angiogenic factors vascular endothelial growth factor (VEGF) and transforming growth factor-beta (TGF-β) [46]. 2D studies, however, fail in some cases to fully recapitulate the native environment in which angiogenesis takes place. Gene expression, behavior, and morphology are often quite different when cells are cultured in 3D hydrogels rather than in a 2D monolayer and it is widely believed that the transition from 2D to 3D cell culture will greatly improve our understanding of many biological processes [47].

Our lab has developed a system capable of inducing co-cultured endothelial and smooth muscle cells to form a complex capillary network in a 3D hydrogel environment, closely mimicking angiogenesis. It is also capable of mechanically stimulating the cells it contains by applying precise

levels of static or cyclic strain to the ECM. It is known that mechanical forces are important regulators of angiogenesis and that endothelial cells will respond to contact guidance dues from the ECM: capillaries sprouting from dissociated microvessels embedded in a collagen matrix will align themselves parallel to the fibers within that matrix [48]. However, it in fibrin-based systems the ECM alignment due to strain is less significant, and it is unknown how, or if, cells will respond to mechanical strain in such a matrix. Improved understanding of the cues that affect directional capillary sprouting will be beneficial for engineering intricately patterned replacement tissues that accurately mimic those found in the body.

Two key molecular players in cellular mechanosensing are the small GTPase RhoA and its downstream target Rho-kinase (ROCK). These promote the assembly of actin filaments, are involved in control of cell motility, and promote increased cell traction force generation [38]. Rho kinases have also been implicated in directional migration in 2D and 3D environments [49], highlighting their potential importance for patterning in tissue engineering applications. In addition to cytoskeletal remodeling, RhoA also affects pericellular remodeling of the ECM. The structure of fibronectin fibers deposited by endothelial cells relies on actomyosin generated tension to expose cryptic sites in the protein, and fibers of

varying thickness are created when RhoA activity is modulated [50, 51], presumably due to its effects on traction force generation. With such an intimate connection between cell traction force and the ECM, it is likely that applied strains will have profound effects on complex morphogenetic processes like angiogenesis.

1.4 Hypothesis

We hypothesize that cyclic mechanical strain will alter the extent to which angiogenesis occurs and cause vascular network alignment mediated by a RhoA-dependent mechanism.

This hypothesis will be tested using a three-dimensional cell culture model of angiogenesis that was originally developed by Nehls and Drenckhahn [52], and adapted by previous researchers in our laboratory [53-55] to study how physical changes in the ECM influence cell function.

1.5 Specific Aims

Specific Aim 1: Build and characterize a bioreactor to apply cyclic strain to hydrogels. Characterization will verify the relationship between applied strain and the amount of strain present in the gel.

Specific Aim 2: Study the effects of strain on angiogenesis using the system developed in Aim 1. Alignment of vessels (relative to the direction of applied strain), the length of the resultant vascular network, and changes to the ECM will be quantified.

Specific Aim 3: Understand how the interplay between cellular traction force and cyclic strain affects angiogenesis, paying specific attention to a RhoA-dependent pathway.

1.6 Translational Potential

Understanding the mechanical cues and culture conditions necessary for successfully patterning vasculature is a key step in advancing the field of tissue engineering. One future *in vivo* application of this line of research includes the possibility to create an implantable graft with pre-patterned vasculature, which would allow researchers to study various configurations of capillary networks *in vivo* and parse out the patterns which best allow for integration with host vasculature and promote cell survival in implanted tissues. It will also allow researchers to create grafts that are perfused in a predictable way rather than through purely random growth, as in the case of implantation of dissociated cells into the host. Also, provided the general

mechanical environment around the implantation site is known, more accurate predictions of how vasculature will form can be made if it is known how mechanical forces affect vasculature *in vitro*.

Vascular tissues are not alone in experiencing, responding to, or creating mechanical stresses and strains, nor are they unique in their branched architecture. Vascular, nerve, and lymphatic tissues all undergo branching morphogenesis to generate intricate patterns in development, and share some common responses to soluble cues, most notably VEGF [56-58]. Epithelial tissues such as lung and gut are also known for their highly branched morphology. They may additionally share common responses to applied strains and thus protocols used to pattern one tissue may be generally applicable to others. For example, rearrangement of the cytoskeleton is necessary for cell migration and proliferation, key processes in many cell types. This study will shed light on how mechanical stretch affects RhoA and its downstream processes, potentially shedding light on RhoA-dependent mechanisms in other cell types.

1.7 Overview

This dissertation is organized as follows. Chapter 2 is a review of the key concepts pertinent to the thesis. The extracellular matrix, with an

emphasis on fibrin, is discussed with respect to its roles in normal tissue and during angiogenesis. Strategies for modifying fibrin, taking advantage of its pro-angiogenic qualities, and its unique mechanics are discussed. Chapter 3 describes the invention and characterization of a bioreactor used to apply mechanical strains to 3D hydrogels. Chapter 4 outlines the use of this bioreactor to apply strain to a 3D model of angiogenesis that permits the creation of vessels containing patent lumens. Characterization of the length and orientation of the resultant vascular networks is presented and an analysis of the extracellular matrix under static and strained conditions is shown. Chapter 5 examines a possible mechanism behind the effects observed in chapter 4, looking specifically at RhoA- and myosin-dependent pathways. Chapter 6 provides a summary of the key findings and presents possible future directions for understanding the role of mechanotransduction in tissue patterning.

1.8 References

[1] Hoyert DL, Xu J. Deaths: preliminary data for 2011. Natl Vital Stat Rep 2012;61:1-65.

[2] NHS. Transplant activity in the UK activity report 2010–11. 2012.

[3] Wolfe R, Roys E, Merion R. Trends in organ donation and transplantation in the United States, 1999–2008. American Journal of Transplantation 2010;10:961-72.

[4] Cima L, Vacanti J, Vacanti C, Ingber D, Mooney D, Langer R. Tissue engineering by cell transplantation using degradable polymer substrates. Journal of biomechanical engineering 1991;113:143.

[5] Bell E. Tissue engineering: a perspective. J Cell Biochem 1991;45:239-41.

[6] Lanza R, Langer R, Vacanti JP. Principles of tissue engineering: Academic press; 2011.

[7] Parenteau NL, Nolte CM, Bilbo P, Rosenberg M, Wilkins LM, Johnson EW, et al. Epidermis generated in vitro: practical considerations and applications. J Cell Biochem 1991;45:245-51.

[8] Atala A, Bauer SB, Soker S, Yoo JJ, Retik AB. Tissue-engineered autologous bladders for patients needing cystoplasty. Lancet 2006;367:1241-6.

[9] L'Heureux N, Dusserre N, Konig G, Victor B, Keire P, Wight TN, et al. Human tissue-engineered blood vessels for adult arterial revascularization. Nat Med 2006;12:361-5.

[10] L'Heureux N, McAllister TN, de la Fuente LM. Tissue-engineered blood vessel for adult arterial revascularization. N Engl J Med 2007;357:1451-3.

[11] Folkman J, Hochberg M. Self-regulation of growth in three dimensions. J Exp Med 1973;138:745-53.

[12] Thomlinson RH, Gray LH. The histological structure of some human lung cancers and the possible implications for radiotherapy. Br J Cancer 1955;9:539-49.

[13] Carmeliet P, Jain RK. Angiogenesis in cancer and other diseases. Nature 2000;407:249-57.

[14] Djonov V, Schmid M, Tschanz SA, Burri PH. Intussusceptive angiogenesis: its role in embryonic vascular network formation. Circ Res 2000;86:286-92.

[15] De Spiegelaere W, Casteleyn C, Van den Broeck W, Plendl J, Bahramsoltani M, Simoens P, et al. Intussusceptive angiogenesis: a biologically relevant form of angiogenesis. J Vasc Res 2012;49:390-404.

[16] Carmeliet P, Jain RK. Molecular mechanisms and clinical applications of angiogenesis. Nature 2011;473:298-307.

[17] Adams RH, Alitalo K. Molecular regulation of angiogenesis and lymphangiogenesis. Nat Rev Mol Cell Biol 2007;8:464-78.

[18] Jakobsson L, Franco CA, Bentley K, Collins RT, Ponsioen B, Aspalter IM, et al. Endothelial cells dynamically compete for the tip cell position during angiogenic sprouting. Nat Cell Biol 2010;12:943-53.

[19] Fantin A, Vieira JM, Gestri G, Denti L, Schwarz Q, Prykhozhij S, et al. Tissue macrophages act as cellular chaperones for vascular anastomosis downstream of VEGF-mediated endothelial tip cell induction. Blood 2010;116:829-40.

[20] Cheng G, Liao S, Kit Wong H, Lacorre DA, di Tomaso E, Au P, et al. Engineered blood vessel networks connect to host vasculature via wrapping-and-tapping anastomosis. Blood 2011;118:4740-9.

[21] Tung JJ, Tattersall IW, Kitajewski J. Tips, stalks, tubes: notch-mediated cell fate determination and mechanisms of tubulogenesis during angiogenesis. Cold Spring Harb Perspect Med 2012;2:a006601.

[22] Chung AS, Ferrara N. Developmental and pathological angiogenesis. Annu Rev Cell Dev Biol 2011;27:563-84.

[23] Timar J, Dome B, Fazekas K, Janovics A, Paku S. Angiogenesis-dependent diseases and angiogenesis therapy. Pathol Oncol Res 2001;7:85-94.

[24] Folkman J, Haudenschild C. Angiogenesis in vitro. Nature 1980;288:551-6.

[25] Montesano R, Orci L, Vassalli P. In vitro rapid organization of endothelial cells into capillary-like networks is promoted by collagen matrices. J Cell Biol 1983;97:1648-52.

[26] Papapetropoulos A, Garcia-Cardena G, Madri JA, Sessa WC. Nitric oxide production contributes to the angiogenic properties of vascular endothelial growth factor in human endothelial cells. J Clin Invest 1997;100:3131-9.

[27] Sankar S, Mahooti-Brooks N, Bensen L, McCarthy TL, Centrella M, Madri JA. Modulation of transforming growth factor beta receptor levels on microvascular endothelial cells during in vitro angiogenesis. J Clin Invest 1996;97:1436-46.

[28] Schechner JS, Nath AK, Zheng L, Kluger MS, Hughes CC, Sierra-Honigmann MR, et al. In vivo formation of complex microvessels lined by human endothelial cells in an immunodeficient mouse. Proc Natl Acad Sci U S A 2000;97:9191-6.

[29] Staton CA, Reed MW, Brown NJ. A critical analysis of current in vitro and in vivo angiogenesis assays. Int J Exp Pathol 2009;90:195-221.

[30] Kniazeva E, Kachgal S, Putnam AJ. Effects of extracellular matrix density and mesenchymal stem cells on neovascularization in vivo. Tissue Eng Part A 2011;17:905-14.

[31] Grainger SJ, Putnam AJ. Assessing the permeability of engineered capillary networks in a 3D culture. PLoS One 2011;6:e22086.

[32] Grainger SJ, Carrion B, Ceccarelli J, Putnam AJ. Stromal cell identity influences the in vivo functionality of engineered capillary networks formed by co-delivery of endothelial cells and stromal cells. Tissue Eng Part A 2013;19:1209-22.

[33] Chen X, Aledia AS, Ghajar CM, Griffith CK, Putnam AJ, Hughes CC, et al. Prevascularization of a fibrin-based tissue construct accelerates the formation of functional anastomosis with host vasculature. Tissue Eng Part A 2009;15:1363-71.

[34] Laschke MW, Menger MD. Vascularization in tissue engineering: angiogenesis versus inosculation. Eur Surg Res 2012;48:85-92.

[35] Keller R, Shook D, Skoglund P. The forces that shape embryos: physical aspects of convergent extension by cell intercalation. Physical biology 2008;5:015007.

[36] Honda H, Motosugi N, Nagai T, Tanemura M, Hiiragi T. Computer simulation of emerging asymmetry in the mouse blastocyst. Development 2008;135:1407-14.

[37] Wennekamp S, Mesecke S, Nedelec F, Hiiragi T. A self-organization framework for symmetry breaking in the mammalian embryo. Nat Rev Mol Cell Biol 2013.

[38] Peyton SR, Putnam AJ. Extracellular matrix rigidity governs smooth muscle cell motility in a biphasic fashion. J Cell Physiol 2005;204:198-209.

[39] Engler AJ, Sen S, Sweeney HL, Discher DE. Matrix elasticity directs stem cell lineage specification. Cell 2006;126:677-89.

[40] Huveneers S, de Rooij J. Mechanosensitive systems at the cadherin-F-actin interface. J Cell Sci 2013;126:403-13.

[41] Califano JP, Reinhart-King CA. Exogenous and endogenous force regulation of endothelial cell behavior. J Biomech 2010;43:79-86.

[42] Lim SM, Trzeciakowski JP, Sreenivasappa H, Dangott LJ, Trache A. RhoA-induced cytoskeletal tension controls adaptive cellular remodeling to mechanical signaling. Integr Biol (Camb) 2012;4:615-27.

[43] Zheng W, Seftor EA, Meininger CJ, Hendrix MJ, Tomanek RJ. Mechanisms of coronary angiogenesis in response to stretch: role of VEGF and TGF-beta. Am J Physiol Heart Circ Physiol 2001;280:H909-17.

[44] Yung YC, Chae J, Buehler MJ, Hunter CP, Mooney DJ. Cyclic tensile strain triggers a sequence of autocrine and paracrine signaling to regulate angiogenic sprouting in human vascular cells. Proc Natl Acad Sci U S A 2009;106:15279-84.

[45] Putnam AJ, Cunningham JJ, Pillemer BB, Mooney DJ. External mechanical strain regulates membrane targeting of Rho GTPases by controlling microtubule assembly. Am J Physiol Cell Physiol 2003;284:C627-39.

[46] Baker AB, Ettenson DS, Jonas M, Nugent MA, Iozzo RV, Edelman ER. Endothelial cells provide feedback control for vascular remodeling through a mechanosensitive autocrine TGF-beta signaling pathway. Circ Res 2008;103:289-97.

[47] Baker BM, Chen CS. Deconstructing the third dimension: how 3D culture microenvironments alter cellular cues. J Cell Sci 2012;125:3015-24.

[48] Krishnan L, Underwood CJ, Maas S, Ellis BJ, Kode TC, Hoying JB, et al. Effect of mechanical boundary conditions on orientation of angiogenic microvessels. Cardiovasc Res 2008;78:324-32.

[49] Breyer J, Samarin J, Rehm M, Lautscham L, Fabry B, Goppelt-Struebe M. Inhibition of Rho kinases increases directional motility of microvascular endothelial cells. Biochem Pharmacol 2012;83:616-26.

[50] Geiger B, Bershadsky A, Pankov R, Yamada KM. Transmembrane crosstalk between the extracellular matrix and the cytoskeleton. Nature Reviews Molecular Cell Biology 2001;2:793-805.

[51] Fernandez-Sauze S, Grall D, Cseh B, Van Obberghen-Schilling E. Regulation of fibronectin matrix assembly and capillary morphogenesis in endothelial cells by Rho family GTPases. Exp Cell Res 2009;315:2092-104.

[52] Nehls V, Drenckhahn D. A novel, microcarrier-based in vitro assay for rapid and reliable quantification of three-dimensional cell migration and angiogenesis. Microvasc Res 1995;50:311-22.

[53] Ghajar CM, Blevins KS, Hughes CC, George SC, Putnam AJ. Mesenchymal stem cells enhance angiogenesis in mechanically viable prevascularized tissues via early matrix metalloproteinase upregulation. Tissue Eng 2006;12:2875-88.

[54] Kachgal S, Putnam AJ. Mesenchymal stem cells from adipose and bone marrow promote angiogenesis via distinct cytokine and protease expression mechanisms. Angiogenesis 2011;14:47-59.

[55] Kniazeva E, Putnam AJ. Endothelial cell traction and ECM density influence both capillary morphogenesis and maintenance in 3-D. Am J Physiol Cell Physiol 2009;297:C179-87.

[56] Emanueli C, Salis MB, Pinna A, Graiani G, Manni L, Madeddu P. Nerve growth factor promotes angiogenesis and arteriogenesis in ischemic hindlimbs. Circulation 2002;106:2257-62.

[57] Sondell M, Lundborg G, Kanje M. Vascular endothelial growth factor has neurotrophic activity and stimulates axonal outgrowth, enhancing cell survival and Schwann cell proliferation in the peripheral nervous system. The Journal of neuroscience 1999;19:5731-40.

[58] Hirakawa S, Kodama S, Kunstfeld R, Kajiya K, Brown LF, Detmar M. VEGF-A induces tumor and sentinel lymph node lymphangiogenesis and promotes lymphatic metastasis. J Exp Med 2005;201:1089-99.

Chapter 2

Literature Review

2.1 Introduction

Fibrin is a natural biomaterial and the primary extracellular constituent of blood clots, halting the flow of the blood from open wounds. Given fibrin's role in the earliest stages of wound healing, it is not a surprise that it has been explored for use in regenerative therapies. Fibrin's structure and bioactive properties encourage sprouting of new blood vessels (angiogenesis) into the wound, and cells readily degrade it during healing. Biodegradable matrices such as fibrin are ideal for tissue engineering applications because they potentially allow for complete tissue regeneration, leaving no trace of the original scaffolding material. Although fibrin can support many complex morphogenetic processes, this review will highlight its strength as a material capable of supporting angiogenesis. Coupled with the fact that it has been extensively characterized and studied

as a biomaterial, fibrin's permissiveness of vascular morphogenesis makes it useful for studying the engineering principles governing cellular behavior in native three-dimensional ECMs [1]. Furthermore, fibrin structure-function relationships are currently being exploited in two primary contexts: modifying native fibrin to achieve specific functionalities, and guiding synthetic biomaterial engineering to more closely mimic native tissue.

2.2 Structure and Degradation of Native Fibrin

Fibrin's complexity confers many functions, which are primarily dictated by the protein's structure. Although this acknowledgement appears elementary, understanding structure-function relationships of well-characterized extracellular proteins, such as fibrin, is fundamentally essential to dictate the design of novel biomaterials. To act reproducibly and controllably, engineered biomaterials must possess similar structure-function properties as the proteins they wish to emulate. In a decade of research in our own laboratory, we've come to appreciate that fibrin's structure is not an unnecessary clutter that can be swept away by clean synthetic biomaterials, but rather that it is a blueprint for superior biomaterial design.

2.2.1 Fibrinogen and Fibrin Polymerization

The fibrin matrix is a web of cross-linked fibrils generated by cleavage of fibrinogen, a soluble plasma protein which circulates in the body at a concentration of approximately 3 mg/ml [2]. Fibrinogen is a hexameric protein containing two identical sets of three disulfide-linked peptides, termed the Aα, Bβ, and γ chains. These peptides form a symmetric, extended protein composed of two flanking D-domains and a central E-domain linked by two coiled-coil regions [3]. This dumbbell-shaped structure is central to the polymerization of fibrin, the insoluble protein formed from fibrinogen when fibrinopeptides A and B are cleaved by thrombin during the clotting cascade [4]. These cleavages expose the knob- "A" and knob- "B" regions, and their complementary binding sites, holes "a" and "b" [5]. Fibrinopeptides A and B, and therefore knobs "A" and "B," are located in the E-domain, at the molecule's center, while holes "a" and "b" are located in the D-domains. In addition, two αC regions are liberated upon cleavage of fibrinopeptide A. These regions are long and thin with a globular head, which can interact with the heads of other αC regions to allow for lateral aggregation of fibrils [6]. Studies of the knob:hole interactions support John Ferry's 1952 hypothesis of fibrin fiber formation [3, 7, 8], which suggests that cleavage of the fibrinopeptides leads to aggregation of fibrinogen monomers through

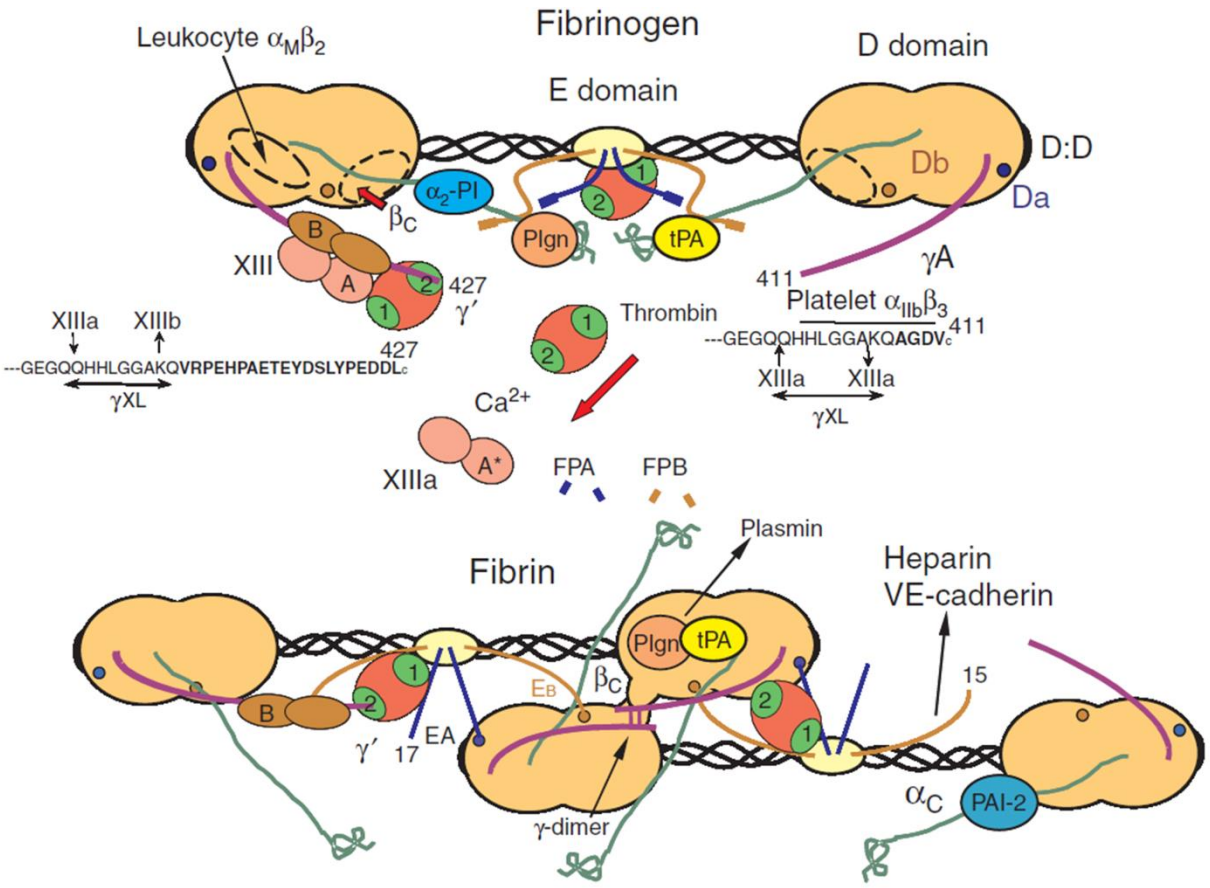

Figure 2-1. Schematic of fibrinogen and its assembly into fibrin. This cartoon representation shows the central E domain of fibrinogen flanked by the two globular D domains linked together by coiled-coil regions. Thrombin cleavage of fibrinopeptides A and B from the E domain leads to dimerization of soluble fibrin molecules into fibrin dimers, the first step of fibrin polymerization. Additionally, thrombin cleavage of factor XIII produces factor XIIIa, which crosslinks adjacent chains, linking the D domains in the growing fibrin polymer. Figure adapted from [6] with permission from John Wiley and Sons.

binding of the D and E domains, with lateral aggregation through the αC regions promoting aggregation into protofibrils and larger fibers [9]. This is illustrated in Figure 2-1, which depicts fibrinogen structure and the early polymerization events of fibrin. Upon assembly, fibrin protofibrils exist in a twisted conformation, reflected in the full fibrin fiber, causing it to twist as well. As additional protofibrils bind the fiber and increase its radius, the

fibers undergo ever greater stretching. Once the energy required to stretch a protofibril exceeds the energy of binding, thickening of fibers ceases, limiting fibrin fiber diameter [10].

The transglutaminase factor XIII is critical for improving the stiffness and stability of the fibrin matrix. Factor XIII is carried by fibrinogen in the blood, bound to fibrinogen's γ-domain [11], ensuring the presence of ample factor XIII during clotting (Fig. 2-1). Like fibrinogen, factor XIII is cleaved by thrombin to generate its active form, factor XIIIa. Factor XIIIa reinforces the fibrin matrix by cross-linking laterally-adjacent γ chains, creating γ-γ dimers in protofibrils and accelerating fibrillogenesis. These Factor XIIIa-mediated cross-links are believed to contribute to the extensibility of fibrin fibers [12]. Factor XIII also creates αC-αC cross-links in the fibrin matrix to further stabilize laterally-aggregated protofibrils, increase the elastic modulus of the matrix, and decrease its susceptibility to proteolysis [9, 13, 14].

2.2.2 Fibrinolysis

Within the lumens of blood vessels, vascular patency is chiefly regulated by the plasmin/plasminogen system, which serves to dissolve clots and prevent fibrin from depositing in various organs. Urokinase-type plasminogen activator (uPa) and tissue-type plasminogen activator (tPa) are capable of cleaving plasminogen and converting it to its active form,

plasmin, the protein most responsible for fibrin proteolysis and maintenance of vascular patency in vivo. Plasminogen is a soluble, inactive pro-peptide found in serum that also binds to the αC region of fibrin, at residues Aα392-610. Plasminogen is converted to plasmin via cleavage of Arg561-Val562 [15] in the presence of a ternary complex in which plasminogen and tPa are both bound to fibrin, localizing proteolysis to the clot [16]. Plasmin cleaves fibrin in a series of steps resulting in fragments of various sizes being solubilized and freed from the clot; the size of the final degradation products is believed to be dependent on the presence of blood flow, which can carry away larger fragments [17].

Additionally, cell-surface receptors for plasminogen are hypothesized to be of use for localizing fibrin proteolysis during various cell processes [18]. For example, ECs have been shown to express the cell membrane protein urokinase plasminogen activator receptor (uPaR), which binds uPa, and in certain contexts is required for tube formation [19]. However, as we will discuss later in this review, it is now pretty clear that an alternate fibrinolytic mechanism that depends on matrix metalloproteineases (MMPs) is responsible for EC-mediated degradation of the provisional fibrin matrix during sprouting angiogenesis.

2.2.3 Cell Binding to Fibrin

Cells can adhere to fibrin directly via multiple motifs, and indirectly via interactions between fibrin and other ECM proteins. Discussing all of the possible mechanisms by which cells can bind to fibrin is beyond the scope of this review, but we would like to highlight a few that are particularly important in how endothelial cells (ECs) interact with fibrin. Perhaps the most significant adhesive interaction between ECs and fibrin occurs indirectly via fibronectin, which has the capacity to bind directly to fibrin. Like fibrinogen itself, fibronectin is present in blood serum, which ensures it is readily available to bind to fibrin during clot formation *in vivo*. Multiple adhesive domains within fibronectin are then available for binding of ECs and other cells. Furthermore, ECs [20, 21] and fibroblasts [22] can also both bind to Arg-Gly-Asp (RGD) sequences in fibrin using the $\alpha_v\beta_3$ integrin receptor, although there is evidence that this binding mechanism is not required for endothelial tube formation [23]. Alternatively, the β15-42 segment of fibrin, a heparin binding domain exposed upon cleavage of fibrinopeptide B [24, 25], can also play a role in EC attachment to fibrin via their VE-cadherin receptors [26-28], and exposure of this sequence may be critical for EC spreading and capillary formation in fibrin gels [23, 25]. Additional peptide sequences accommodate leukocyte [29] and platelet [21] binding.

2.3 Using fibrin to study angiogenesis

2.3.1 Conventional angiogenesis assays

Fibrin supports robust angiogenesis in a variety of assays including 2D and 3D environments, mono- and co-culture systems, and other systems capable of examining the influences of mechanical stimuli and microfluidic gradients. The simplest 2D assay performed on a fibrin gel is a cord formation assay, where endothelial cells (ECs) are seeded atop the gel and induced to form cords [30]. This assay typically requires only 18-24 hours to generate cord structures, making it a popular assay. Although many molecules regulating angiogenesis have been discovered via this type of assay, a major weakness is that non-EC types have also been shown to form cords [30].

By contrast, many truly 3D assays have been developed in fibrin and other natural hydrogels. One of the most convenient and widely-used 3D assays was originally developed by Nehls and Drenckhahn, who coated calf pulmonary artery ECs onto microcarrier beads, embedded them in a fibrin gel, and showed they migrate off the beads and undergo angiogenesis when stimulated by certain soluble factors [31]. An advantage of this type of technique is that the microcarrier provides a

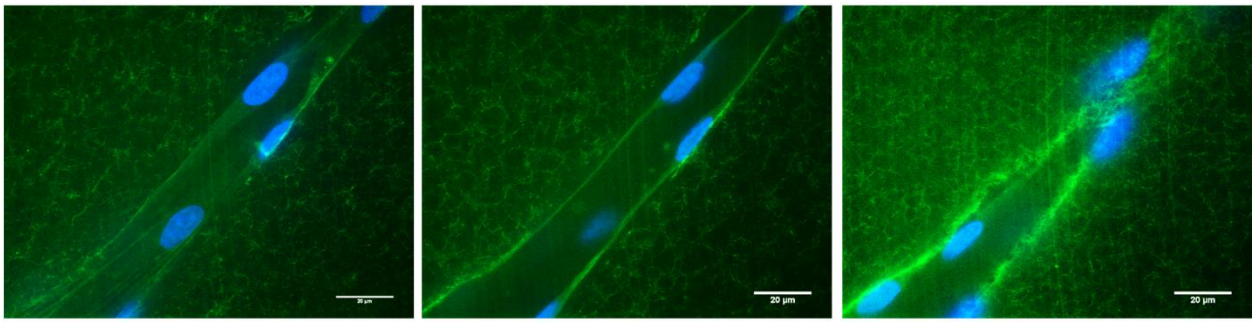

Figure 2-1. Fibrin hydrogels are useful as 3D model systems of angiogenic sprouting. High magnification confocal images of a sprouting capillary in a 3D fibrin matrix containing FITC-conjugated fibrinogen. HUVECs cultured in fibrin gels form capillaries with hollow lumens as demonstrated by confocal sections obtained at the bottom (left), center (middle), and top (right) z-planes of a capillary. HUVECs were stained with Oregon Green 488 phalloidin and nuclei were counterstained with DAPI. The HUVECs create a 3D channel in the fibrin matrix via proteolysis.

reference point for easy quantification of vessel length and direction. The microcarrier-based technique has been expanded upon to include various EC types, but modification of the assay was required for translation to human cells. Human umbilical vein endothelial cells (HUVECs) were shown to form capillaries only when co-cultured with a supporting cell type. Human dermal and lung fibroblasts cultured atop the gel stimulated the formation of robust, lumen-bearing capillaries (Figure 2-2) [32, 33]. Attenuation of angiogenesis was achieved by increasing the distance between the two cell types [34] and by increasing matrix density [32, 35]. Distributing either mesenchymal stem cells (MSCs) [32] or lung fibroblasts [35] throughout the matrix resulted in a nearly complete rescue of capillary network length, demonstrating that this system can be used to study more intimate interactions between different cell types and their effects on

angiogenic sprouting.

A variation of the microcarrier model uses EC spheroids, generated by culturing ECs in non-adherent dishes, causing them to aggregate. When these spheroids are placed into fibrin and collagen gels, they are capable of forming capillaries containing hollow lumens [36]. This assay was originally performed as a mono-culture but has also been adapted for co-culture. Microcarrier and spheroid assays have two additional advantages: first, ECs begin the assay very close together and thus have a large "reserve" of cells to from which to form extensive capillary networks; second, the assay is more representative of an in vivo angiogenic program because the cells begin as a confluent monolayer.

Another simpler 3D assay is more representative of vasculogenesis. ECs randomly distributed in a hydrogel are induced to form a de novo capillary network. The advantage of this system is that the homogeneous cell distribution is amenable to in vivo, microfluidic, and multi-well plate formats. Systems with homogeneously distributed ECs have been used to examine integrin attachments during EC vacuolation, a result that would be difficult to observe in 2D culture [37]. Fibrin/collagen composite matrices containing a co-culture of ECs and MSCs have also been created to probe the role of matrix composition on vascular network formation. Notably,

increasing the relative fibrin content improved vasculogenesis in these gels [38]. Although more difficult to quantify than microcarrier-based angiogenesis assays, vasculogenesis assays replicate many of the same features and may also be more representative of the process by which a bolus of cells injected within a supporting ECM in vivo form new vasculature.

3.2 Microfluidic Systems

Studying angiogenesis, and specifically the perivascular niche, is simplified in microfluidic systems [39, 40]. Our laboratory has used one such device to image vasculogenesis in fibrin gels, and discovered that MSC recruitment to perivascular locations is $\alpha_6\beta_1$ integrin-dependent [39]. Recently, systems with perfusable vasculature have been developed to improve the physiological relevance of these in vitro microfluidic assays. In one study, human endothelial colony forming cell-derived ECs (ECFC-ECs) and normal human lung fibroblasts were co-cultured in a microfluidic device containing daisy-chained tissue chambers and shown to produce vasculature that inosculates with a perfusable flow chamber [41]. Another device used fibrin-filled parallel chambers that allowed invading ECs to form perfusable lumens spanning the length of the chamber [42].

3.3 Structure-Function Relationships in Angiogenesis

Fibrin provides a permissive matrix for angiogenesis, circumventing the need to engineer a new material to study cell behavior in this context. As a result, fibrin-based systems remain useful tools in which to study morphogenesis, but understanding the precise signals fibrin provides to the constituent cells remains an ongoing challenge.

There are several unanswered questions about fibrin's ability to support angiogenesis. Few studies directly compare performance between ECM materials, and those that do use widely differing protocols and materials [38, 43, 44], making it difficult to compare across studies. Additionally, the differences between the cues fibrin presents to constituent cells and the cues other ECM materials present are not well understood. Parsing out how the structural properties of fibrin differentiate it from other materials, with respect to how it presents morphogenetic cues to constituent cells, can guide the development of future biomaterials capable of more intricate control of cell behavior.

2.4 Protease-mediated migration and angiogenesis in fibrin

The present and the future of biomaterial design lies in the concept of biomimicry. Generating materials that interact with living tissues in predictable, therapeutically-useful ways is dependent on understanding

how cells interact with native tissues in vivo, especially in both regenerative and pathologic microenvironments. The presence of fibrin-rich matrices in both of these microenvironments has led to investigation of cell migration and signaling in fibrin gels.

Damage to existing vessels as a consequence of wounding results in fibrinogen leaking from existing vessels and forming a provisional clot upon enzymatic cleavage by thrombin. This clot serves as an interstitial matrix that must be actively remodeled by resident cells for a wounded tissue bed to be revascularized. Furthermore, during sprouting angiogenesis in vivo, fibrinogen may leak from budding neovessels and generate a fibrin-rich matrix that must be negotiated by invading cells. The MMP family of zinc-dependent endopetidases break down a variety of matrix proteins, and are now known to complement, and sometimes replace, the plasmin/plasminogen system during angiogenesis. Membrane type-1 matrix metalloproteinase (MT1-MMP) was first implicated in angiogenesis when it was observed that plasmin deficiency did not inhibit revascularization of mouse skin wounds [45] or fibrin neovascularization [46], leading to the discovery that MT1-MMP is a critical, and perhaps required, fibrinolytic enzyme during angiogenesis [46]. Our own lab has expanded upon this work with in vitro studies using primary human cells,

where we have shown that both MMPs and plasmin can be employed for neovascularization in fibrin gels. Which proteases are involved depends in part on the choice of supporting stromal cells used to support angiogenesis in our fibrin-based co-culture system [47, 48]. In addition, silencing MMP-2 and MMP-9 exhibited no effect on angiogenesis in our co-culture model, implying that MT1-MMP is the most important, and possibly only, MMP used by endothelial cells in this system [49]. When plasmin is employed, MT1-MMP is still active and may play a role in regulating vessel width [48]. This illustrates that in addition to understanding how particular cell types interact with the ECM in isolation, it is critical to understand how paracrine cross-talk affects cell-matrix interactions.

An evolving mechanistic understanding of these and other types of cell-matrix interactions continues to enhance efforts to engineer ECM mimetics tailored for specific microenvironments. Although fibrin can be degraded by multiple proteases, polyethylene glycol (PEG) based blank-slate materials can be generated with proteolytic susceptibility that is more restricted in a customized manner [50, 51], facilitating mechanistic studies of proteolysis [52, 53]. Building on these concepts, several promising in vitro models of neovascularization have been created in the context of synthetic hydrogels containing adhesive and proteolytically-sensitive

peptides [54-57]. These studies are particularly remarkable considering that these gels present a fairly minimal set of instructive cues, relative to a natural material like fibrin. Tethering or sequestering angiogenic growth factors adds an additional element of biomimicy to protease-susceptible synthetic hydrogels, and such systems have shown potential to enhance angiogenesis in vivo [56, 58, 59]. Although it cannot be said that these materials are directly "fibrin-inspired," there is at least one strategy that claims inspiration directly from fibrin: factor XIIIa has been used to create hydrogels of PEG-peptide conjugates [60]. An enzymatic cross-linking step, which is completed under more physiological conditions than other chemical cross-linking strategies, represents a step toward bridging the gap between natural and synthetic materials. We believe that synthetic materials can be further improved by mimicking additional, perhaps undiscovered, features present within natural hydrogels like fibrin.

2.5 Studying mechanotransduction with fibrin

As the provisional matrix in wound healing, fibrin's main function is to plug wounds and stop blood loss, resisting the blood pressure and shear stress to stay in place. Fibrin fibers and clots exhibit unique mechanical properties that are likely to assist in its primary function, although the

details of how are as yet incompletely known. Understanding the mechanical design principles behind fibrin clots is already facilitating strategies to engineer new biomaterials, but also led to efforts to understand how cells embedded within fibrin sense and respond to mechanical cues.

Fibrin is one of the most extensible proteins known, exceeding even elastin [61]. Individual fibers can be strained to approximately 330% [62] and whole clots to at least 150% [63, 64], and still recover elastically. Fibrin also exhibits strain stiffening, like most biological matrix proteins. These characteristics are believed to be caused by the unique unfolding of the individual fibrin monomers under strain, maintaining gel integrity and extensibility while possessing a low volume of protein [61-64]. These effects are typically not present in synthetic gels. Furthermore, fibrin's nonlinear elasticity enables cell-cell communication through mechanical means across relatively long distances. For example, fibroblasts sparsely seeded on (2D) and within (3D) fibrin matrices were able to communicate and form patterns at distances of approximately 0.5 mm, or about 5 cell-lengths away. This effect was not present when linearly elastic polyacrylamide gels were used [65].

One potential mechanism by which both externally applied and cell-generated forces can potentially alter cell responses in fibrin is via force-induced alignment of the matrix. However, there are discrepant views about fibrin's potential for contact guidance. Korff and Augustin reported that sprouts from EC-containing spheroids cultured close together grew toward each other in 3D collagen gels [36]. They also cultured EC spheroids atop collagen and fibrin gels, and observed directional migration only on collagen. They concluded that alignment of the large (several microns long) collagen fibers was responsible for the directional migration, while the fibrin fibers were too short to align and thus unable to provide as a contact-guidance cue. This study was a key step in the examination of how fibrillar structure can be exploited to guide cell growth, but the 2D nature of the comparison between collagen and fibrin limited its utility. Later work has shown that fibrin can play a role in contact guidance.

Recent studies in fibrin have shown the importance of mechanical effects such as fiber alignment and gradients in fiber stiffness for directing cellular alignment, migration, and angiogenesis. Fibrin clots undergo pronounced fiber alignment at only 25% strain, which induces alignment of smooth muscle and endothelial cells cultured within the gels [66], and EC sprouts have been shown to align parallel to fibers aligned magnetically

and by cell traction forces [67]. Fiber alignment also affects ECM deposition by embedded cells; however it is difficult to separate the effects of fiber alignment from those of matrix stress generated by cell traction forces [68].

Cell alignment in fibrin gels also appears to be dependent on local anisotropies in matrix stiffness. Using a device capable of applying small strains to fibrin gels, combined with laser tweezers for measuring local matrix stiffness, it has been demonstrated that applied strains generate stiffness gradients in fibrin matrices without detectable changes in fiber architecture. Smooth muscle cells cultured within these strained gels aligned perpendicular to the gradient (or parallel to the applied strain), showing that cells respond to gradients of matrix stiffness within natural biomaterials [69]. Such matrix anisotropies may also be important in angiogenesis. For example, we have shown that the matrix surrounding growing capillaries is twice as stiff than the matrix elsewhere [70], which complements other results showing that branching morphogenesis occurs in mammary epithelium at regions of high strain [71]. Matrix anisotropies may thus be a general mechanism by which cells orient themselves and communicate with each other in 3D environments, and natural biomaterials are especially conducive to studying these types of phenomena. However,

quantification of stress-strain relationships is difficult in natural materials because they are often inhomogeneous. This complication highlights a potential advantage of synthetic biomaterials in the context of better understanding mechanical influences on cell behavior in 3D. However, the dynamic, strain-stiffening properties of natural materials provide a means for long range cell-cell communication, and ways to replicate this type of behavior in synthetic biomaterials likely need to be incorporated into synthetic biomaterials if they are to support robust morphogenetic programs.

The vast majority of mechanobiology studies of ECs have focused on their response to shear stresses induced by blood flow [72], but ECs are also sensitive to cyclic strain. ECs cultured in vitro have shown increased expression and secretion of tPA [73, 74] and various MMPs [75] when strained, implying a role for cyclic strain in vascular remodeling. Work from our own lab has used a modified version of the microcarrier bead assay described earlier to show that HUVECs will form capillaries parallel to the direction of applied uniaxial strain without affecting total vascular network length [76]. Fibrin enables these experiments because it robustly supports angiogenesis, but improvements in synthetic gel preparation, inspired by structure-function relationships in fibrin, may allow them to support these

experiments as well.

2.6 Clinical Applications of Fibrin

Unmodified fibrin has also been extensively used as a vehicle for cell delivery in many tissue engineering applications, and a broad review can be found in [1]. Notably, fibrin glues and constructs more closely representing physiological fibrin concentrations have been prepared, and cells from virtually all tissues have been implanted into animals using fibrin scaffolds. Cell transplantation is much more effective when using a scaffold material to contain the implanted cells [77, 78], and fibrin is an ideal scaffold for transplantation because precursor solutions containing fibrinogen, thrombin, and cells can be injected in a minimally-invasive manner without the need for open surgery.

The most notable achievement of fibrin research is the use of fibrin glue as a surgical sealant. Tisseel™, cleared for use by the Food and Drug Administration in 1998, was the first commercial fibrin sealant in the United States. Surgeons had earlier been using fibrin glue from noncommercial sources [79]. Fibrin sealants have displayed biocompatibility and performance in surgical hemostatic applications. Although all naturally derived, non-recombinant biomaterials carry a risk of viral or prion infection,

fibrin sealants have benefitted from excellent screening procedures and have not been linked to transmission of any viral pathogen [80]. The sealants are a combination of high-concentration, frozen or lyophilized fibrinogen and thrombin packaged in a double-barreled syringe so that the components mix as the sealant is dispensed [81]. These glues typically contain factor XIII and aprotinin to improve clot mechanics and prevent sealant degradation. Concentrations of fibrinogen and thrombin vary from 60-120 mg/ml and 250-1000 IU/ml, respectively, representing concentrations several orders of magnitude above physiological. These features decrease clotting time and improve clot rigidity [82].

Fibrin matrices have been used to study vascularization strategies for tissue engineering and treatment of ischemic disease. The most prominent of these is ischemia due to myocardial infarction (MI), a leading cause of death in the United States. The first attempt to treat this in mice using fibrin glue showed that the injection of a Tisseel™ fibrin matrix improved cardiac function and neovascularization in the infarct site with and without the inclusion of cardiomyocytes in the gel [83, 84]. Additionally, the fibrin glue supported cardiomyocyte survival in vitro for seven days, demonstrating that high concentrations of fibrin are capable of supporting cells.

Another strategy for treating ischemic conditions is the use of pre-

vascularized, implantable fibrin tissues. HUVECs and lung fibroblasts have been used to generate such tissues prior to subcutaneous implantation into immune-deficient mice, which led to faster inosculation with the host vasculature than cell-laden, non-vascularized tissues [85]. Pre-vascularization is a promising and potentially translational strategy that may prove even more useful once tissue engineering has matured and generates large tissues and even whole organs. However, whole tissue implantation is invasive and therefore not ideal when an organ may be saved through alternative means. One non-invasive option is to inject a fibrin precursor solution containing appropriate cells to an injury site. We have used subcutaneous injection of cell-laden fibrin precursor solutions to study how co-transplantation of HUVECs with various supporting cell types affects the subsequently formed vasculature. The stromal cells supported vasculature of varying quality, with bMSCs and adipose-derived stem cells (ADSCs) supporting slower vessel growth but more mature vasculature that displayed little leakage, possibly indicative of enhanced wound healing with normal vessel ingrowth. By contrast, NHLFs supported vasculature that grew quickly but remained immature and leaky, characteristic of a pathological wound healing environment or tumor vasculature [86]. The 2.5 mg/ml fibrin gels used persisted up to 2 weeks in vivo, demonstrating that

supraphysiological fibrin concentrations are not required in such applications. The versatility of supporting various angiogenic programs and co-culture systems makes fibrin an ideal matrix to study angiogenesis in vivo.

2.7 Re-engineering fibrin for specific applications

2.7.1 Modifying Fibrin for Controlled Growth Factor Presentation

Fibrin can be used as a substrate for studying cell behavior in vitro and as a cell-delivery vehicle in vivo, but a fundamental understanding of fibrin's biochemistry has also led to the ability to augment its capabilities and turn it into a "smart" material. A demonstration of this concept pioneered by Jeffrey Hubbell and colleagues exploits the ability of Factor XIIIa to incorporate bifunctional peptides into the fibrin matrix [87] for novel growth factor presentation and drug delivery applications (Fig. 2-3). In one example, the extracellular domain of chick ephrin-B2 was attached to fibrin via factor XIII and was shown to increase angiogenesis over control fibrin gels [88] in the absence of cells. Other factors, including β-nerve growth factor (β-NGF) and vascular endothelial growth factor (VEGF), have also been tethered to fibrin matrices [89, 90] via an additional plasmin-sensitive

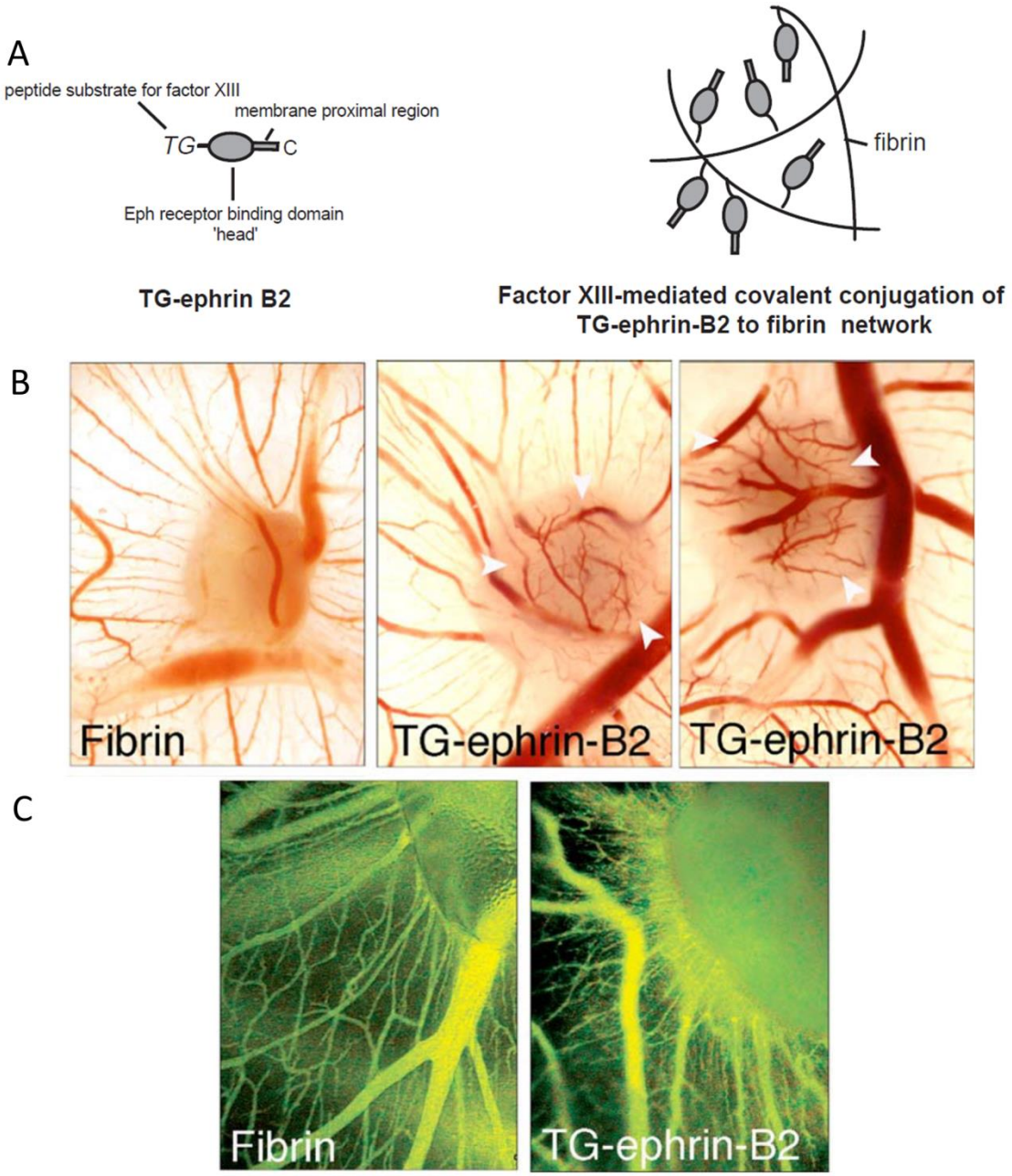

Figure 2-1. Engineering fibrin for controlled growth factor presentation. (A) The recombinant protein TG-ephrin B2, the full length ectodomain of ephrin B2 fused to a transglutaminase-sensitive (TG) motif, was conjugated to fibrin via factor XIIIa through the TG region of the protein. (B) Modifying fibrin in this way improved the angiogenic response of acellular fibrin implants in a chick chorioallantoic membrane (CAM) model, producing localized angiogenesis at the implant site. Pure fibrin implants showed little vessel ingrowth. (B) In vivo examination of microvascular growth on the growing CAM revealed strong and specific induction of new vessels by ephrin-B2 from fibrin grafts. Blood vessels were monitored by in vivo fluorescence microscopy performed after Intravenous injections of FITC-dextran, and showed larger diameters of vessels induced by ephrin-B2 indicative of arterioles or venules; by contrast, no changes of the regular vessel pattern of the CAM were observed in response to plain fibrin. Figure adapted from [88] with permission from Elsevier.

linker that allows the factors to be released from the matrix upon enzymatic digestion. Similar strategies have been used to engineer increased heparin affinity of fibrin by incorporating a heparin-binding domain at the biologically active site at a ratio of up to 8 moles of peptide per mole of fibrinogen [91]. This approach enabled fibrin to efficiently sequester a variety of heparin-binding growth factors, including acidic and basic fibroblast growth factors (aFGF, bFGF) [92], neurotrophin-3 (NT-3), and platelet-derived growth factor-AA (PDGF-AA) [93].

Additional methods of engineering fibrin for controlled release and protein sequestration have emerged as well. In one example, heparin was directly attached to fibrin matrices via carbodiimide chemistry at a molar ratio of approximately 1:1, and then used to control the release of bone morphogenetic protein-2 for bone regenerative therapy [94]. In another example, fibrin knob:pocket interactions were engaged by using custom peptides, which were also conjugated to a fibronectin protein fragment. Characterization of the fibrin gels generated using this method showed improved mechanical properties when the “b” pocket was engaged by its conjugate peptide with no decrease in the angiogenic potential of the gels [95]. Despite the fact that fibrin itself has been studied for over a century,

these and other examples collectively illustrate the ability to customize it in innovative new ways for specific purposes.

2.7.2 Chemical Modification of Fibrin(ogen)

Despite fibrin's versatility in a wide range of regenerative medicine applications, its relatively weak mechanical properties may limit its utility for some applications. One potential means to improve mechanical properties is to conjugate fibrinogen with polyethylene glycol (PEG), either with [96] or without [97, 98] retention of the protein's thrombin-mediated clottability. PEGylation provides an approach to better control the scaffold material properties, maintain the biological activity of the native protein, and provide a mechanism for sequestering growth factors within the gel for drug delivery. We have shown that PEG-fibrinogen supports cell adhesion, spreading, proliferation, and differentiation of some cell types in vitro [98, 99]; however, its potential to support complex morphogenetic processes, such as angiogenesis, remains unrealized in our hands. A similar PEGylated fibrin material has been used to deliver mesenchymal stem cells into the heart, validating the use of these types of gels for cell therapies in vivo [100]. Similarly, PEG-peptide conjugates which mimic the knob:hole interactions of fibrin have also been used to modify fibrin matrix properties

non-covalently by disrupting native knob:hole interactions and decreasing the gel modulus [101]. In this strategy, the fibrin(ogen) molecule was unmodified, leaving its biological functionality intact. It has further been shown that these types of interactions do not disrupt angiogenesis, and thus may lead to improved control of gel mechanics in variety of fibrin-based biomedical applications [102-104].

2.8 Conclusion

Fibrin is an elegant and prototypical material characterized by a long list of features: fibrillar architecture, considerable extensibility, strain stiffening, multiple adhesive domains, susceptible to multiple proteases, and abilities to sequester and release growth factors. These characteristics enable fibrin to outperform all synthetic material platforms engineered to date, particularly in terms of its ability to support angiogenesis. However, these impressive features also complicate the use of fibrin for fundamental studies as it is typically impossible to decouple fibrin's multiple instructive cues in an attempt to ascertain how cells respond to any one particular input; thus, the use of fibrin (or any natural material for that matter) for fundamental works requires caution with respect to interpretation. On one hand, efforts to modify fibrin using natural and synthetic means to enhance

its function from the “top-down” continue to be well-served by an improved understanding of its structure-property relationships, yielding potential new applications without the need to engineer a new material from scratch. On the other hand, an improved understanding of fibrin’s intricacies and complexities continue to inspire “bottom-up” designs of new material platforms. Together, these two paradigms ensure that fibrin, a classic material with an already long history of utility, will continue to be a staple in the biomaterials community.

Acknowledgments

We gratefully acknowledge financial support from the National Institutes of Health (R01-HL085339 and R21-DE021537). The content is solely the responsibility of the authors and does not necessarily represent the official views of the NIH.

2.9 References

[1] Ahmed TA, Dare EV, Hincke M. Fibrin: a versatile scaffold for tissue engineering applications. Tissue Eng Part B Rev 2008;14:199-215.

[2] Clark RA. The molecular and cellular biology of wound repair: Springer; 1996.

[3] Mosesson MW, Siebenlist KR, Meh DA. The structure and biological features of fibrinogen and fibrin. Ann N Y Acad Sci 2001;936:11-30.

[4] Pechik I, Yakovlev S, Mosesson MW, Gilliland GL, Medved L. Structural basis for sequential cleavage of fibrinopeptides upon fibrin assembly. Biochemistry 2006;45:3588-97.

[5] Laudano AP, Doolittle RF. Synthetic peptide derivatives that bind to fibrinogen and prevent the polymerization of fibrin monomers. Proc Natl Acad Sci U S A 1978;75:3085-9.

[6] Mosesson MW. Fibrinogen and fibrin structure and functions. J Thromb Haemost 2005;3:1894-904.

[7] Lord ST. Fibrinogen and fibrin: scaffold proteins in hemostasis. Current opinion in hematology 2007;14:236-41.

[8] Ferry JD. The Mechanism of Polymerization of Fibrinogen. Proc Natl Acad Sci U S A 1952;38:566-9.

[9] Gorkun OV, Veklich YI, Medved LV, Henschen AH, Weisel JW. Role of the alpha C domains of fibrin in clot formation. Biochemistry 1994;33:6986-97.

[10] Weisel JW, Nagaswami C, Makowski L. Twisting of fibrin fibers limits their radial growth. Proc Natl Acad Sci U S A 1987;84:8991-5.

[11] Siebenlist KR, Meh DA, Mosesson MW. Plasma factor XIII binds specifically to fibrinogen molecules containing gamma chains. Biochemistry 1996;35:10448-53.

[12] Mosesson MW, Siebenlist KR, Hainfeld JF, Wall JS. The covalent structure of factor XIIIa crosslinked fibrinogen fibrils. J Struct Biol 1995;115:88-101.

[13] Standeven KF, Ariens RA, Grant PJ. The molecular physiology and pathology of fibrin structure/function. Blood reviews 2005;19:275-88.

[14] Shen LL, Hermans J, McDonagh J, McDonagh RP, Carr M. Effects of calcium ion and covalent crosslinking on formation and elasticity of fibrin cells. Thromb Res 1975;6:255-65.

[15] Castellino FJ, Ploplis VA. Structure and function of the plasminogen/plasmin system. Thromb Haemost 2005;93:647-54.

[16] Medved L, Nieuwenhuizen W. Molecular mechanisms of initiation of fibrinolysis by fibrin. Thromb Haemost 2003;89:409-19.

[17] Marder VJ, Francis CW. Plasmin degradation of cross-linked fibrin. Ann N Y Acad Sci 1983;408:397-406.

[18] Hajjar KA, Harpel PC, Jaffe EA, Nachman RL. Binding of plasminogen to cultured human endothelial cells. J Biol Chem 1986;261:11656-62.

[19] Kroon ME, Koolwijk P, van Goor H, Weidle UH, Collen A, van der Pluijm G, et al. Role and localization of urokinase receptor in the formation of new microvascular structures in fibrin matrices. Am J Pathol 1999;154:1731-42.

[20] Cheresh DA. Human endothelial cells synthesize and express an Arg-Gly-Asp-directed adhesion receptor involved in attachment to fibrinogen and von Willebrand factor. Proc Natl Acad Sci U S A 1987;84:6471-5.

[21] Cheresh DA, Berliner SA, Vicente V, Ruggeri ZM. Recognition of distinct adhesive sites on fibrinogen by related integrins on platelets and endothelial cells. Cell 1989;58:945-53.

[22] Gailit J, Clarke C, Newman D, Tonnesen MG, Mosesson MW, Clark RA. Human fibroblasts bind directly to fibrinogen at RGD sites through integrin alpha(v)beta3. Exp Cell Res 1997;232:118-26.

[23] Chalupowicz DG, Chowdhury ZA, Bach TL, Barsigian C, Martinez J. Fibrin II induces endothelial cell capillary tube formation. J Cell Biol 1995;130:207-15.

[24] Odrljin TM, Francis CW, Sporn LA, Bunce LA, Marder VJ, Simpson-Haidaris PJ. Heparin-binding domain of fibrin mediates its binding to endothelial cells. Arterioscler Thromb Vasc Biol 1996;16:1544-51.

[25] Bunce LA, Sporn LA, Francis CW. Endothelial cell spreading on fibrin requires fibrinopeptide B cleavage and amino acid residues 15-42 of the beta chain. J Clin Invest 1992;89:842-50.

[26] Bach TL, Barsigian C, Yaen CH, Martinez J. Endothelial cell VE-cadherin functions as a receptor for the beta15-42 sequence of fibrin. J Biol Chem 1998;273:30719-28.

[27] Martinez J, Ferber A, Bach TL, Yaen CH. Interaction of fibrin with VE-cadherin. Ann N Y Acad Sci 2001;936:386-405.

[28] Yakovlev S, Medved L. Interaction of fibrin(ogen) with the endothelial cell receptor VE-cadherin: localization of the fibrin-binding site within the third extracellular VE-cadherin domain. Biochemistry 2009;48:5171-9.

[29] Flick MJ, Du X, Witte DP, Jirouskova M, Soloviev DA, Busuttil SJ, et al. Leukocyte engagement of fibrin(ogen) via the integrin receptor alphaMbeta2/Mac-1 is critical for host inflammatory response in vivo. J Clin Invest 2004;113:1596-606.

[30] Vernon RB, Angello JC, Iruela-Arispe ML, Lane TF, Sage EH. Reorganization of basement membrane matrices by cellular traction promotes the formation of cellular networks in vitro. Lab Invest 1992;66:536-47.

[31] Nehls V, Drenckhahn D. A novel, microcarrier-based in vitro assay for rapid and reliable quantification of three-dimensional cell migration and angiogenesis. Microvasc Res 1995;50:311-22.

[32] Ghajar CM, Blevins KS, Hughes CC, George SC, Putnam AJ. Mesenchymal stem cells enhance angiogenesis in mechanically viable prevascularized tissues via early matrix metalloproteinase upregulation. Tissue Eng 2006;12:2875-88.

[33] Nakatsu MN, Sainson RC, Aoto JN, Taylor KL, Aitkenhead M, Perez-del-Pulgar S, et al. Angiogenic sprouting and capillary lumen formation modeled by human umbilical vein endothelial cells (HUVEC) in fibrin gels: the role of fibroblasts and Angiopoietin-1. Microvasc Res 2003;66:102-12.

[34] Griffith CK, Miller C, Sainson RC, Calvert JW, Jeon NL, Hughes CC, et al. Diffusion limits of an in vitro thick prevascularized tissue. Tissue Eng 2005;11:257-66.

[35] Ghajar CM, Chen X, Harris JW, Suresh V, Hughes CC, Jeon NL, et al. The effect of matrix density on the regulation of 3-D capillary morphogenesis. Biophys J 2008;94:1930-41.

[36] Korff T, Augustin HG. Tensional forces in fibrillar extracellular matrices control directional capillary sprouting. J Cell Sci 1999;112 (Pt 19):3249-58.

[37] Bayless KJ, Salazar R, Davis GE. RGD-dependent vacuolation and lumen formation observed during endothelial cell morphogenesis in three-dimensional fibrin matrices involves the alpha(v)beta(3) and alpha(5)beta(1) integrins. Am J Pathol 2000;156:1673-83.

[38] Rao RR, Peterson AW, Ceccarelli J, Putnam AJ, Stegemann JP. Matrix composition regulates three-dimensional network formation by endothelial cells and mesenchymal stem cells in collagen/fibrin materials. Angiogenesis 2012;15:253-64.

[39] Carrion B, Huang CP, Ghajar CM, Kachgal S, Kniazeva E, Jeon NL, et al. Recreating the perivascular niche ex vivo using a microfluidic approach. Biotechnol Bioeng 2010;107:1020-8.

[40] Trkov S, Eng G, Di Liddo R, Parnigotto PP, Vunjak-Novakovic G. Micropatterned three-dimensional hydrogel system to study human endothelial-mesenchymal stem cell interactions. J Tissue Eng Regen Med 2010;4:205-15.

[41] Moya ML, Hsu YH, Lee AP, Hughes CC, George SC. In Vitro Perfused Human Capillary Networks. Tissue Eng Part C Methods 2013.

[42] Yeon JH, Ryu HR, Chung M, Hu QP, Jeon NL. In vitro formation and characterization of a perfusable three-dimensional tubular capillary network in microfluidic devices. Lab Chip 2012;12:2815-22.

[43] Allen P, Melero-Martin J, Bischoff J. Type I collagen, fibrin and PuraMatrix matrices provide permissive environments for human endothelial and mesenchymal progenitor cells to form neovascular networks. J Tissue Eng Regen Med 2011;5:e74-86.

[44] Nicosia RF, Ottinetti A. Modulation of microvascular growth and morphogenesis by reconstituted basement membrane gel in three-dimensional cultures of rat aorta: a comparative study of angiogenesis in matrigel, collagen, fibrin, and plasma clot. In Vitro Cell Dev Biol 1990;26:119-28.

[45] Bugge TH, Kombrinck KW, Flick MJ, Daugherty CC, Danton MJ, Degen JL. Loss of fibrinogen rescues mice from the pleiotropic effects of plasminogen deficiency. Cell 1996;87:709-19.

[46] Hiraoka N, Allen E, Apel IJ, Gyetko MR, Weiss SJ. Matrix metalloproteinases regulate neovascularization by acting as pericellular fibrinolysins. Cell 1998;95:365-77.

[47] Ghajar CM, Kachgal S, Kniazeva E, Mori H, Costes SV, George SC, et al. Mesenchymal cells stimulate capillary morphogenesis via distinct proteolytic mechanisms. Exp Cell Res 2010;316:813-25.

[48] Kachgal S, Putnam AJ. Mesenchymal stem cells from adipose and bone marrow promote angiogenesis via distinct cytokine and protease expression mechanisms. Angiogenesis 2011;14:47-59.

[49] Kachgal S, Carrion B, Janson IA, Putnam AJ. Bone marrow stromal cells stimulate an angiogenic program that requires endothelial MT1-MMP. J Cell Physiol 2012;227:3546-55.

[50] Lutolf MP, Hubbell JA. Synthetic biomaterials as instructive extracellular microenvironments for morphogenesis in tissue engineering. Nat Biotechnol 2005;23:47-55.

[51] Raeber GP, Lutolf MP, Hubbell JA. Molecularly engineered PEG hydrogels: a novel model system for proteolytically mediated cell migration. Biophys J 2005;89:1374-88.

[52] Bott K, Upton Z, Schrobback K, Ehrbar M, Hubbell JA, Lutolf MP, et al. The effect of matrix characteristics on fibroblast proliferation in 3D gels. Biomaterials 2010;31:8454-64.

[53] Patterson J, Hubbell JA. Enhanced proteolytic degradation of molecularly engineered PEG hydrogels in response to MMP-1 and MMP-2. Biomaterials 2010;31:7836-45.

[54] Hanjaya-Putra D, Bose V, Shen YI, Yee J, Khetan S, Fox-Talbot K, et al. Controlled activation of morphogenesis to generate a functional human microvasculature in a synthetic matrix. Blood 2011;118:804-15.

[55] Miller JS, Shen CJ, Legant WR, Baranski JD, Blakely BL, Chen CS. Bioactive hydrogels made from step-growth derived PEG-peptide macromers. Biomaterials 2010;31:3736-43.

[56] Moon JJ, Saik JE, Poche RA, Leslie-Barbick JE, Lee SH, Smith AA, et al. Biomimetic hydrogels with pro-angiogenic properties. Biomaterials 2010;31:3840-7.

[57] Sokic S, Papavasiliou G. Controlled proteolytic cleavage site presentation in biomimetic PEGDA hydrogels enhances neovascularization in vitro. Tissue engineering Part A 2012;18:2477-86.

[58] Phelps EA, Landazuri N, Thule PM, Taylor WR, Garcia AJ. Bioartificial matrices for therapeutic vascularization. Proc Natl Acad Sci U S A 2010;107:3323-8.

[59] Zisch AH, Lutolf MP, Ehrbar M, Raeber GP, Rizzi SC, Davies N, et al. Cell-demanded release of VEGF from synthetic, biointeractive cell ingrowth matrices for vascularized tissue growth. FASEB journal : official publication of the Federation of American Societies for Experimental Biology 2003;17:2260-2.

[60] Ehrbar M, Rizzi SC, Schoenmakers RG, Miguel BS, Hubbell JA, Weber FE, et al. Biomolecular hydrogels formed and degraded via site-specific enzymatic reactions. Biomacromolecules 2007;8:3000-7.

[61] Guthold M, Liu W, Sparks EA, Jawerth LM, Peng L, Falvo M, et al. A comparison of the mechanical and structural properties of fibrin fibers with other protein fibers. Cell Biochem Biophys 2007;49:165-81.

[62] Liu W, Jawerth LM, Sparks EA, Falvo MR, Hantgan RR, Superfine R, et al. Fibrin fibers have extraordinary extensibility and elasticity. Science 2006;313:634.

[63] Ferry JD, Morrison PR. Preparation and properties of serum and plasma proteins; the conversion of human fibrinogen to fibrin under various conditions. Journal of the American Chemical Society 1947;69:388-400.

[64] Brown AE, Litvinov RI, Discher DE, Purohit PK, Weisel JW. Multiscale mechanics of fibrin polymer: gel stretching with protein unfolding and loss of water. Science 2009;325:741-4.

[65] Winer JP, Oake S, Janmey PA. Non-linear elasticity of extracellular matrices enables contractile cells to communicate local position and orientation. PLoS One 2009;4:e6382.

[66] Matsumoto T, Sasaki J, Alsberg E, Egusa H, Yatani H, Sohmura T. Three-dimensional cell and tissue patterning in a strained fibrin gel system. PLoS One 2007;2:e1211.

[67] Morin KT, Tranquillo RT. Guided sprouting from endothelial spheroids in fibrin gels aligned by magnetic fields and cell-induced gel compaction. Biomaterials 2011;32:6111-8.

[68] Sander EA, Barocas VH, Tranquillo RT. Initial fiber alignment pattern alters extracellular matrix synthesis in fibroblast-populated fibrin gel

cruciforms and correlates with predicted tension. Ann Biomed Eng 2011;39:714-29.

[69] Kotlarchyk MA, Shreim SG, Alvarez-Elizondo MB, Estrada LC, Singh R, Valdevit L, et al. Concentration independent modulation of local micromechanics in a fibrin gel. PLoS One 2011;6:e20201.

[70] Kniazeva E, Weidling JW, Singh R, Botvinick EL, Digman MA, Gratton E, et al. Quantification of local matrix deformations and mechanical properties during capillary morphogenesis in 3D. Integr Biol (Camb) 2012;4:431-9.

[71] Gjorevski N, Nelson CM. Endogenous patterns of mechanical stress are required for branching morphogenesis. Integr Biol (Camb) 2010;2:424-34.

[72] Hahn C, Schwartz MA. Mechanotransduction in vascular physiology and atherogenesis. Nat Rev Mol Cell Biol 2009;10:53-62.

[73] Sumpio BE, Chang R, Xu WJ, Wang XJ, Du W. Regulation of tPA in endothelial cells exposed to cyclic strain: role of CRE, AP-2, and SSRE binding sites. The American journal of physiology 1997;273:C1441-8.

[74] Diamond SL, Eskin SG, McIntire LV. Fluid flow stimulates tissue plasminogen activator secretion by cultured human endothelial cells. Science 1989;243:1483-5.

[75] Cummins PM, von Offenberg Sweeney N, Killeen MT, Birney YA, Redmond EM, Cahill PA. Cyclic strain-mediated matrix metalloproteinase regulation within the vascular endothelium: a force to be reckoned with. Am J Physiol Heart Circ Physiol 2007;292:H28-42.

[76] Ceccarelli J, Cheng A, Putnam AJ. Mechanical Strain Controls Endothelial Patterning During Angiogenic Sprouting. Cellular and Molecular Bioengineering 2012;5:463-73.

[77] Putnam AJ, Mooney DJ. Tissue engineering using synthetic extracellular matrices. Nat Med 1996;2:824-6.

[78] Langer R, Vacanti JP. Tissue engineering. Science 1993;260:920-6.

[79] Spotnitz WD. Fibrin sealant: past, present, and future: a brief review. World journal of surgery 2010;34:632-4.

[80] Dunn CJ, Goa KL. Fibrin sealant: a review of its use in surgery and endoscopy. Drugs 1999;58:863-86.

[81] Radosevich M, Goubran HI, Burnouf T. Fibrin sealant: scientific rationale, production methods, properties, and current clinical use. Vox sanguinis 1997;72:133-43.

[82] Jackson MR. Fibrin sealants in surgical practice: An overview. American journal of surgery 2001;182:1S-7S.

[83] Christman KL, Fok HH, Sievers RE, Fang Q, Lee RJ. Fibrin glue alone and skeletal myoblasts in a fibrin scaffold preserve cardiac function after myocardial infarction. Tissue Eng 2004;10:403-9.

[84] Christman KL, Vardanian AJ, Fang Q, Sievers RE, Fok HH, Lee RJ. Injectable fibrin scaffold improves cell transplant survival, reduces infarct expansion, and induces neovasculature formation in ischemic myocardium. J Am Coll Cardiol 2004;44:654-60.

[85] Chen X, Aledia AS, Ghajar CM, Griffith CK, Putnam AJ, Hughes CC, et al. Prevascularization of a fibrin-based tissue construct accelerates the formation of functional anastomosis with host vasculature. Tissue Eng Part A 2009;15:1363-71.

[86] Grainger SJ, Carrion B, Ceccarelli J, Putnam AJ. Stromal Cell Identity Influences the In Vivo Functionality of Engineered Capillary Networks Formed by Co-delivery of Endothelial Cells and Stromal Cells. Tissue Eng Part A 2013;19:1209-22.

[87] Schense JC, Hubbell JA. Cross-linking exogenous bifunctional peptides into fibrin gels with factor XIIIa. Bioconjugate chemistry 1999;10:75-81.

[88] Zisch AH, Zeisberger SM, Ehrbar M, Djonov V, Weber CC, Ziemiecki A, et al. Engineered fibrin matrices for functional display of cell membrane-

bound growth factor-like activities: study of angiogenic signaling by ephrin-B2. Biomaterials 2004;25:3245-57.

[89] Sakiyama-Elbert SE, Panitch A, Hubbell JA. Development of growth factor fusion proteins for cell-triggered drug delivery. Faseb J 2001;15:1300-2.

[90] Zisch AH, Schenk U, Schense JC, Sakiyama-Elbert SE, Hubbell JA. Covalently conjugated VEGF--fibrin matrices for endothelialization. Journal of controlled release : official journal of the Controlled Release Society 2001;72:101-13.

[91] Sakiyama SE, Schense JC, Hubbell JA. Incorporation of heparin-binding peptides into fibrin gels enhances neurite extension: an example of designer matrices in tissue engineering. Faseb J 1999;13:2214-24.

[92] Sakiyama-Elbert SE, Hubbell JA. Development of fibrin derivatives for controlled release of heparin-binding growth factors. Journal of controlled release : official journal of the Controlled Release Society 2000;65:389-402.

[93] Johnson PJ, Tatara A, McCreedy DA, Shiu A, Sakiyama-Elbert SE. Tissue-engineered fibrin scaffolds containing neural progenitors enhance functional recovery in a subacute model of SCI. Soft matter 2010;6:5127-37.

[94] Yang HS, La WG, Bhang SH, Jeon JY, Lee JH, Kim BS. Heparin-conjugated fibrin as an injectable system for sustained delivery of bone morphogenetic protein-2. Tissue Eng Part A 2010;16:1225-33.

[95] Soon AS, Stabenfeldt SE, Brown WE, Barker TH. Engineering fibrin matrices: the engagement of polymerization pockets through fibrin knob technology for the delivery and retention of therapeutic proteins. Biomaterials 2010;31:1944-54.

[96] Barker TH, Fuller GM, Klinger MM, Feldman DS, Hagood JS. Modification of fibrinogen with poly(ethylene glycol) and its effects on fibrin clot characteristics. Journal of biomedical materials research 2001;56:529-35.

[97] Almany L, Seliktar D. Biosynthetic hydrogel scaffolds made from fibrinogen and polyethylene glycol for 3D cell cultures. Biomaterials 2005;26:2467-77.

[98] Peyton SR, Kim PD, Ghajar CM, Seliktar D, Putnam AJ. The effects of matrix stiffness and RhoA on the phenotypic plasticity of smooth muscle cells in a 3-D biosynthetic hydrogel system. Biomaterials 2008;29:2597-607.

[99] Kim PD, Peyton SR, VanStrien AJ, Putnam AJ. The influence of ascorbic acid, TGF-beta1, and cell-mediated remodeling on the bulk mechanical properties of 3-D PEG-fibrinogen constructs. Biomaterials 2009;30:3854-64.

[100] Zhang G, Hu Q, Braunlin EA, Suggs LJ, Zhang J. Enhancing efficacy of stem cell transplantation to the heart with a PEGylated fibrin biomatrix. Tissue Eng Part A 2008;14:1025-36.

[101] Soon AS, Lee CS, Barker TH. Modulation of fibrin matrix properties via knob:hole affinity interactions using peptide-PEG conjugates. Biomaterials 2011;32:4406-14.

[102] Stabenfeldt SE, Gourley M, Krishnan L, Hoying JB, Barker TH. Engineering fibrin polymers through engagement of alternative polymerization mechanisms. Biomaterials 2012;33:535-44.

[103] Zhang G, Wang X, Wang Z, Zhang J, Suggs L. A PEGylated fibrin patch for mesenchymal stem cell delivery. Tissue Eng 2006;12:9-19.

[104] Zhang G, Drinnan CT, Geuss LR, Suggs LJ. Vascular differentiation of bone marrow stem cells is directed by a tunable three-dimensional matrix. Acta biomaterialia 2010;6:3395-403.

Chapter 3

Using Cyclic Strain to Pattern Angiogenesis

3.1 Introduction

Mechanical signals are key regulators of cell behavior [1], and serve as an important link to the extracellular environment. Cells exist in a force-balance between external mechanical inputs and internal, cell-generated traction forces. This "tug-of-war" induces a state of pre-stress in the system, making cells exquisitely sensitive to changes in their mechanical environment [2]. Changes in tissue mechanics are symptomatic of many disease states. For example, tumor extracellular matrices are generally much stiffer than surrounding tissues, and tumors often have higher interstitial fluid pressure, both of which alter cell behavior [3]. Increases in stiffness affect the vasculature within a tumor as well [4], contributing to vessel leakiness and metastasis. Changes in the mechanical microenvironment can contribute to changes in cell behavior, which in turn

lead to changes in tissue function.

While such mechanical changes in the microenvironment have been linked with numerous pathologies [5, 6], mechanical stimulation can also be applied to induce desirable changes in cell behavior. Cells not only respond to passive mechanical cues, such as ECM stiffness, but to forces that are actively applied to the matrix, providing a robust way to modify cell behavior. Mechanical stimulation has been shown to improve the integrity of engineered vascular grafts [7, 8], demonstrating the utility of using mechanical signals to improve outcomes. Despite the success of mechanical preconditioning in engineered tissue applications, a better understanding of how the ECM transduces mechanical signals to resident cells might enable the use of applied mechanical forces as a way to control tissue patterning and morphogenesis. Endothelial cell behavior is relatively well characterized in 2D [9] but it is less clear how strain alters their behavior when challenged to undergo a complex morphogenetic program in 3D, such as angiogenesis [10, 11].

We have developed a system to study the effects of mechanical inputs on angiogenesis by adapting a 3D, microcarrier-based angiogenesis assay, first described by Nehls and Drenckhahn [12]. Human umbilical vein endothelial cells (HUVECs) adhering to gelatin-coated dextran

microcarrier beads are embedded in a fibrin matrix and co-cultured with a monolayer of human aortic smooth muscle cells (HASMCs) atop the gel. This 3D culture model is contained with a custom-designed polydimethylsiloxane (PDMS) multi-well platform capable of housing natural and synthetic hydrogels. When clamped into a linear stage, a well-defined static or cyclic uniaxial strain may be applied to the PDMS, which propagates the strain to the ECM and the embedded cells. We show that the application of cyclic strain causes sprouting parallel to the applied strain, and that this biasing is lost if strain is removed. We also show that the observed directional biasing is not simply explained via contact guidance.

3.2 Methods

3.2.1 PDMS Multi-Well Plate and Stretch Device

A PDMS multi-well slab was designed to support 3D cell cultures and to enable them to be subjected to strain (Fig. 3-1 a). To fabricate the multi-well slab, a Teflon® mold was machined to house the PDMS during curing. The wells within the PDMS slab are cubic, 5 mm on a side, and spaced 5 mm apart with a 10 mm gap between the end of the outside wells and the

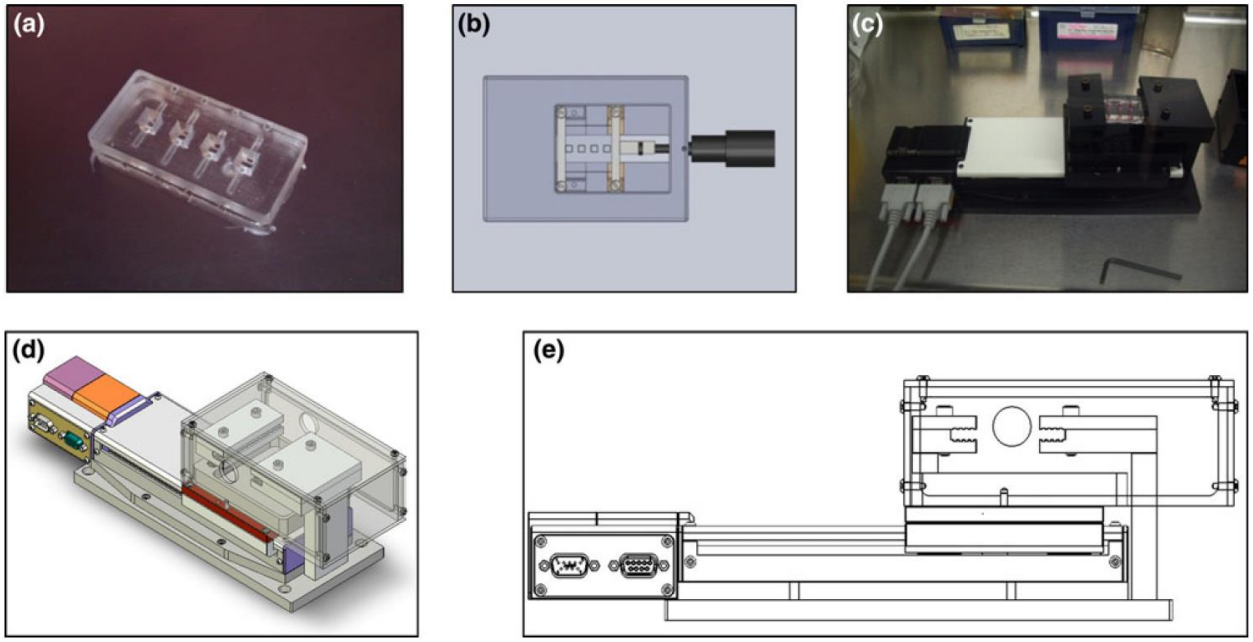

Figure 3-1. Devices used to house and apply strain to hydrogels. (A) PDMS multi-well plate, (b) schematic of microscope stage insert used for calibration of micro-scale strain, and (c-e) linear stage used to apply cyclic strain to PDMS multi-well plate.

edge of the PDMS to facilitate clamping. During strain experiments, the PDMS slab was clamped into a linear stage (Newmark Systems, Mission Viejo, CA) capable of providing precise, reproducible strain (Figs. 3-1 c–e). The clamp apparatus was covered with a lid to improve sterility and a reservoir to keep the semi-open culture system at 100% humidity during cell culture. The reservoir was filled with sterile ddH2O at the start of the experiment and replenished as necessary. Once the wells of the plate were loaded, the system was placed into a standard cell culture incubator.

3.2.2 Cell Culture

HUVECs were isolated from freshly harvested umbilical cords as

previously described [13]. The cords were obtained via a process considered exempt by the University of Michigan's institutional review board because the tissue is normally discarded, and no identifying information is provided to the researchers who receive the cords. Cord veins were flushed with Dulbecco's phosphate-buffered saline (DPBS, Gibco, Carlsbad, CA), then a 0.1% collagenase type 1 (Worthington, Lakewood, NJ) digestion was performed for 15 minutes to release the endothelial cells from the vessel wall. The vessel was flushed with DPBS and the resulting cell suspension centrifuged, plated, and washed after 24 hours with DPBS to remove any residual erythrocytes. HUVECs were cultured in Endothelial Growth Medium-2 (EGM-2, Lonza, Walkersville, MD) and used at passage 3. Primary HASMCs (Cascade Biologics, Portland, Oregon) were cultured in Medium 231 supplemented with Smooth Muscle Growth Supplement (SMGS, both Invitrogen). HASMCs were used before passage 15. All cell culture was performed in a 37°C, 5.0% CO_2 incubator. Media was changed every other day.

3.2.3 3D Cell Culture and Fibrin Gel Construction

The 3D cell culture model of angiogenesis was modified from previously established protocols [12, 13]. Briefly, HUVECs were allowed to

attach to gelatin-coated Cytodex® 3 microcarrier beads (Sigma-Aldrich, St. Louis, MO) as follows. HUVECs were trypsinized, pelleted, counted, and $4x10^6$ cells were suspended in 5 ml of EGM-2. This suspension was transferred into an upright T-25 culture flask with ten-thousand sterilized microcarrier beads and was gently agitated every 30 minutes. After 4 hours, the suspension was supplied with an additional 5 ml EGM-2 and moved to a fresh T-25, and incubated in normal cell culture position. Coated beads were used within 48 hours.

To create fibrin tissues for 3D cell cultures, 490 μl of 2.5 mg/ml bovine fibrinogen (lot# 029K7636V, Sigma-Aldrich) solutions containing approximately 100 HUVEC-coated microcarrier beads were combined with 10 μl thrombin stock solution (50 U/ml, Sigma-Aldrich). Then, 63 μl of this mixture was quickly transferred into each well of the autoclaved PDMS multi-well plate. Acellular fibrin gels used for confocal reflectance imaging were created in an identical manner using microcarrier beads with no HUVECs attached. All gels were left at room temperature for 5 minutes to allow the beads to settle to the bottom of the well, and incubated an additional 25 minutes in a 37°C, 5.0% CO_2 incubator to allow for complete gelation. After incubation, 5,000 HASMCs were plated on top of each fibrin gel. Within 30 minutes of plating HASMCs, gels to be used in stretched

conditions were clamped into a linear stage and the cyclic strain protocol (10% strain, 0.7 Hz) commenced. PDMS plates cultured statically were placed into petri dishes for sterility. Both strained and static conditions were cultured in a 37°C, 5.0% CO_2 incubator. Media was changed daily for all experiments in PDMS multi-well plates.

3.2.4 Determination of the Kinetics and Robustness of Directional Sprouting

To determine the effects of cyclic strain on angiogenesis, cell-seeded PDMS multi-well slabs were prepared as described above, divided into static and stretched conditions, and cultured for 5 days. On days 2 through 5, all of the beads within each PDMS slab were imaged.

To determine the robustness of directional sprouting in this system, PDMS multi-well slabs were again prepared. Two slabs were subjected to cyclic strain (Fig. 3-4 A, Groups 1 and 2), while two were left under static conditions initially (Fig. 3-4 A, Groups 3 and 4) for four days. On day 4, plates were imaged. After imaging, one of the previously strained samples was transferred to a static condition, while a previously unstrained PDMS slab was placed in the linear stage and subjected to cyclic strain (Fig. 3-4 A). On day 8, the plates were imaged again. Four experiments were

performed for each condition.

3.2.5 Calibration of Strain in 3D Hydrogels

To determine the extent to which various levels of strain deform fibrin hydrogels embedded within the PDMS slab, 2.5 mg/ml fibrin gels containing Fluospheres® were prepared as described above and the PDMS slab was clamped into a custom-built microscope stage insert (Fig. 3-1 B). A micrometer attached to the insert was used to reposition the moving clamp to apply strain to the PDMS slab. Determination of the internal strain in the gel was performed as previously described [14, 15]. In short, triads of fluorescent beads randomly distributed within the gel were imaged at 0-12% strain in increments of 2%. Relative distances between these beads at each strain level were used to calculate the first and second principle strains using Lagrangian finite strain analysis (Fig. 3-2 A).

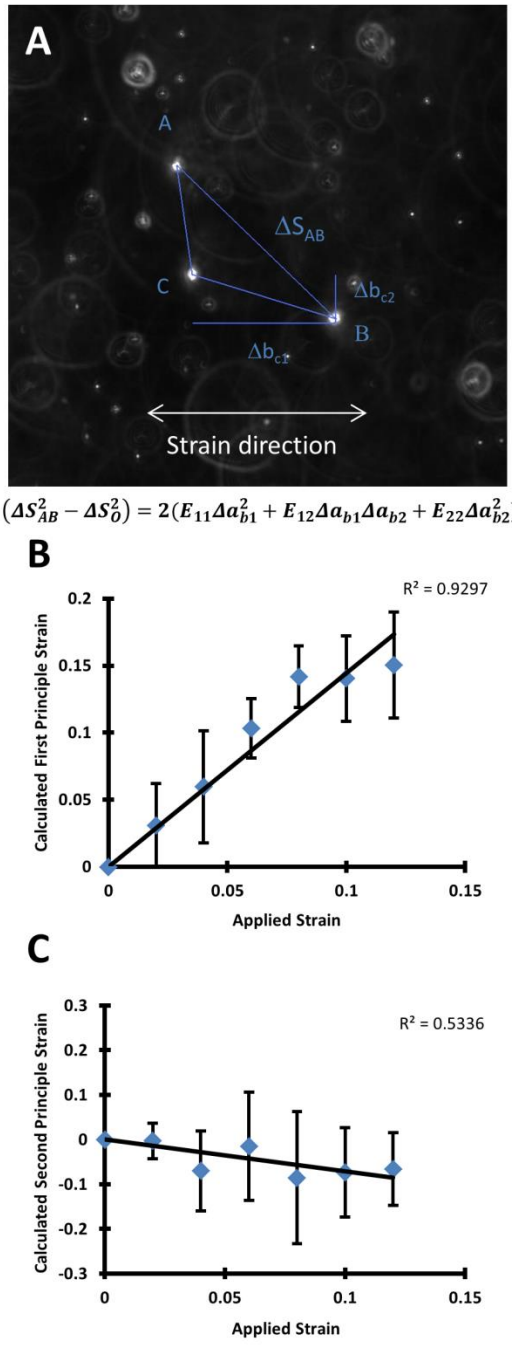

Figure 3-2. Relationship between applied strain and strain within the fibrin gel. (a) Representative image of a triad used in strain calibration. A system of equations was solved for E11, E12, and E22 and were used to calculate the principle strains. Shown are the first (b) and second (c) principle strains within the fibrin matrix. 15 triads were used for this analysis.

3.2.6 Quantification of Network Length and Sprout Angle

Quantification of total network length was performed as described previously [13]. Briefly, vessels from each bead were traced using ImageJ software and summed to determine total network length. For each condition, the network lengths of sprouts coming from 10 individual beads were averaged to determine the total average network length for that condition. To determine the average angle of sprouts coming off of the bead, ImageJ software was used to measure the acute angle of each sprout as it projected from the bead relative to the direction of applied

strain (horizontal). Angle measurements from each bead were averaged, followed by averaging of the results across 10 beads to determine the average sprout angle. For all quantifications, 4 independent experiments were performed.

3.2.7 Finite Element Model

To further analyze the local strain within the fibrin gel, a 2D finite element model of the strain field surrounding a single microcarrier bead was created using COMSOL Multiphysics (COMSOL Inc., Burlington, MA). The model assumes 10% uniaxial strain applied to a slab of fibrin gel containing the bead. The fibrin surrounding the bead is modeled as an elastic solid of elastic modulus (E) 3147 Pa, Poisson's ratio (υ) of 0.4992, and density 2.5 mg/ml. The diameter of the bead in the model is 150 μm, which corresponds to the approximate diameter of the Cytodex beads used experimentally (after swelling). The bead is modeled as a rigid solid of modulus 10MPa.

3.2.8 Staining of HUVEC plasma membranes for imaging

To facilitate imaging, HUVEC plasma membranes were stained with the lipophilic carbocyanine SP-DiIC$_{18}$(3) (Molecular Probes®, Grand Island,

NY). Cells were washed once with DPBS, then incubated in DPBS containing 2.5 μM SP-DiIC$_{18}$(3) at 37°C for 5 minutes, followed by a 15 minute incubation at 4°C to prevent endocytosis of the dye. After the incubation at 4°C, a final DPBS wash was performed, and EGM-2 was replaced.

3.2.9 Confocal Reflectance and Fluorescence Microscopy

Unlabeled fibrin matrices were visualized using confocal reflectance microscopy. Confocal reflectance images were taken on a Zeiss LSM 510-META Laser Scanning Confocal microscope using a 63x water immersion objective (C-Aprochromat, Carl Zeiss, Thornwood, NY). Fibrin gels were illuminated using a 488 nm Argon laser through an 80/20 filter. Other fluorescence images were taken on an Olympus IX81 microscope equipped with a 100-W high pressure mercury lamp (Olympus, Center Valley, PA) and Hammamatsu camera (Bridgewater, NJ).

3.2.10 Statistical Analysis

Statistical analysis was performed using open source R software (www.r-project.org). Two-way analysis of variance (ANOVA) was performed and pairwise comparisons were made using Tukey's method.

The threshold for statistical significance was set at $p < 0.05$. Data are reported as mean ± SEM.

3.3 Results

3.3.1 Quantification of microscale strain confirms that strain applied to the PDMS propagates into the fibrin gel

The first step in this study was to confirm that strain applied to the PDMS slab was propagated into the fibrin, and to subsequently calibrate the measured strain with the applied strain. To accomplish this goal, red fluorescent microcarrier beads were embedded in the fibrin gels. Displacements of the microspheres under strain (0-12%) were measured, revealing that the first principle strain in the system responded linearly ($R^2 = 0.9297$) to the applied strain (Fig. 3-2 B). The second principle strain, a metric of strain in the direction orthogonal to the applied strain, showed a weaker, but still linear ($R^2 = 0.5336$), negative trend with increasing applied strain (Fig. 3-2 C). These calibration results show that uniaxial strain applied to the PDMS slab propagates into the fibrin gels in our system.

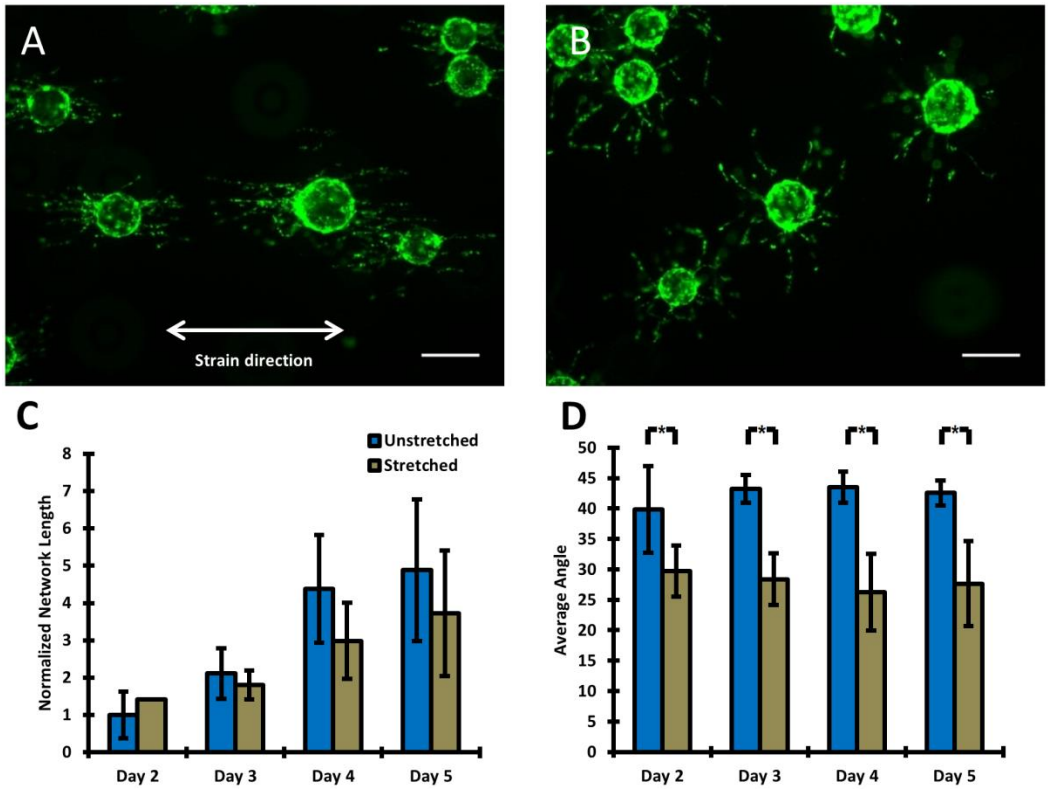

Figure 3-1. Effects of cyclic strain on angiogenesis. (a, b) Representative pictures of HUVEC-coated dextran microcarrier beads at day 5 in 3D angiogenesis assay under strained (left) and static (right) conditions. (c) Normalized network lengths of strained and static capillaries. Data for each condition were normalized to the day 2 static condition. No significant differences were observed between the strained and static conditions at each time point. (d) A significant decrease in average sprout angle was observed in the strained conditions (relative to static) for all time points. Random alignment corresponds to an average angle of 45°, and perfect alignment in the direction of strain corresponds to 0°. Data reported as mean 6 SEM. Scale bars = 100 μm.

3.3.2 Cyclic strain alters the direction, but not the magnitude, of angiogenic sprouting

Following calibration, we used our mechanical strain device to apply cyclic strain (10% strain, 0.7 Hz) to the 3D fibrin-based model of angiogenesis. This regimen was chosen to conform with published experiments showing directional alignment in 3D assays [11, 16, 17]. Representative images of capillaries formed under static and strained conditions, respectively (Fig. 3A-B), reveal clear differences in capillary

sprouting in strained versus control cultures. No statistically significant differences in average total network lengths were observed between the strained and static conditions on days 2-5 (Fig. 3C). However, significant differences were observed in sprouting direction. By day 2, the static cultures contained capillary sprouts with an average sprout angle of 39.9±7.1°, showing nearly perfectly random radial outward growth from a bead (Fig. 3D). In contrast, cells in the strained cultures yielded capillary sprouts with an average sprout angle of 29.7±4.2°, significantly lower ($p < 0.05$) than that for the static cultures (Fig. 3D).

3.3.3 Direction of angiogenic sprouting is sensitive to changes in strain regimen

In order to test the stability of the directional biasing, four experimental groups were created (Fig. 4A). The magnitude of capillary sprouting was not significantly different across any of these four groups at day 4 or 8 (Fig. 4B), consistent with the data presented earlier (Fig. 3C). By contrast, there were significant adjustments in sprout angle when the strain regimen was altered. Image analysis revealed that the conditions with constant regimens [i.e., the condition cultured under strain for 8 days

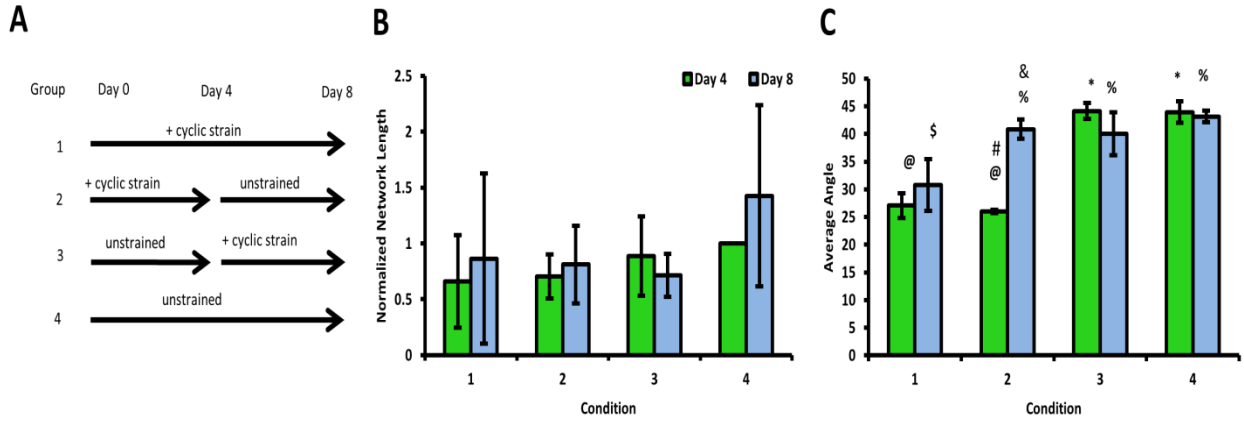

Figure 3-2. Effects of a change in strain regimen on angiogenesis. A. Schematic depicting the four different experimental groups, each of which was quantified for total network length and average sprout angle on day 4 and day 8. Strained conditions were subjected to 10% strain, 0.7Hz. B. Quantification of network lengths, normalized to the day 4 unstrained condition, showed that the magnitude of sprouting was unaffected by changes in the strain regimen. C. Cells under strain showed biasing parallel to the direction of strain at day 4. When the strain stimulus was removed, biasing disappeared. @ and * are statistically different, $ and % are statistically different, # and & are statistically different. Other comparisons are either not significant or were not made. Random alignment corresponds to an average angle of 45 degrees, while perfect alignment in the direction of strain corresponds to 0 degrees. Data reported as mean +/- S.E.M.

(Group 1) and the condition cultured statically for 8 days (Group 4)] showed no changes in the angle of capillary sprouting between days 4 and 8, as expected. The condition that was cultured statically for 4 days then cyclically strained for 4 days (Group 3) showed a slightly negative, but not statistically significant, change in sprout angle at day 8. In contrast, however, the condition that was strained for 4 days then cultured statically for 4 days (Group 2) showed a complete loss of directional biasing, with sprouts growing radially outward from the bead at day 8.

3.3.4 Matrix architecture shows only modest changes due to the applied strain

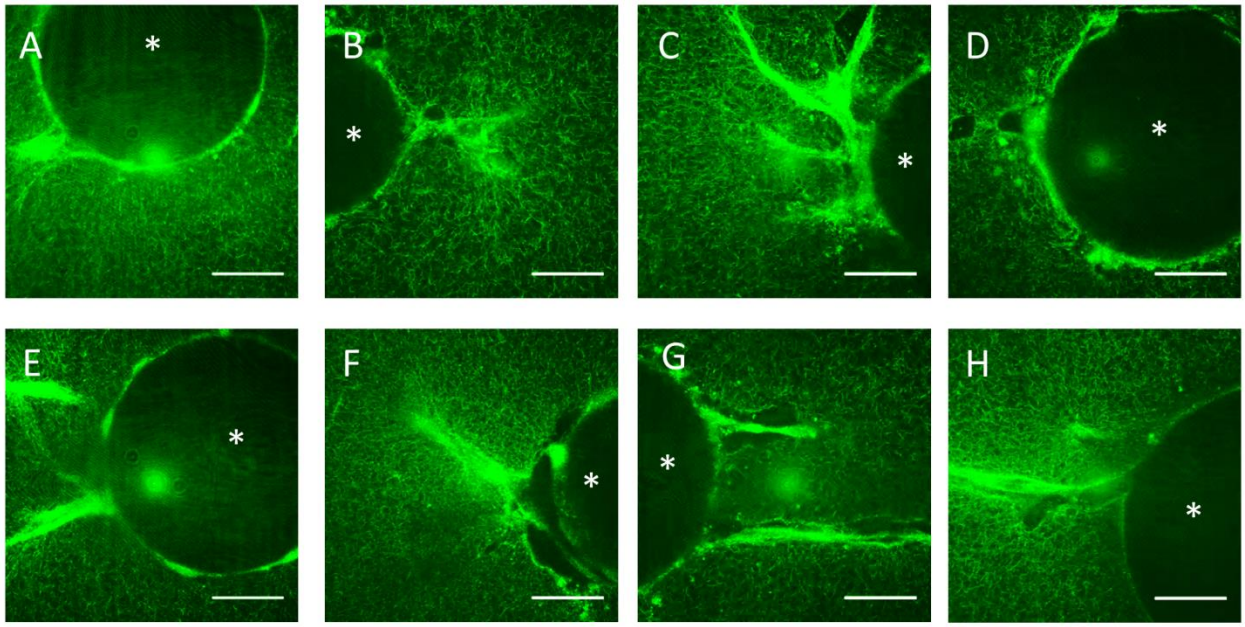

Figure 3-3. Confocal reflectance images of the fibrin matrix at days 2-5 of the angiogenesis assay. A,E. Day 2, B,F. Day 3, C,G. Day 4 D,H. Day 5 of the microcarrier bead angiogenesis assay. A-D. Static conditions, E-H. Stretched conditions. The asterisk in each image denotes the microcarrier bead. Images pseudo-colored green for clarity. Scale bars = 50 μm.

Confocal reflectance images of the angiogenesis assay, taken under static conditions on days 2-5, showed significant remodeling of the extracellular matrix caused by the invading endothelial cells, but no visible alignment of fibrin fibers (Fig. 5A-H). To examine the strain field surrounding a microcarrier bead, a finite element model was generated (Fig. 6A, B). Under an applied strain of 10%, the model shows 10% first principle strain throughout the gel, as well as distortions to the strain field surrounding the embedded microcarrier. Near the regions of the bead normal to the applied strain, the simulation shows strains increasing to approximately 14%; by contrast, near the regions of the bead tangential to the applied strain, the simulation shows strains of approximately 7%.

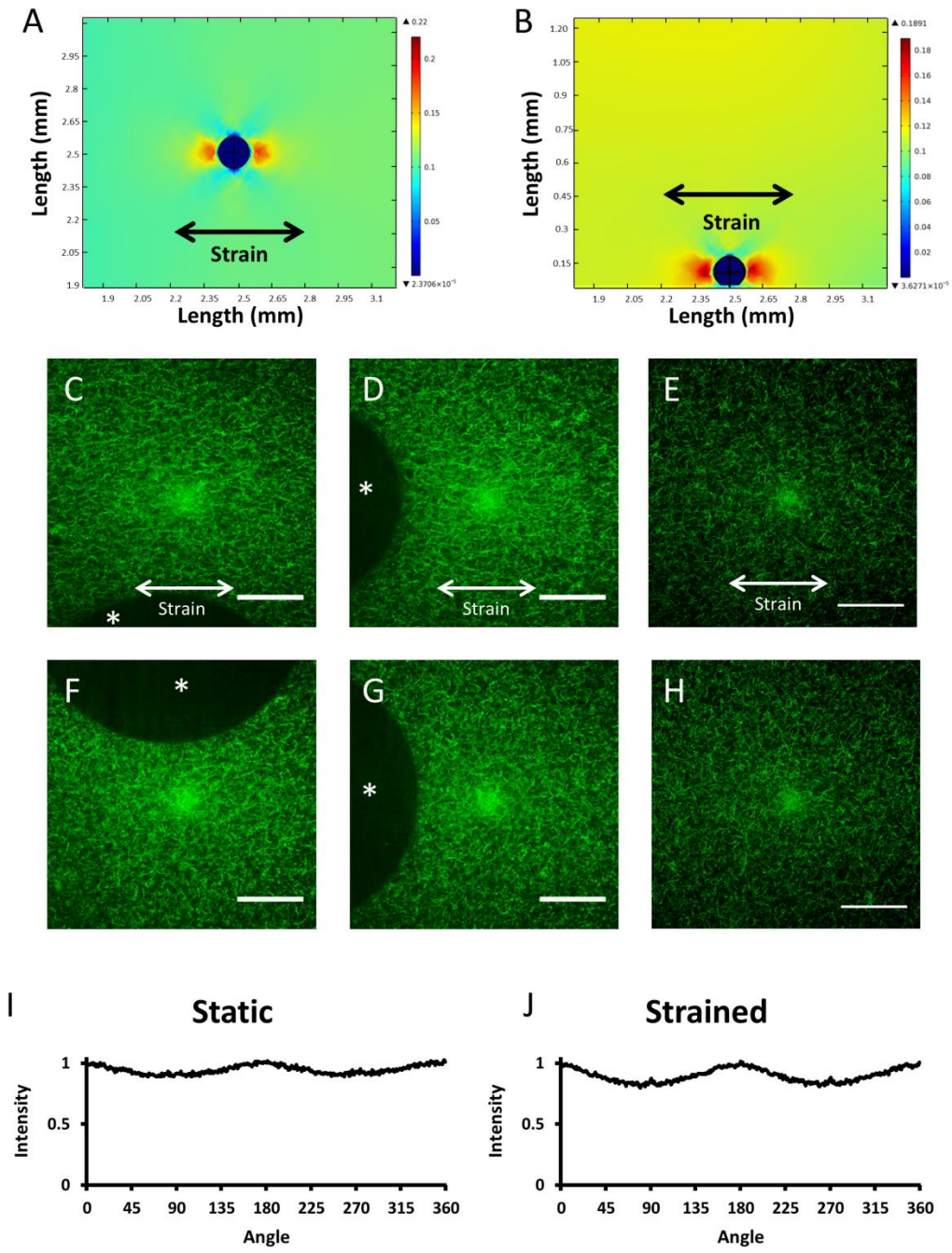

Figure 3-4. The effects of strain on ECM architecture. A-B. Linear elastic models of a fibrin hydrogel containing a microcarrier bead and subjected to 10% strain. In both the x-y (A) and x-z (B) planes, strain is amplified on the left and right faces of the bead, normal to the applied strain; strain is dampened on the faces tangential to the applied strain. C, D, F, G. Confocal reflectance images of fibrin matrix surrounding a strained bead show modest fiber alignment when the gel is strained 10% (C,D) and random orientation when static (F,G). The asterisk in each image denotes the microcarrier bead. There appear to be no differences in matrix architecture far from any boundary condition in the strained (E) and unstrained (H) conditions. FFT Analysis (I, J) of images D and G shows a similar degree of fiber alignment in the strained and static conditions in the horizontal direction, with moderate peaks at 0, 180, and 360 degrees. Strain direction is horizontal. Images pseudo-colored green for clarity. Scale bars = 50 µm.

These data suggest that the microcarrier beads themselves can both slightly amplify and slightly dampen the applied strain, depending on the face of the bead considered.

Confocal reflectance images of acellular fibrin gels containing microcarriers, but no cells, were taken to complement the finite element model (Fig. 6C-F). When imaged under 10% strain, only modest alignment of the fibrin fibers parallel to the direction of strain was observed (Fig. 6C-D, strain direction is horizontal) when visually compared to the unstrained conditions (Fig. 6E-F). Reflectance pictures of acellular gels containing no beads (Fig. 6G-H) showed no visual difference in fiber alignment between strained and unstrained conditions.

To further characterize the orientation of the fibers under static and strained conditions, Fourier transforms of the images in Figs. 6D and 6G were generated and analyzed using NIH ImageJ (Figs. 6I and 6J). Computed intensity values for each angle represent the degree of fiber orientation in the image at that angle. Results normalized to the raw values computed at 0° in each image show slight peaks in intensity at 0°, 180°, and 360°, indicating some possible alignment of the fibers in the horizontal direction; however, there were no significant differences in these peaks between the static and strained conditions.

3.4 Discussion

In this study, we developed and characterized a custom-made mechanical strain device that supports a 3D co-culture model of angiogenic sprouting widely used in the literature [12, 13, 16, 18]. With this new device, we showed here that cyclic strain applied to endothelial cells in a 3D hydrogel controls angiogenic pattern formation. Specifically, cyclic strain promoted alignment parallel to the direction of strain when the strain regimen was initiated at the beginning of the culture period. Moving strained samples to a static environment caused a randomization of sprout angle, implying that the direction of sprouting does have a degree of plasticity even after vessels have formed. Applying cyclic strain to the cultures after vessel-like structures had already formed induced a slight change in the subsequent sprouting direction as well, but the change was not quite statistically significant. However, the challenge of accurately measuring changes in capillary orientation in a pre-formed network without a fixed starting point may have contributed to an increased measurement uncertainty in this particular condition.

The results of our study here add to the growing body of evidence that collectively supports the idea that applied mechanical forces can direct

the formation of capillary networks. However, consensus has not been reached as to whether mechanical forces positively or negatively influence vessel growth due to many contradictory studies. For example, Kilarski, et al. showed that forces generated by endogenous fibroblasts promote the development and growth of new vessels during wound healing *in vivo* [19]. By contrast, Boerckel, et al. recently showed that externally applied mechanical loads can actually reduce vessel invasion in a bone injury model when applied at early time points, while enhancing vascular remodeling when the load is applied after a delay [20]. Our quantitative data here show that ECs subjected to cyclic strain form capillary networks to the same extent as those cultured in static conditions, similar to a study by Krishnan, et al. which found no differences in segment length distribution in strained and unstrained collagen gels [17]. Beyond the magnitude of capillary sprouting, there are also contradictory publications with respect to the influence of applied strain on directionality. Our observation that capillary sprouting occurs parallel to the direction of applied strain is consistent with the Krishnan, et al. study in which new sprouts initiated from isolated microvessels embedded in 3D collagen gels aligned parallel to the direction of applied cyclic strain (6% strain, 1 Hz) [17]. However, a study using a similar microcarrier-based model system

reported sprouting in a direction perpendicular to the applied cyclic strain [11].

In order to put our results in the context of these earlier studies, it is important to understand two key differences with respect to our model system and data. First, our model system contains a monolayer of smooth muscle cells on top of the fibrin gel. In prior studies using our model, we have found that some type of stromal cell is essential to stimulate the HUVECs to form robust capillary-like structures with hollow, well-defined lumens [21, 22]. These supporting cells may fundamentally alter the mechanics of the matrix under strain, the behavior of the endothelial cells in their presence, or a combination of those factors. However, our experiments with HUVECs alone did not induce alignment perpendicular to the applied strain in our system, but instead compromised the formation of sprouts altogether (data not shown).

A second important distinction of our findings is our data showing that cyclic strain did not significantly align the fibrin matrix, at least as detected via confocal reflection microscopy. On one hand, this finding is consistent with those of Matsumoto, et al., who showed that cyclic strain of 7% amplitude did not induce any perceptible alignment of fibrin fibrils [23]. On the other hand, Korff and Augustin showed that ECM alignment in

response to endothelial cell-generated tensile forces caused directional sprouting [10]. A more recent study showed that endothelial sprouting from spheroids occurred in a directional fashion in fibrin gels that had been aligned via an applied magnetic field or EC-generated forces [24]. In our model system, the mechanism by which applied strain induced directional alignment of the capillary-like networks is not simply explained by ECM realignment and contact guidance. The randomization of capillary sprouting after the strain is removed further supports this statement, and implies that any subtle strain-induced local anisotropies in matrix architecture are not permanent.

While we cannot rule out that subtle ECM realignment may play a role in directional capillary sprouting in our system, an alternative explanation is that the applied strain may induce local changes in ECM stiffness, without significantly disrupting fiber architecture. A previous study has shown that fibrin begins strain stiffening at approximately 10% strain, and that this stiffening occurs before fiber alignment can be detected by birefringence [25]. Matrix alignment itself can also increase the apparent stiffness of the ECM in the direction of alignment [26], but any potential change in local fibrin mechanics here in our study occurred independently of matrix alignment. Local matrix anisotropy is difficult to measure and

therefore possible local matrix strain stiffening is rarely examined. To address the question of how strain affects local matrix mechanics and cell behavior, Kotlarchyk et al. showed that applied strain induces local changes to fibrin stiffness in 3D gels, leading to differential cell behavior in regions of different stiffness [27]. Our finite element results showing strain amplification on the face of the bead normal to the strain direction agree with previous work showing that a rigid inclusion on a deformable membrane [28], as well as in a fibrin gel [29], can cause strain amplification in the vicinity of the inclusion. Although strain stiffening in fibrin begins at 10% strain, strain amplification around microcarriers may cause substantial strain, and stiffness, gradients.

Our data show that cyclic strain can be used to produce directional capillary growth during angiogenesis without a diminishing the extent of network formation, which is encouraging from a tissue engineering perspective. It has already been established that the implantation of a pre-vascularized tissue improves the rate of anastomosis with the host vasculature [30], an important factor in the survival of large tissue implants. Pre-vascularization and alignment will be important in engineered metabolic tissues which require alignment to function properly, such as cardiac muscle tissue. As our understanding of the mechanical

environment surrounding cells undergoing complex morphogenetic programs improves, it will illuminate the engineering parameters necessary to create large, implantable tissues. Finally, we highlight an interaction between a tissue and a rigid boundary, providing insight into the interaction between implanted medical devices and the surrounding vasculature. In light of the modeling data presented here and the pronounced angiogenic response surrounding a microcarrier bead, understanding the mechanical environment surrounding an implant is necessary to effectively combat, or take advantage of, the host response.

3.5 References

[1] Peyton SR, Ghajar CM, Khatiwala CB, Putnam AJ. The emergence of ECM mechanics and cytoskeletal tension as important regulators of cell function. Cell Biochem Biophys 2007;47:300-20.

[2] Ingber DE. Mechanical signaling and the cellular response to extracellular matrix in angiogenesis and cardiovascular physiology. Circ Res 2002;91:877-87.

[3] Baker EL, Bonnecaze RT, Zaman MH. Extracellular matrix stiffness and architecture govern intracellular rheology in cancer. Biophys J 2009;97:1013-21.

[4] Lopez JI, Kang I, You WK, McDonald DM, Weaver VM. In situ force mapping of mammary gland transformation. Integr Biol (Camb) 2011;3:910-21.

[5] Malek AM, Alper SL, Izumo S. Hemodynamic shear stress and its role in atherosclerosis. JAMA 1999;282:2035-42.

[6] Cecchi E, Giglioli C, Valente S, Lazzeri C, Gensini GF, Abbate R, et al. Role of hemodynamic shear stress in cardiovascular disease. Atherosclerosis 2011;214:249-56.

[7] Jeong SI, Kwon JH, Lim JI, Cho SW, Jung Y, Sung WJ, et al. Mechano-active tissue engineering of vascular smooth muscle using pulsatile perfusion bioreactors and elastic PLCL scaffolds. Biomaterials 2005;26:1405-11.

[8] Yazdani SK, Tillman BW, Berry JL, Soker S, Geary RL. The fate of an endothelium layer after preconditioning. J Vasc Surg 2010;51:174-83.

[9] Thodeti CK, Matthews B, Ravi A, Mammoto A, Ghosh K, Bracha AL, et al. TRPV4 channels mediate cyclic strain-induced endothelial cell reorientation through integrin-to-integrin signaling. Circ Res 2009;104:1123-30.

[10] Korff T, Augustin HG. Tensional forces in fibrillar extracellular matrices control directional capillary sprouting. J Cell Sci 1999;112 (Pt 19):3249-58.

[11] Matsumoto T, Yung YC, Fischbach C, Kong HJ, Nakaoka R, Mooney DJ. Mechanical strain regulates endothelial cell patterning in vitro. Tissue Eng 2007;13:207-17.

[12] Nehls V, Drenckhahn D. A novel, microcarrier-based in vitro assay for rapid and reliable quantification of three-dimensional cell migration and angiogenesis. Microvasc Res 1995;50:311-22.

[13] Ghajar CM, Blevins KS, Hughes CC, George SC, Putnam AJ. Mesenchymal stem cells enhance angiogenesis in mechanically viable prevascularized tissues via early matrix metalloproteinase upregulation. Tissue engineering 2006;12:2875-88.

[14] Barbee KA, Macarak EJ, Thibault LE. Strain measurements in cultured vascular smooth muscle cells subjected to mechanical deformation. Ann Biomed Eng 1994;22:14-22.

[15] Lee AA, Delhaas T, Waldman LK, MacKenna DA, Villarreal FJ, McCulloch AD. An equibiaxial strain system for cultured cells. Am J Physiol 1996;271:C1400-8.

[16] Yung YC, Chae J, Buehler MJ, Hunter CP, Mooney DJ. Cyclic tensile strain triggers a sequence of autocrine and paracrine signaling to regulate angiogenic sprouting in human vascular cells. Proc Natl Acad Sci U S A 2009;106:15279-84.

[17] Krishnan L, Underwood CJ, Maas S, Ellis BJ, Kode TC, Hoying JB, et al. Effect of mechanical boundary conditions on orientation of angiogenic microvessels. Cardiovasc Res 2008;78:324-32.

[18] Newman AC, Nakatsu MN, Chou W, Gershon PD, Hughes CC. The requirement for fibroblasts in angiogenesis: fibroblast-derived matrix proteins are essential for endothelial cell lumen formation. Molecular biology of the cell 2011;22:3791-800.

[19] Kilarski WW, Samolov B, Petersson L, Kvanta A, Gerwins P. Biomechanical regulation of blood vessel growth during tissue vascularization. Nat Med 2009;15:657-64.

[20] Boerckel JD, Uhrig BA, Willett NJ, Huebsch N, Guldberg RE. Mechanical regulation of vascular growth and tissue regeneration in vivo. Proc Natl Acad Sci U S A 2011;108:E674-80.

[21] Kniazeva E, Putnam AJ. Endothelial cell traction and ECM density influence both capillary morphogenesis and maintenance in 3-D. American journal of physiology Cell physiology 2009;297:C179-87.

[22] Ghajar CM, Kachgal S, Kniazeva E, Mori H, Costes SV, George SC, et al. Mesenchymal cells stimulate capillary morphogenesis via distinct proteolytic mechanisms. Exp Cell Res 2010;316:813-25.

[23] Matsumoto T, Sasaki J, Alsberg E, Egusa H, Yatani H, Sohmura T. Three-dimensional cell and tissue patterning in a strained fibrin gel system. PLoS One 2007;2:e1211.

[24] Morin KT, Tranquillo RT. Guided sprouting from endothelial spheroids in fibrin gels aligned by magnetic fields and cell-induced gel compaction. Biomaterials 2011;32:6111-8.

[25] Kang H, Wen Q, Janmey PA, Tang JX, Conti E, MacKintosh FC. Nonlinear elasticity of stiff filament networks: strain stiffening, negative normal stress, and filament alignment in fibrin gels. J Phys Chem B 2009;113:3799-805.

[26] Tranquillo RT, Durrani MA, Moon AG. Tissue engineering science: consequences of cell traction force. Cytotechnology 1992;10:225-50.

[27] Kotlarchyk MA, Shreim SG, Alvarez-Elizondo MB, Estrada LC, Singh R, Valdevit L, et al. Concentration independent modulation of local micromechanics in a fibrin gel. PLoS One 2011;6:e20201.

[28] Mori D, David G, Humphrey JD, Moore JE, Jr. Stress distribution in a circular membrane with a central fixation. J Biomech Eng 2005;127:549-53.

[29] Balestrini JL, Skorinko JK, Hera A, Gaudette GR, Billiar KL. Applying controlled non-uniform deformation for in vitro studies of cell mechanobiology. Biomech Model Mechanobiol 2010;9:329-44.

[30] Chen X, Aledia AS, Ghajar CM, Griffith CK, Putnam AJ, Hughes CC, et al. Prevascularization of a fibrin-based tissue construct accelerates the formation of functional anastomosis with host vasculature. Tissue Eng Part A 2009;15:1363-71.

Chapter 4

Endothelial Response to Cyclic Strain is Unhindered by Modulation of Cell Traction Force

4.1 Introduction

Biological systems almost universally contain intricate patterns that help to optimize tissue function. For example, the lung is highly branched to maximize vascular surface area and promote gas exchange, and in cardiac muscle capillaries align parallel to the tissue mimicking its aligned conformation [1]. Although the presence of patterns is ubiquitous, how they are formed remains subject to debate. Morphogen gradients have been shown to be important in certain types of pattern formation, but they do not fully explain the complex patterns seen in many tissues [2].

Integrin connections link the cytoskeleton to the ECM, mechanically coupling the cell to its surroundings, and allowing the cell to be an active player in the force-balance between it and its microenvironment. Recently,

mechanical cues such as extracellular matrix (ECM) stiffness, cell-mediated traction forces, and strains applied to the ECM have been shown to influence cell migration [3, 4] and pattern formation [5-7], especially in the context of angiogenesis, and there is considerable evidence linking cytoskeletal dynamics to these phenomena [8]. The small GTPase RhoA is of particular significance as a regulator of cytoskeletal organization and traction force generation [9, 10] and it is known to modulate endothelial cell responses to shear stress during migration and angiogenesis [11, 12]. More broadly, however, endothelial cell traction force generation, regulated by RhoA and other participants in the pathway leading to actomyosin-generated traction force, are critical for robust angiogenesis [13].

Cells regulate their cytoskeletal conformation in response to changes in stiffness and applied forces [14]. In addition, they are believed to sense mechanical forces via their cytoskeletal components, and impairment of these structures impairs their mechanosensitivity [15, 16]. This effect is well-characterized in 2D but has not been studied as extensively in 3D systems, especially in the context of complex morphogenetic programs like angiogenesis. Although it has been suggested that angiogenic sprouting will follow contact guidance cues mediated by aligned collagen fibers [17], a role for cyclic stretch in fibrin gels, which align very little when subjected

to low magnitude strains, has not been definitively established [6, 18, 19].

By adapting a system originally developed by Nehls and Drenckhahn to recapitulate angiogenesis in fibrin gels [20], we have designed a bioreactor capable of applying cyclic strain to an in vitro model of angiogenesis. Previous studies using this system have shown that sprouts form parallel to the direction of strain, but the mechanism by which this occurs remains to be elucidated [6]. Here we explore the effects of cyclic strain on angiogenesis in the presence of multiple genetic and pharmacological modulators of cell traction force, specifically chosen to explore a pathway involved in regulating, sensing, and responding to cell-mediated and externally-imposed forces, to test the hypothesis that this pathway is involved in the persistent directional sprouting of angiogenic capillaries in the presence of cyclic strain.

4.2 Methods

4.2.1 Cell Culture

HUVECs were isolated from fresh umbilical cords as described previously [21]. In brief, cord veins were cannulated and residual blood was flushed out with sterile Dulbecco's phosphate buffered saline (DPBS, Gibco, Carlsbad, CA), then 0.1% collagenase type 1 (Worthington,

Lakewood, NJ) digestion was performed for 15 minutes at 37°C to release endothelial cells from the vessel wall. The vessel was again flushed with DPBS and the cell suspension was centrifuged, re-suspended in Endothelial Growth Medium 2 (EGM-2, Lonza, Walkersville, Maryland), and plated. Cells were washed with DPBS after 24 hours to remove residual erythrocytes. HUVECs were expanded to passage 2 and frozen. All microcarrier bead assays were performed with HUVECs at passage 3. Human aortic smooth muscle cells (HASMCs, Cascade Biologics, Portland, OR) were cultured in M231 supplemented with smooth muscle growth supplement (Life Technologies, Grand Island, NY). Medium was changed every other day. All cell culture was performed in a 37°C, 5% CO_2 incubator.

4.2.2 Modulation of Endothelial Cell Traction Force by Application of Cytoskeletal Inhibitors

Three drugs were chosen to inhibit cell traction force generation: Y27632 (EMD Millipore, Billerica, MA), which inhibits Rho-associated protein kinase (ROCK) activity and subsequently myosin light chain phosphorylation via ROCK; ML-7 (Sigma-Aldrich, St. Louis, MO), which inhibits myosin light chain kinase (MLCK) activity, and thus myosin light

chain phosphorylation via MLCK; and the myosin ATPase inhibitor 2,3-butanedione 2-Monoxime (BDM, Calbiochem). Concentrations used in angiogenesis experiments were as follows: Y27632 at 30 μM, ML-7 at 10 μM, BDM at 10 mM, chosen based on previous studies from our laboratory [13, 22].

4.2.3 Creation of RhoA Mutant Constructs and Transduction

The mutant RhoA and eGFP transgenes were subcloned from pcDNA3-EGFP-RhoA-Q63L (constitutively active form of RhoA, Addgene plasmid 12968), and pcDNA3-EGFP-RhoA-T19N (dominant negative form of RhoA, Addgene plasmid 12967). The transgenes were then inserted into the multiple cloning site of a tetracycline inducible backbone, TetO-FUW-MCS, derived from Addgene plasmid 20321 (TetO-FUW-OSKM) to construct the plasmids TetO-FUW-eGFP-RhoA-Q63L, TetO-FUW-eGFP-RhoA-T19N, and TetO-FUW-eGFP. HUVECs were transduced with the respective viruses at a multiplicity of infection of approximately 1.5 in the presence of 8 μg/ml Polybrene (EMD Millipore. Cat# TR-1003-G).

4.2.4 Pull-down Assay, SDS-PAGE, and Immunoblotting

HUVECs transduced with T19N and Q63L RhoA mutants, or the

eGFP control, were lysed on ice in modified RIPA buffer without SDS (50 mM Tris, pH 7.6, 150 mM NaCl, 10 mM $MgCl_2$, 1% TritonX-100, 1 mM PMSF, 10 μg/ml leupeptin, 10 μg/ml aprotinin, 1 mM $NaVO_4$, 0.5 μg/ml pepstatin A). Lysates were cleared by centrifugation and protein concentration was determined by bicinchoninic acid assay. To verify the activity of the RhoA mutants, pull-down assays were performed as follows. Equal masses of protein were incubated with 30 μg of Rhotekin-RBD Protein GST Beads (Cytoskeleton, Denver, CO) at 4 °C for 1 hour, collected by centrifugation and washed with lysis buffer. After the final wash the supernatant was aspirated, 25 μl Laemmli sample buffer was added to the bead slurry was heated to 95 °C for 10 minutes then run on a 16% polyacrylamide gel. Presence of total mutant protein was determined similarly, without the pull-down step. All samples were subjected to SDS-polyacrylamide gel electrophoresis after which protein was transferred to a PVDF membrane for immunoblotting. PVDF membranes were blocked with 5% BSA in Tris-buffered saline plus 0.1% Tween 20 (TBST) for 2 hours, followed by incubation with a mouse anti-human RhoA antibody in TBST containing 5% BSA for an additional 2 hours (Santa Cruz Biotechnology, Dallas, TX). After 6 10-minute washes, membranes were incubated with a donkey anti-mouse-IgG-HRP secondary antibody (Santa

Cruz Biotechnology, Dallas, TX) for 2 hours, washed as before, and detected via an enhanced chemiluminescence detection system. Quantification of immunoblots was performed using NIH ImageJ software.

4.2.5 Fibrin Tissue Construction and Application of Cyclic Strain

Fibrin tissues were constructed as previously described [6]. HUVECs were trypsinized, counted, and 4 x 10^6 were suspended with ten-thousand Cytodex® 3 microcarrier beads (Sigma-Aldrich, St. Louis, MO) in 5 ml of EGM-2 in an upright T-25 flask. The flask was gently agitated every 30 minutes. After 4 hours an additional 5 ml EGM-2 was added to the flask and the entire suspension was transferred to a fresh T-25 and incubated in normal cell culture position. The next day, 490 μl of fibrinogen (Sigma-Aldrich, St. Louis, MO) solution containing 100 microcarrier beads coated with the appropriately transduced, or non-transduced, HUVECs was combined with 10 μl 50 U/ml thrombin stock solution (Sigma-Aldrich, St. Louis, MO) and 63 μl of this solution was pipetted into each well of a PDMS multi-well plate. All gels were left at room temperature for 5 minutes to allow the beads to settle, then were cultured at 37°C for an additional 25 minutes to allow for complete gelation. After generation of the fibrin gel, HASMCs were trypsinized, counted, re-suspended in EGM-2, and 5,000

were added to the top of each fibrin gel. Within 30 minutes of plating, PDMS multi-well plates used in strained conditions were loaded onto linear stages and 10% strain was applied at 0.7 Hz. All fibrin tissues were cultured in a 37°C, 5% CO_2 incubator.

4.2.6 Quantification of Network Length and Sprout Angle

Quantification of total network length was performed as described previously [6, 21]. For each condition, vessels branching from at least 10 beads were traced using ImageJ software and averaged to determine total average network length. ImageJ software was also used to measure the acute angle of each sprout as it projected from the bead relative to the direction of applied strain (horizontal) to determine the angle at which capillaries sprouted from the bead. Angle measurements from each bead were averaged, followed by averaging of the results across at least 10 beads to determine the average sprout angle. For all quantifications, at least three independent experiments were performed.

4.2.7 Statistical Analysis

Statistical analysis was conducted with open source R software (www.r-project.org). The threshold for statistical significance was set at $p <$

0.05. Data are reported as mean ± 95% confidence interval.

4.3 Results

4.3.1 Transduced HUVECs Express RhoA Mutants

Western blots and pull-down assays were performed to verify that HUVECs transduced with RhoA mutants Q63L (constitutively active) and T19N (dominant negative) expressed the proteins in question and to verify their activity. Expression of all three constructs (including eGFP) was also verified by fluorescence microscopy (data not shown). Western blotting for RhoA indicated that in the presence of 100 ng/ml and 0 ng/ml doxycycline the Q63L-RhoA and T19N-RhoA constructs showed high and low levels of construct expression, respectively (Figure 4-1 A). Notably, both proteins showed a basal level of expression in the absence of doxycycline. Pull-down assays confirmed the activity of Q63L-RhoA and the presence of a basal level of expression of this construct (Figure 4-1 B). Activity levels of T19N-RhoA were below the levels of Q63L-RhoA in the 100 ng/ml and 0 ng/ml doxycycline conditions (Figure 4-1 B), despite comparable total expression levels, indicating that the T19N- RhoA mutant had low activity.

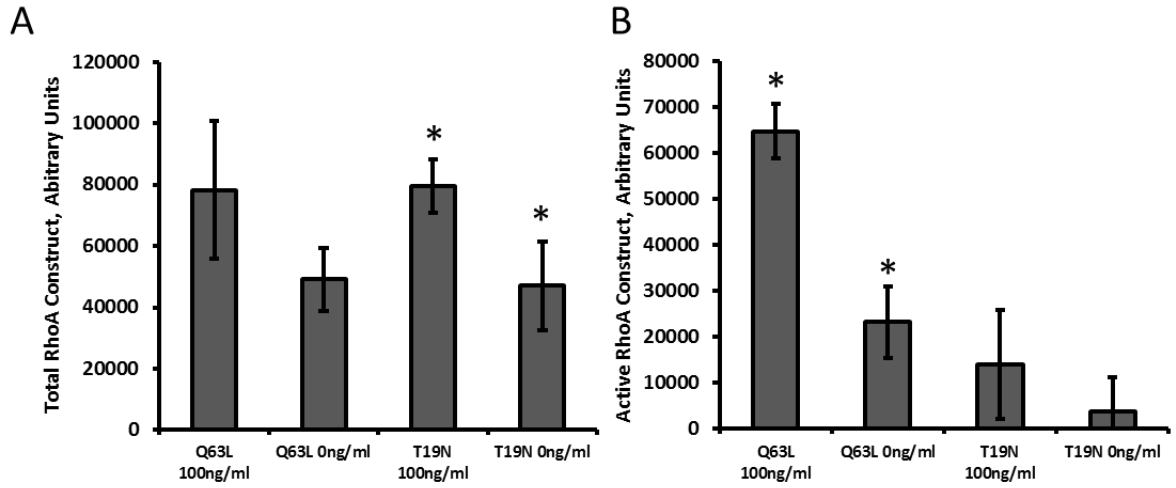

Figure 4-1. RhoA construct expression is modulated by doxycycline concentration. (A) Quantification of Western blots showing total Q63L-RhoA and T19N-RhoA construct in the presence of 100 ng/ml or 0 ng/ml doxycycline. Both constructs are expressed equally in the presence of equal concentrations of doxycycline, and both show decreased expression when doxycycline is not present. (B) Quantification of pull-down assay indicating the presence of GTP-bound constructs. When induced by doxycycline the RhoA-Q63L shows strong expression. A basal level of expression persists even in the absence of doxycycline. The T19N-RhoA construct shows a low level of activity in the presence of doxycycline and nearly zero activity in its absence. Conditions with * are statistically different from each other ($p < 0.05$). Data is reported as mean +/- S.E.M.

4.3.2 Presence of RhoA Mutants Affects Network Length but Not Capillary Alignment

Angiogenesis assays using transduced HUVECs coated onto microcarrier beads were performed to determine if altered RhoA activity in endothelial cells affected capillary network length or alignment in the presence of cyclic strain. In assays carried out to day 4 (Figure 4-2) and day 8 (Figure 4-3) the expression of either RhoA mutant led to a decrease in average network length relative to the eGFP control under both static and strained conditions. However, the application of cyclic strain did

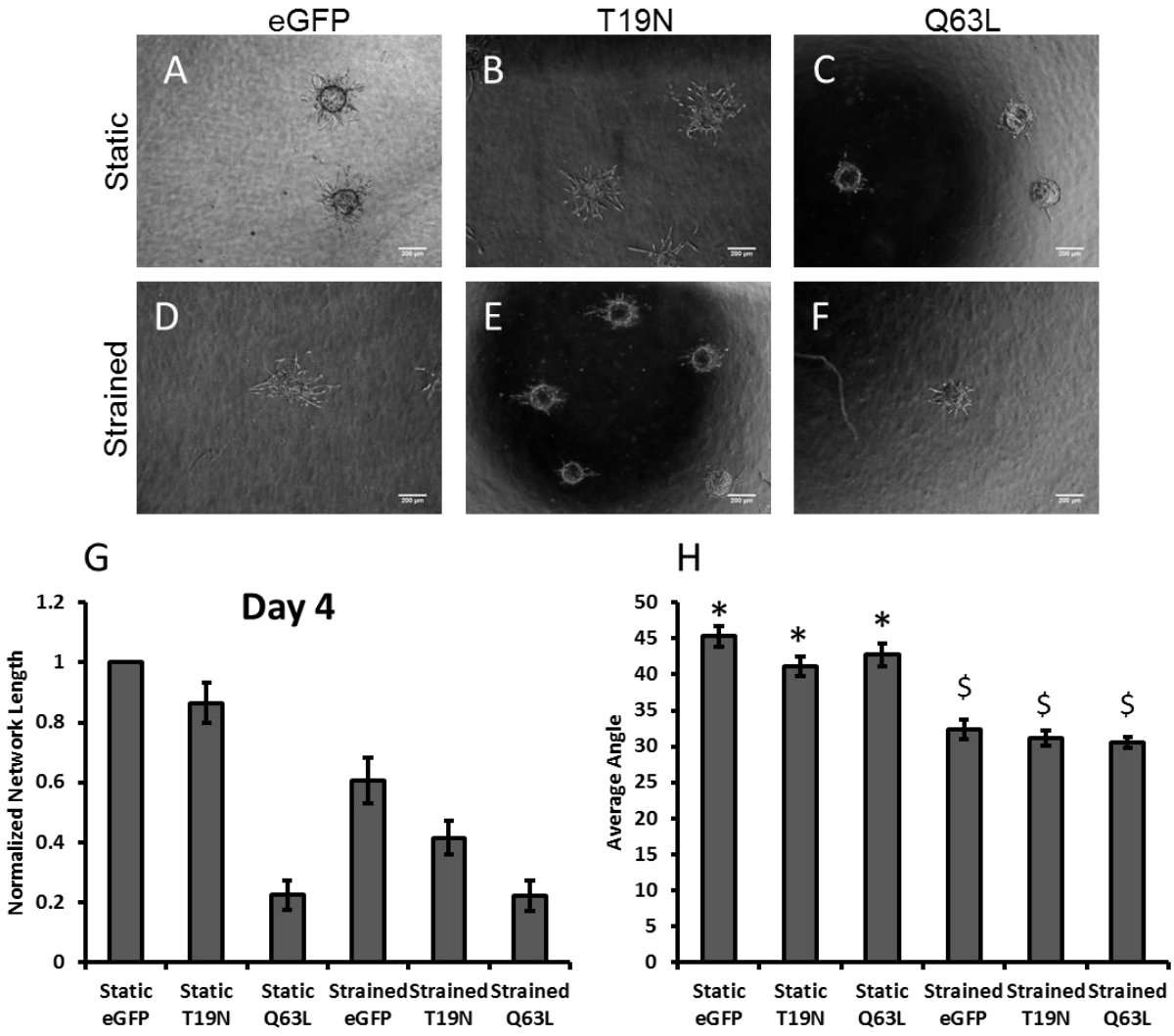

Figure 4-2. Presence of RhoA mutants affects network length but not directional sprouting at day 4. (A, D) eGFP transduced HUVECs at day 4, (B, E) T19N-RhoA transduced HUVECs at day 4, (C, F) Q63L-RhoA transduced HUVECs at day 4. (G) Presence of a RhoA mutant decreases the network length relative to eGFP control under both static and strained conditions. The magnitude of this decrease is greater for the Q63L-RhoA mutant. (H) The presence of either a RhoA mutant or the eGFP control has no effect on the directional biasing induced by cyclic strain. Columns with * are statistically different from corresponding condition with $ ($p < 0.05$). Data is reported as mean +/- S.E.M. Scale bars = 200 µm.

significantly reduce network length in both the control and T19N-RhoA conditions but not the Q63L-RhoA condition on both days.

Expression of the mutants had no effect on capillary alignment in the presence of cyclic strain. Static controls displayed radial outgrowth with average sprout angles of approximately 45 degrees at both day 4 (Figure 4-2 H) and day 8 (Figure 4-3 H). By contrast, growth of cyclically strained HUVECs was biased in the direction parallel to the applied strain and this bias was unaffected by the presence of either the constitutively active (Q63L) or dominant negative (T19N) RhoA mutants.

4.3.3 Pharmacological Inhibition of Cell Traction Force Affects Network Length but not Capillary Alignment

To modulate cell traction force, hydrogels were treated with the drugs BDM (an inhibitor of myosin ATPase), ML7 (an inhibitor of myosin light chain kinase), and Y27632 (an inhibitor of ROCK). Treatment with all of the drugs except for ML7 produced networks of similar length at day 4 (Figure 4-4 G) or eight (Figure 4-5 G). Interestingly, ML7 produced capillary networks of widely varying length that were, on average, longer than those produced in the presence of the other drugs. None of the drugs prevented the capillaries from aligning parallel to the cyclic strain at either

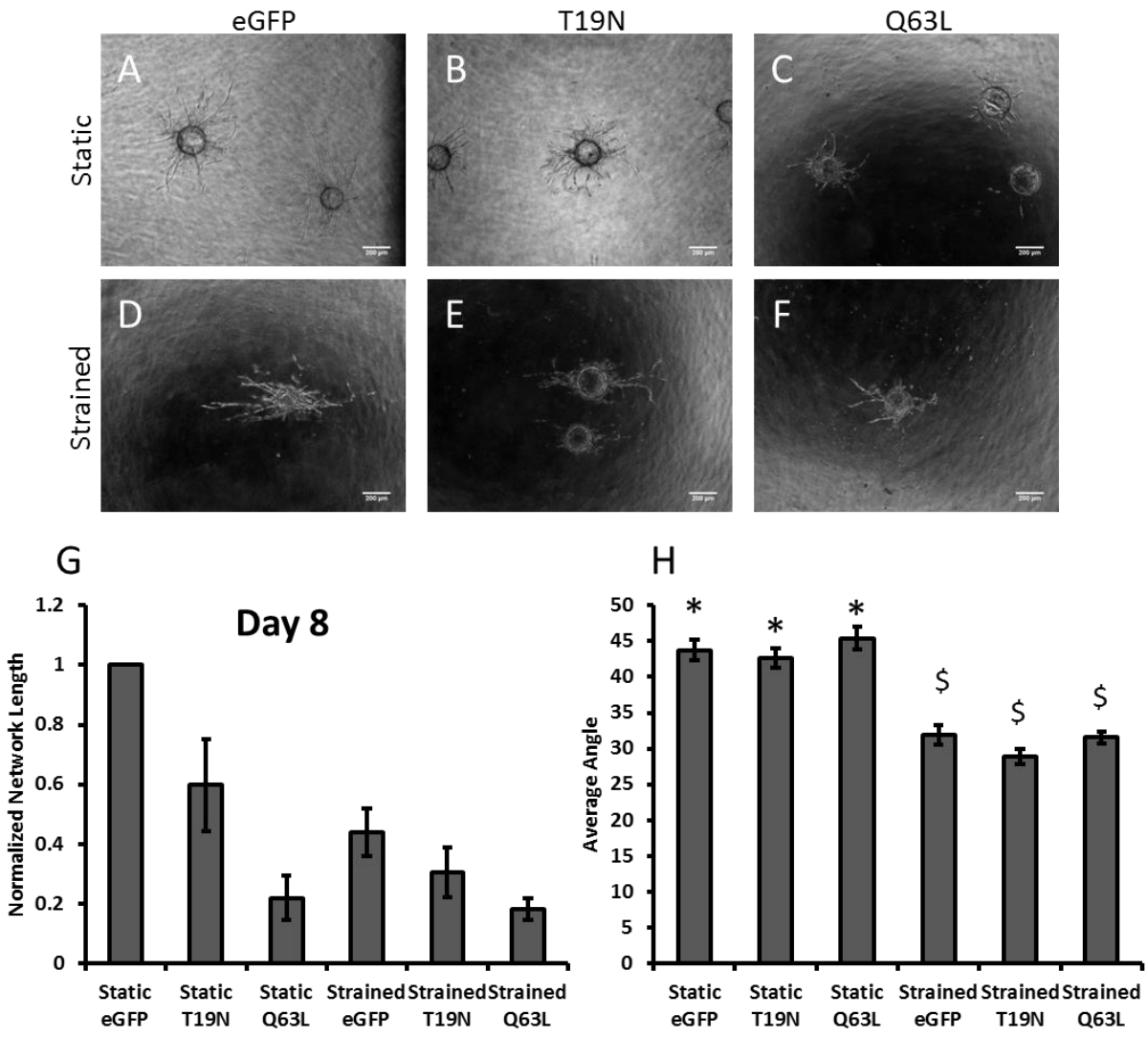

Figure 4-3. Presence of RhoA mutants affects network length but not directional sprouting at day 8. (A, D) eGFP transduced HUVECs at day 8, (B, E) T19N-RhoA transduced HUVECs at day 8, (C, F) Q63L-RhoA transduced HUVECs at day 8. (G) Presence of a RhoA mutant decreases the network length relative to eGFP control under both static and strained conditions. The magnitude of this decrease is greater for the Q63L-RhoA mutant. (H) The presence of either a RhoA mutant or the eGFP control has no effect on the directional biasing induced by cyclic strain. Columns with * are statistically different from corresponding condition with $ ($p < 0.05$). Data is reported as mean +/- S.E.M. Scale bars = 200 µm.

day 4 or 8 (Figure 4-4 H and Figure 4-5 H), indicating that the presence of these drugs does not prevent HUVECs from sensing their mechanical microenvironment despite inhibition of their ability to apply traction force.

4.4 Discussion

We have previously shown that HUVECs induced to undergo angiogenesis while being exposed to cyclic strain produce capillaries that are aligned parallel to that strain [6]. However, the mechanism that caused this effect remained unclear. We aimed to test the hypothesis that during angiogenesis, HUVECs used a RhoA-dependent mechanism to sense local forces and determine their direction of growth. This pathway is known to be involved in the generation of cytoskeletal pre-stress, which closely couples the strain state of the cell with that of the ECM [23]. Transduction with inducible dominant negative and constitutively active RhoA mutants allowed for modulation of RhoA activity, and thus the state of pre-stress, within the cultured HUVECs. We subsequently demonstrated that changes in RhoA activity had no effect on the alignment of our cultured HUVECs in the presence of cyclic strain, although significant decreases in network length were noted in the presence of both mutants. Despite reports

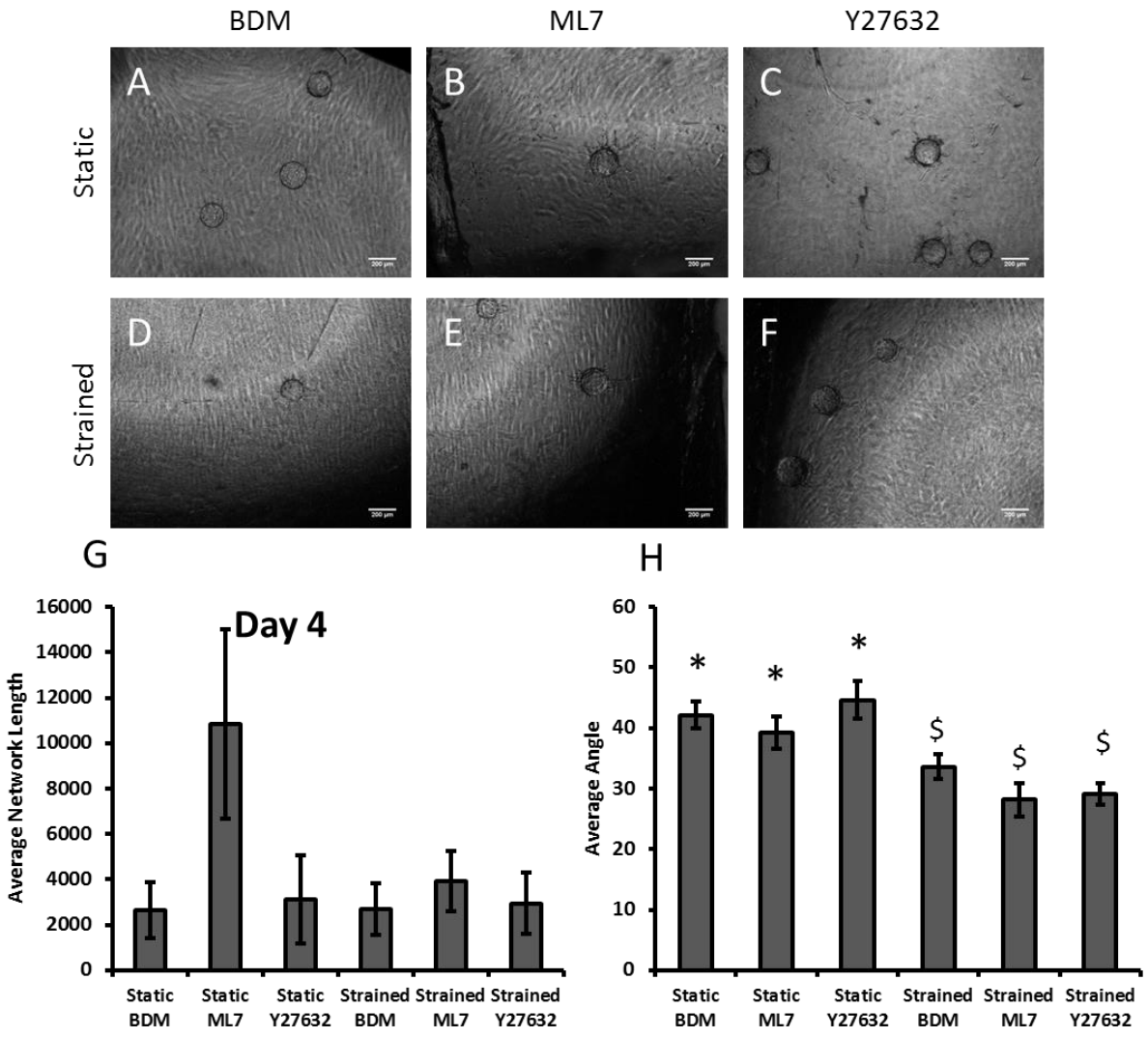

Figure 4-4. Modulation of cell traction force affects both network length and sprout angle. (A, D) HUVECs treated with BDM at day 4, (B, E) HUVECs treated with ML7 at day 4, (C, F) HUVECs treated with Y27632 at day 4. (G) Modulation of traction force produced no statistical differences between static controls and strained conditions treated with the same drug, indicating that strain neither counteracts nor amplifies the effects of drug treatment. (H) All strained networks have lower average sprout angles than their static controls, implying that the drugs did not affect their ability to align parallel to the applied strain. Columns with * are statistically different from corresponding condition with $ ($p < 0.05$). Data is reported as mean +/- S.E.M. Scale bars = 200 μm.

that ECs expressing constitutively active V14-RhoA exhibited increased angiogenic sprouting [24, 25], we believe that in this case the decreases in network length found in HUVECs expressing our constructs are due to leaky expression of the constructs as shown in Figure 1. In the case of the Q63L mutant, it appears that the levels of RhoA mutant generated by the construct is so great, even when not induced, that the traction force produced by the ECs goes beyond the pro-angiogenic optimum seen previously to an over-contractile, less angiogenic state.

This finding led us to expand our search to include three downstream effectors: ROCK, MLCK, and Myosin ATPase to better parse where, and if, this pathway sensed the applied strain. We observed varying levels of network formation in both static and strained tissues at both time points, as shown previously [6, 26], but presence of the drugs did not inhibit capillary alignment parallel to the direction of strain at either time point.

Neither Y27632 nor ML7 altered the alignment behavior of the angiogenic capillaries. ROCK is a known regulator of cell polarity [27] and is directly involved in traction force generation during cell migration [28], yet inhibition of this protein did not result in detectable changes in cell alignment in the presence of cyclic strain. This is not completely surprising because cases of aberrant increases in RhoA and ROCK activity, as in the

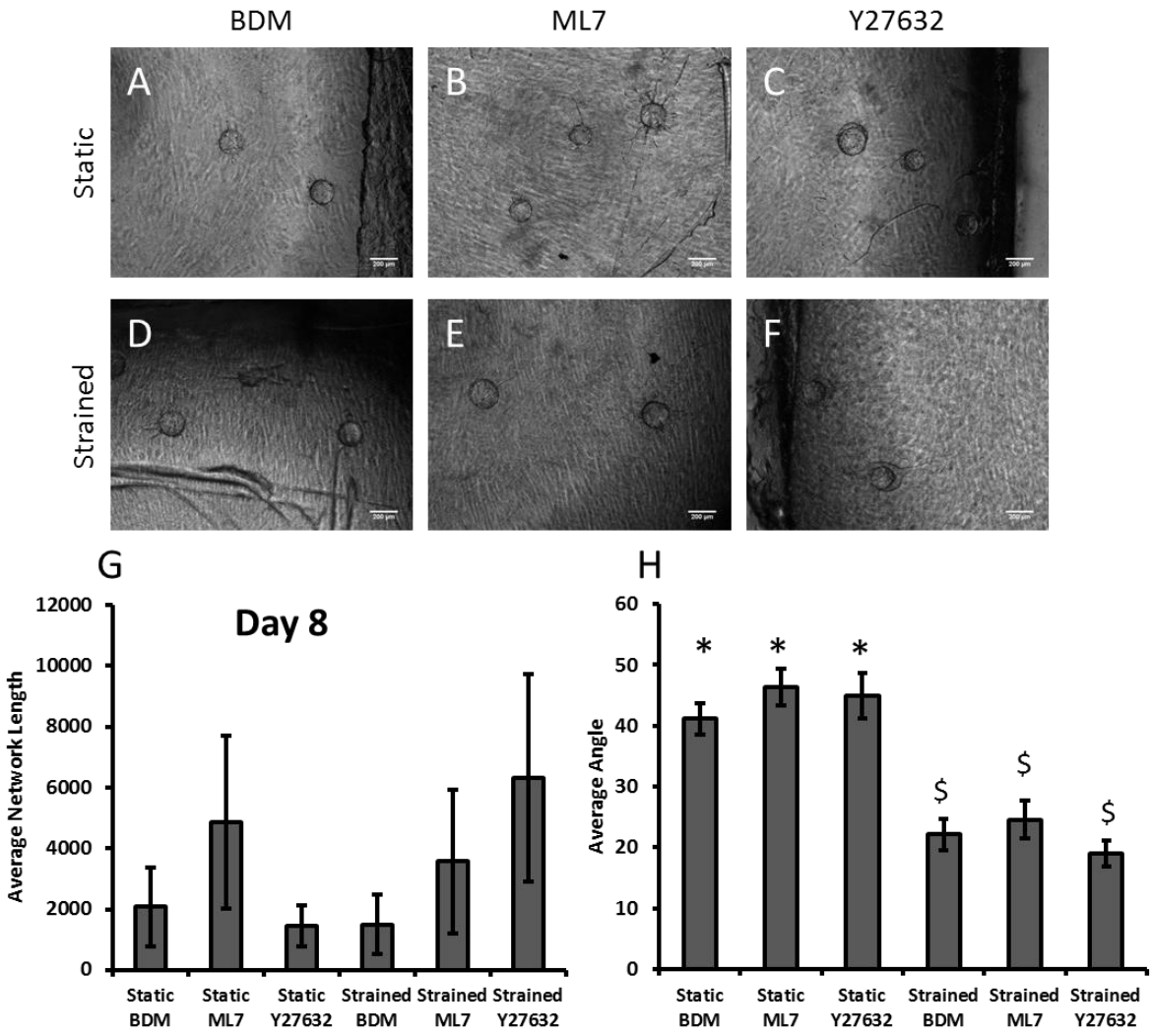

Figure 4-5 Modulation of cell traction force affects both network length and sprout angle. (A, D) HUVECs treated with BDM at day 8, (B, E) HUVECs treated with ML7 at day 8, (C, F) HUVECs treated with Y27632 at day 8. (G) Modulation of traction force produced no statistical differences between static controls and strained conditions treated with the same drug, indicating that strain neither counteracts nor amplifies the effects of drug treatment. (H) At day 8 all strained networks have lower means than their corresponding static controls, indicating alignment parallel to strain. Columns with * are statistically different from corresponding condition with $ ($p < 0.05$). Data is reported as mean +/- S.E.M. Scale bars = 200 µm.

tumor microenvironment, inhibition of ROCK can encourage normal responses to mechanical stimuli [29] and improve vessel function. Thus, sub-physiological ROCK activity may still allow the endothelial cells to polarize and migrate in response to mechanical cues. Also, strain is a known activator of the RhoA/ROCK pathway. While the application of an inhibitor may somewhat decrease this [30], it does not interfere with alignment in our system. Interestingly, application of ML7 and Y27632 to endothelial cells on 2D substrates has been shown to reverse the polarizing cue, causing stress fiber alignment parallel to the applied strain, rather than perpendicular as in the control cells [31]. By contrast, in 3D and while undergoing angiogenesis, our results show that HUVECs are robust to perturbations of their traction force generating pathways and consistently align parallel to the strain direction. Stress fibers in 3D matrices may play a lesser role than they appear to play in 2D, as evidenced by their lack of prominence in 3D matrices [32], and thus disruption of the signaling pathways controlling them may be less influential over directional cell migration.

Additionally, BDM, a myosin ATPase inhibitor, failed to prevent capillaries from aligning parallel to the strain direction. This suggests that myosin ATPase is not a direct mechanosensor and supports an alternative

hypothesis that traction force production and mechanosensing are controlled by different pathways in endothelial cells during angiogenesis. However, BDM is only a moderately specific myosin inhibitor, strongly inhibiting myosin II but not several other myosin isoforms [33]. It is also an inhibitor of calcium influx in muscle and non-muscle cells [34, 35]. These disadvantages indicate that the use of BDM should be complemented with alternative myosin inhibitor, such as blebbistatin, a drug capable of broader myosin inhibition [36], in future experiments.

Alternatively, the strain applied to our system may be overcoming the effects of cell traction force inhibition by tensing the cellular force transduction elements independently of actomyosin contractility. For example, actin stress fibers treated with the drugs used in this study most likely exhibit decreased levels of pre-stress, similarly to how cells under sudden compression display buckled actin stress fibers [37]. Normal levels of pre-stress were recovered after application of strain, and it is possible that the applied strain in our system similarly compensates for a lack of pre-stress in our capillary ECs. This could be tested by lowering the strain amplitude applied to the system to determine at what point the application of strain no longer induced capillaries to align in the presence and absence of myosin inhibition. Another possibility is that tension induced by

actomyosin contraction increases integrin-ECM bond strength, which has been shown to be enhanced by applied strains even in the presence of BDM [38]. Similarly, applied strain in our system may be compensating for the decrease in actomyosin-generated tension and overcoming any loss of mechanosensitivity due to inhibitory drugs.

4.5 References

[1] Bassingthwaighte JB, Yipintsoi T, Harvey RB. Microvasculature of the dog left ventricular myocardium. Microvasc Res 1974;7:229-49.

[2] Lander AD. Pattern, growth, and control. Cell 2011;144:955-69.

[3] Peyton SR, Putnam AJ. Extracellular matrix rigidity governs smooth muscle cell motility in a biphasic fashion. J Cell Physiol 2005;204:198-209.

[4] Zaman MH, Trapani LM, Sieminski AL, Mackellar D, Gong H, Kamm RD, et al. Migration of tumor cells in 3D matrices is governed by matrix stiffness along with cell-matrix adhesion and proteolysis. Proc Natl Acad Sci U S A 2006;103:10889-94.

[5] Ingber DE. Mechanical signaling and the cellular response to extracellular matrix in angiogenesis and cardiovascular physiology. Circ Res 2002;91:877-87.

[6] Ceccarelli J, Cheng A, Putnam AJ. Mechanical Strain Controls Endothelial Patterning During Angiogenic Sprouting. Cellular and Molecular Bioengineering 2012;5:463-73.

[7] Kilarski WW, Samolov B, Petersson L, Kvanta A, Gerwins P. Biomechanical regulation of blood vessel growth during tissue vascularization. Nat Med 2009;15:657-64.

[8] Mammoto A, Ingber DE. Cytoskeletal control of growth and cell fate switching. Curr Opin Cell Biol 2009;21:864-70.

[9] Hanley PJ, Xu Y, Kronlage M, Grobe K, Schon P, Song J, et al. Motorized RhoGAP myosin IXb (Myo9b) controls cell shape and motility. Proc Natl Acad Sci U S A 2010;107:12145-50.

[10] Provenzano PP, Keely PJ. Mechanical signaling through the cytoskeleton regulates cell proliferation by coordinated focal adhesion and Rho GTPase signaling. J Cell Sci 2011;124:1195-205.

[11] Shiu YT, Li S, Marganski WA, Usami S, Schwartz MA, Wang YL, et al. Rho mediates the shear-enhancement of endothelial cell migration and traction force generation. Biophys J 2004;86:2558-65.

[12] Song JW, Daubriac J, Tse JM, Bazou D, Munn LL. RhoA mediates flow-induced endothelial sprouting in a 3-D tissue analogue of angiogenesis. Lab Chip 2012;12:5000-6.

[13] Kniazeva E, Putnam AJ. Endothelial cell traction and ECM density influence both capillary morphogenesis and maintenance in 3-D. Am J Physiol Cell Physiol 2009;297:C179-87.

[14] Wang JH, Goldschmidt-Clermont P, Yin FC. Contractility affects stress fiber remodeling and reorientation of endothelial cells subjected to cyclic mechanical stretching. Ann Biomed Eng 2000;28:1165-71.

[15] Iba T, Sumpio BE. Morphological response of human endothelial cells subjected to cyclic strain in vitro. Microvasc Res 1991;42:245-54.

[16] Shirinsky VP, Antonov AS, Birukov KG, Sobolevsky AV, Romanov YA, Kabaeva NV, et al. Mechano-chemical control of human endothelium orientation and size. J Cell Biol 1989;109:331-9.

[17] Krishnan L, Underwood CJ, Maas S, Ellis BJ, Kode TC, Hoying JB, et al. Effect of mechanical boundary conditions on orientation of angiogenic microvessels. Cardiovasc Res 2008;78:324-32.

[18] Korff T, Augustin HG. Tensional forces in fibrillar extracellular matrices control directional capillary sprouting. J Cell Sci 1999;112 (Pt 19):3249-58.

[19] Matsumoto T, Yung YC, Fischbach C, Kong HJ, Nakaoka R, Mooney DJ. Mechanical strain regulates endothelial cell patterning in vitro. Tissue Eng 2007;13:207-17.

[20] Nehls V, Drenckhahn D. A novel, microcarrier-based in vitro assay for rapid and reliable quantification of three-dimensional cell migration and angiogenesis. Microvasc Res 1995;50:311-22.

[21] Ghajar CM, Blevins KS, Hughes CC, George SC, Putnam AJ. Mesenchymal stem cells enhance angiogenesis in mechanically viable prevascularized tissues via early matrix metalloproteinase upregulation. Tissue Eng 2006;12:2875-88.

[22] Kniazeva E, Weidling JW, Singh R, Botvinick EL, Digman MA, Gratton E, et al. Quantification of local matrix deformations and mechanical properties during capillary morphogenesis in 3D. Integr Biol (Camb) 2012;4:431-9.

[23] Chiquet M, Renedo AS, Huber F, Flück M. How do fibroblasts translate mechanical signals into changes in extracellular matrix production? Matrix biology 2003;22:73-80.

[24] Hoang MV, Whelan MC, Senger DR. Rho activity critically and selectively regulates endothelial cell organization during angiogenesis. Proc Natl Acad Sci U S A 2004;101:1874-9.

[25] Kniazeva E, Weidling JW, Singh R, Botvinick EL, Digman MA, Gratton E, et al. Quantification of local matrix deformations and mechanical properties during capillary morphogenesis in 3D. Integr Biol (Camb) 2012;4:431-9.

[26] Kniazeva E, Putnam AJ. Endothelial cell traction and ECM density influence both capillary morphogenesis and maintenance in 3-D. Am J Physiol Cell Physiol 2009;297:C179-87.

[27] Daley WP, Gervais EM, Centanni SW, Gulfo KM, Nelson DA, Larsen M. ROCK1-directed basement membrane positioning coordinates epithelial tissue polarity. Development 2012;139:411-22.

[28] Lamalice L, Le Boeuf F, Huot J. Endothelial cell migration during angiogenesis. Circ Res 2007;100:782-94.

[29] Ghosh K, Thodeti CK, Dudley AC, Mammoto A, Klagsbrun M, Ingber DE. Tumor-derived endothelial cells exhibit aberrant Rho-mediated mechanosensing and abnormal angiogenesis in vitro. Proc Natl Acad Sci U S A 2008;105:11305-10.

[30] Teramura T, Takehara T, Onodera Y, Nakagawa K, Hamanishi C, Fukuda K. Mechanical stimulation of cyclic tensile strain induces reduction of pluripotent related gene expressions via activation of Rho/ROCK and subsequent decreasing of AKT phosphorylation in human induced pluripotent stem cells. Biochem Biophys Res Commun 2012;417:836-41.

[31] Lee CF, Haase C, Deguchi S, Kaunas R. Cyclic stretch-induced stress fiber dynamics - dependence on strain rate, Rho-kinase and MLCK. Biochem Biophys Res Commun 2010;401:344-9.

[32] Hakkinen KM, Harunaga JS, Doyle AD, Yamada KM. Direct comparisons of the morphology, migration, cell adhesions, and actin cytoskeleton of fibroblasts in four different three-dimensional extracellular matrices. Tissue Eng Part A 2011;17:713-24.

[33] Ostap EM. 2,3-Butanedione monoxime (BDM) as a myosin inhibitor. J Muscle Res Cell Motil 2002;23:305-8.

[34] Sellin LC, McArdle JJ. Multiple effects of 2,3-butanedione monoxime. Pharmacol Toxicol 1994;74:305-13.

[35] Zhu Y, Ikeda SR. 2,3-butanedione monoxime blockade of Ca2+ currents in adult rat sympathetic neurons does not involve 'chemical phosphatase' activity. Neurosci Lett 1993;155:24-8.

[36] Limouze J, Straight AF, Mitchison T, Sellers JR. Specificity of blebbistatin, an inhibitor of myosin II. J Muscle Res Cell Motil 2004;25:337-41.

[37] Lu L, Feng Y, Hucker WJ, Oswald SJ, Longmore GD, Yin FC. Actin stress fiber pre-extension in human aortic endothelial cells. Cell Motil Cytoskeleton 2008;65:281-94.

[38] Friedland JC, Lee MH, Boettiger D. Mechanically activated integrin switch controls alpha5beta1 function. Science 2009;323:642-4.

Chapter 5

Conclusions and Future Directions

5.1 Contributions of This Dissertation

This work has demonstrated that the application of cyclic strain causes capillaries formed during angiogenesis to form parallel to the applied strain. It has also demonstrated that this alignment is robust to treatments known to modulate the ability of endothelial cells to apply traction to their surroundings. Three specific aims were addressed to formulate these conclusions.

Specific Aim 1

Build and characterize a bioreactor to apply cyclic strain to hydrogels.

Specific Aim 2

Study the effects of strain on angiogenesis

Specific Aim 3

Understand how the interplay between cellular traction force and cyclic strain affects angiogenesis

One cell culture platform and two devices were created to support the completion of these aims. The cell culture platform was created from PDMS, a biocompatible silicone elastomer commonly used in microfluidic applications for cell culture. Static and cyclic strains were applied to this platform using either of two devices. The first of these can be mounted on a microscope stage for visualization of the ECM under load, and the second can apply cyclic or static strains to the PDMS platform under cell-culture conditions. Using these devices, it was demonstrated that angiogenesis occurs parallel to the direction of applied strain and that the alignment is reversible if subsequent culture is performed at 0% strain. It was also discovered that cell-mediated remodeling of the ECM was not a significant factor in capillary alignment and that ECM alignment was modest under 10% applied strain. Modulation of a mechanosensitive biochemical pathway involving RhoA, ROCK, MLCK, and myosin ATPase revealed that inhibition of this pathway does not diminish the directional response to applied strain.

5.2 Expanded Summary

Fulfillment of Specific Aim 1 required the development of 2 devices capable of applying strain to a PDMS multi-well plate. Validation of the

PDMS platform required designing a device for the application of static strain: a microscope stage-insert containing a clamp and micrometer for applying precise strain to the PDMS culture plate. This allowed hydrogels within the plate to be visualized while under strain. Lagrangian finite strain analysis performed on 1 μm fluorescent beads embedded in the fibrin gel revealed a linear relationship between the applied strain and the strain present in the fibrin gel up to an applied strain of 12%. The second device, used for cell culture, consists of a motorized linear stage with a clamping mechanism that can hold up to two PDMS multi-well plates. It can apply a large enough force to deform the PDMS to 10% strain in repeated cycles lasting for weeks, and if necessary can apply even greater strains. The stage can also be left running in a standard cell culture incubator (100% humidity, 5% CO_2, and temperature of 37 °C) during this time period, as it was during all experiments. This platform has shown itself to be extremely robust, requiring minimal maintenance despite heavy use over the course of nearly 5 years.

Fulfillment of Specific Aim 2 required the use of the 3D cell culture platform to study the effects of cyclic strain on an in vitro model of angiogenesis. This model consisted of a fibrin gel containing HUVECs attached to microcarrier beads. The HUVECs were supported by factors

excreted from smooth muscle cells cultured on the top of the fibrin gels, providing physical separation of the two cell types but still allowing cross-talk via diffusion of soluble factors. We successfully showed that cyclic strain did not negatively impact capillary network formation, an important observation due to the possibility of having to mechanically condition engineered tissues prior to implantation into patients. We have also demonstrated that cyclic strain can be used to exert control over the direction of capillary formation during angiogenesis. Capillaries cultured under cyclic strain in our system grow parallel to the direction of strain; if the strain is removed, they will begin growing in a random orientation even after the pre-establishment of an aligned network. These findings provide a foundation for improved control over engineered tissue architecture that will be essential for developing large and complex organs in vitro.

Attempts to ascertain a mechanism for the observed alignment ruled out causes based on ECM architecture. Direct visualization of the fibrin matrix via confocal reflectance microscopy showed that fiber alignment was minimal, suggesting that the presence of a contact guidance cue generated by the applied strain was not responsible for the observed alignment. However, finite element modeling of the system presented the basis for a hypothesis: straining fibrin at low strain (10%) may induce small strain

gradients in the fibrin matrix, which could in turn cause stiffness gradients in the matrix, and provide increased resistance to traction in the direction of applied strain. The endothelial cells may be sensing these gradients and following the stiffer regions of the gel. This hypothesis provided the basis for the study of a pathway known to regulate cell traction force in an effort to understand how the endothelial cells were biochemically responding to the strain and how this might affect their ability to respond by aligning the capillaries they formed.

Fulfillment of Specific Aim 3 required the addition of several factors that influence a signaling pathway controlling cell traction force generation. The first were mutant genetic constructs of a small GTP-binding protein, RhoA, known to be influential in cytoskeletal rearrangement, cell polarization, and traction force generation. HUVECs transduced with either the constitutively active or dominant negative forms of these genes displayed decreased network length compared to a vector control but still aligned parallel to applied strain. This refuted the hypothesis that changes in the levels of active RhoA were mediating the alignment response and led to a broader analysis of a pathway involved in myosin-based traction force generation. Three candidate proteins - ROCK, MLCK, and myosin ATPase - were inhibited via a battery of drugs in an effort to understand how

inhibition of cell traction force generation would affect alignment. In nearly all cases, pharmacologic inhibition of traction force caused the capillaries to be extremely short (HUVECs treated with ML7 displayed longer but widely variable network lengths) but had no effect on the HUVEC's ability to align parallel to the applied strain. Similarly, inhibition of myosin ATPase by BDM drastically shortened the total network length produced by the HUVECs and did not prevent the capillaries from aligning parallel to the applied strain.

5.2 Future Directions

The observations made in this thesis opened up several avenues for additional research. In addition, the experimental setup can be improved to increase throughput and make the device easier to use.

We have shown that aligned capillary networks formed under cyclic strain will randomize their growth direction when strain is ceased and they are cultured statically, but it is unclear how they may respond to alternative strain regimens. The observation that strain can align capillaries implies the possibility of finer control over capillary direction via the application of strain at different angles over the course of an experiment. The simplest of these would be the application of strain in one direction followed by

application of strain in the direction perpendicular, ideally providing a stark contrast between the capillary networks before and after the change in strain direction. Such experiments were not possible in the scope of this thesis due to the rectangular shape of the devices designed (the device was not wide enough to fit into the clamps if rotated 90°). However, a simple re-design of the mold could make it fit in multiple configurations. Eventually this technique could be expanded to form more complex shapes by using multiple stretch directions in series.

The reason for the use of a rectangular mold was throughput: two devices could be clamped onto each linear stage. However, although each PDMS multi-well plate contained 4 wells, for a total of 8 on each linear stage, throughput was often an issue when various strain regimens were being tested because both devices in a given linear stage experience an identical strain regimen. This problem will be compounded if wider devices are produced because only 1 will be able to fit into the stage. There are several solutions to this problem. First, shorter time points can be selected. Although it takes 3-4 days for bona fide capillaries to form, sprout direction can be determined in only 1-2 days and experiments with multiple strain regimens can thus be completed in 2-4 days. The clamps can also be

widened to accommodate more devices, especially for experiments studying the effects of two or more different strain regimens in series.

Another, less expected throughput limitation was the size and number of wells. Because of the difficulty in distributing beads in such a small well, all four wells of each device were often used for a given condition. This could be problematic if multiple cell types, drugs, or genetic manipulations are used in strain experiments. The simplest fix for this would be to lengthen the devices. The linear stage can easily accommodate devices of over twice the length of those used in these studies, potentially doubling or even tripling the number of wells. Additionally, widening the clamp to accommodate more devices would alleviate this issue [1].

One of the biggest limitations of the experiments presented here is the exploration of only 2 strain regimens. This was done for consistency and simplicity, but should be expanded on in future research. Capillaries in vivo are generally shielded from the strong pulsatile flow experienced by larger vessels but do experience strains from neighboring cells during wound healing. It would be interesting to test their response to a very low, continuous strain rate like they might experience as myofibroblasts contract a wound at the earliest stages of repair. This could take the form of a low frequency cyclic strain or of a continuous, slow, unidirectional strain for

several days during capillary formation. The latter of these would more closely simulate the gradual straining of tissue during wound healing and may lend insight into the wound revascularization process.

From a tissue engineering perspective, control of pattern formation is critical, but it is unknown how different strain regimens than the two we have tested will affect capillary network alignment. HUVECs whose traction force generating machinery was altered were remarkable in that their ability to align parallel to the strain was unperturbed. However, alternative strain regimens may attenuate or enhance this response. Both the frequency and amplitude of the strain can be modulated to test if the response is mediated by the magnitude of the strain or its rate. Most likely, moderate values of amplitude and frequency will yield the greatest response and other regimens weaker responses, revealing a biphasic relationship. In addition, the effects of strain rate and amplitude on network length are equally ambiguous. The suggested experiments would allow an investigation of how these factors affect network length as well.

We have also put forth the hypothesis that cyclic strain induces the fibrin matrix to locally stiffen surrounding a microcarrier bead, or possibly even the capillary tip itself, and present a stiffness gradient that the cells may follow. This hypothesis was supported by a finite element model of

the system in question but validation of this model was not possible within the scope of this work. It would require the measurement of individual fibrin fibers at various locations throughout the matrix using highly specialized equipment to build a map of matrix stiffness around a microcarrier bead or around a sprouting capillary. Laser tweezers microrheology is the ideal method for such measurements because it can produce a micron-scale resolution map. Building a stiffness map of the fibrin gel could elucidate differences in how the stiffness profile of the ECM is changed by invading capillaries exposed to strain as opposed to those that are not.

The device presented here is capable of supporting many hydrogel formulations and cell types, and this work should be expanded using both. Endothelial progenitor cells are easily obtainable from adult blood and represent a clinically relevant cell type for future cell therapies [2]. However, it must be determined if they respond similarly to strain as the HUVECs used in these studies. Additionally, although aortic smooth muscle cells were used to support angiogenesis here, mesenchymal stem cells from bone marrow or isolated from blood represent the more likely clinical option, and thus their ability to support angiogenesis under cyclic strain must be investigated to validate their use in tissue engineering systems that must undergo cyclic strain. Additionally, tissue-specific cell

types may also be tested. Cells in the lung undergo consistent cyclic stretch very similar to that tested here, and it would be advisable to test engineered lung tissue under cyclic strain in 3D using this device.

Rather than leading to a dead end, the ability of capillary networks to align in the presence of traction force inhibition hints at the possibility of new mechanosensitive pathways that may be active during angiogenesis. Cadherin-mediated contacts are critically important for endothelial cells because of the continuous monolayer they create to line the interior of blood vessels. These are known to mechanically couple the cells and may thus provide a means of communication between them [3]. VE-cadherin is also known to interact with fibrin directly [4-6] and could be a possible candidate for transducing mechanical forces to endothelial cells during angiogenesis. Blocking antibodies could be used to impair this interaction by blocking the beta15-42 region of fibrin, rather than blocking the activity of VE-cadherin. This would prevent circumvent the possibility of a blocking antibody disrupting the cell-cell contacts present in growing capillaries, ideally allowing angiogenesis to occur unabated. Alternatively, recombinant fibrin could also be used to test this hypothesis. Point mutations could be introduced that prevent various integrins or VE-cadherin

from binding fibrin and thus block mechanotransduction through this pathway, again without significant disruption to angiogenesis.

The final avenue that could be exploited to understand how HUVECs are responding to cyclic strain is by viewing them in real-time. Building a microscope stage-mounted strain device and environmental chamber would allow for cell culture to be performed under cyclic strain with periodic, automated stoppage and imaging. This method would greatly simplify the study of how changes in strain regimen affect the reaction of the capillary network. In addition, drugs could be added to pre-formed networks and their changes could be monitored in a similar fashion. It is still unclear whether capillaries that initially grew in a random orientation will align in the presence of strain, and real-time monitoring would be an ideal way to test this.

We have demonstrated that angiogenic sprouting can be patterned via the application of cyclic strain and that this response is robust to perturbation by a host of pharmacologic and genetic manipulations. A deeper understanding of the relationship between cells and the ECM will lay the foundation for the greater control of complex morphogenetic processes, including angiogenesis. The work presented here represents a

step toward the generation of vascularized engineered tissues and the development of implantable whole organs.

5.4 References

[1] Yung YC, Vandenburgh H, Mooney DJ. Cellular strain assessment tool (CSAT): precision-controlled cyclic uniaxial tensile loading. J Biomech 2009;42:178-82.

[2] Melero-Martin JM, De Obaldia ME, Kang SY, Khan ZA, Yuan L, Oettgen P, et al. Engineering robust and functional vascular networks in vivo with human adult and cord blood-derived progenitor cells. Circ Res 2008;103:194-202.

[3] Borghi N, Sorokina M, Shcherbakova OG, Weis WI, Pruitt BL, Nelson WJ, et al. E-cadherin is under constitutive actomyosin-generated tension that is increased at cell–cell contacts upon externally applied stretch. Proceedings of the National Academy of Sciences 2012;109:12568-73.

[4] Bach TL, Barsigian C, Yaen CH, Martinez J. Endothelial cell VE-cadherin functions as a receptor for the beta15-42 sequence of fibrin. J Biol Chem 1998;273:30719-28.

[5] Martinez J, Ferber A, Bach TL, Yaen CH. Interaction of fibrin with VE-cadherin. Ann N Y Acad Sci 2001;936:386-405.

[6] Yakovlev S, Medved L. Interaction of fibrin(ogen) with the endothelial cell receptor VE-cadherin: localization of the fibrin-binding site within the third extracellular VE-cadherin domain. Biochemistry 2009;48:5171-9.

Appendix 1 : Production of PDMS Multi-well Plates

Materials

- Polydimethylsiloxane (PDMS) and cross-linker (Sylgard 184 kit)
- Teflon mold
- Binder clips
- Surgical tubing (Tygon, ADF00001)
- Polyester Film Tape (3M, UPC# 00021200393273)
- Oven set to 60-70 °C
- X-Acto knife
- Forceps
- Plastic knife
- Plastic cup
- Vacuum desiccator
- Vacuum pump

Protocol

<u>PDMS precursor preparation</u>

- Dispense PDMS into disposable plastic cup
- Pour cross-linker into cup at 1 part crosslinker for 10 parts PDMS
    - You will need 16-18 g PDMS/cross-linker mixture to fill 1 mold
- Stir PDMS and cross-linker using plastic knife until the mixture is white and completely opaque with tiny bubbles. This ensures good mixing
- Place PDMS-filled cup into vacuum desiccator and draw a vacuum
    - The bubbles in the mixture will expand and the volume will increase dramatically. Be careful not to spill!
- Leave in desiccator until all bubbles have disappeared (30-60 minutes)

Mold preparation

- Clean any residual PDMS off of Teflon molds
- Using the tape, cut tiny rectangles and place them on the top of the pillars in the bottom piece of the mold
    - THIS IS CRITICAL! Without the tape the surface of the PDMS at these locations will not be transparent
- Thread the surgical tubing through the holes in the bottom piece
- Place the top and bottom pieces together and clamp them with the binder clips, leaving the input holes clear

Pouring the molds

- Pour PDMS carefully into one of the holes of the mold
    - You should be able to see the PDMS as it fills the mold by looking into the other hole
- Once the mold is full, place it into the oven at 60 °C for at least 90 minutes
    - Do not pour the mold so full that the PDMS makes contact with the top surface. This will make the device prone to ripping during strain experiments and it will make the bottom opaque

Removing the PDMS from the mold

- Using the X-Acto knife, pry the two mold pieces apart
- Remove the tubing from the mold and PDMS
- Carefully pry the PDMS out of the mold
- Examine the wells of the PDMS piece and remove any tape that is present
- Replace the tape on the mold with fresh tape
- The long holes in the PDMS should then be plugged with PDMS and left in the hood for 1 hour

Appendix 2 : Care and use of the linear stage

The linear stage is a product of Newmark Systems (www.newmarksystems.com) and uses a custom software package called “Quickmotion” to control it. The device consists of three parts: the linear stage itself, the lid, and the controller. The linear stage is connected to the controller via two cords that plug into the “motor” and “signals” ports on the stage. They have corresponding ports on the controller. The controller has additional ports: power, which connects the power cable, and the RS-232 port, which connects to a computer. I have attached the RS-232 port to another cable, an RS-232 to USB cable, so that computers without an RS-232 port can access the controller.

Figure A-1 contains a picture of the software interface provided by Quickmotion. It allows you to set the position of the clamp, set a “zero” position, and set positions relative to the zero. The red circle next to the word “Connected” will turn green when the device is connected to a computer. It is recommended to connect the device to your computer first, and then start the software. Clicking on the “Virtual Joystick” box brings up the dialogue in Figure A-2. The Virtual Joystick is used to program

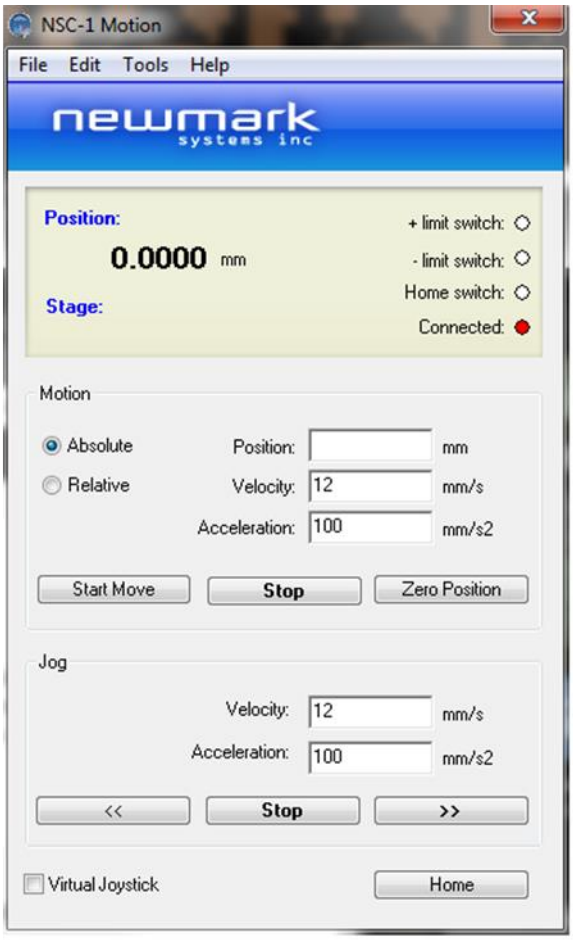

Figure A-1. Quickmotion interface

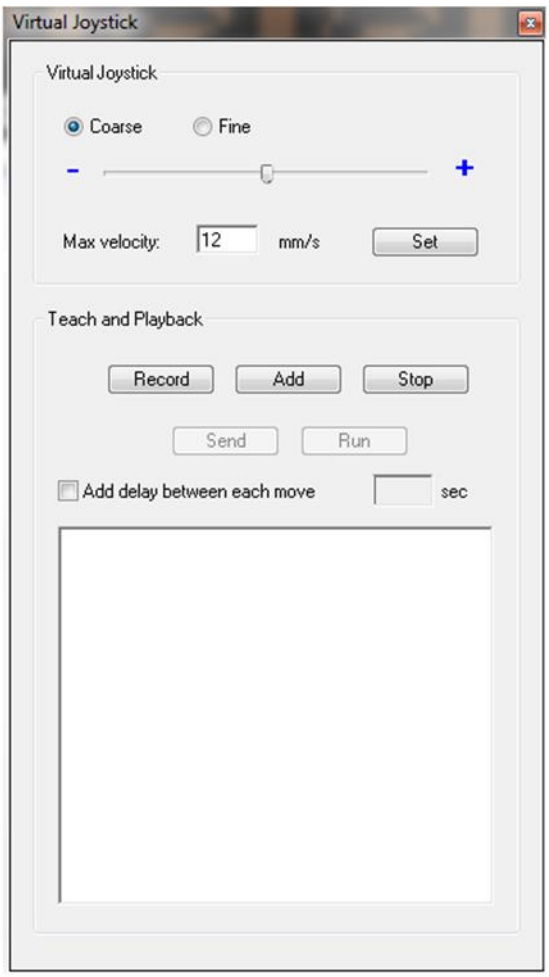

Figure A-2. Virtual Joystick interface

commands into the controller and drive the device. The “Record” function can also be used in conjunction with the standard interface to record motions that you input. It can then play those back if a particular sequence of movements is desired. The program also allows the user to save and load protocols for the stage to follow. In the “Tools” menu, click “Program Editor” to bring up the editor dialogue, as shown in Figure A-3. Attempts to program the stage using this dialogue have not been successful. To open

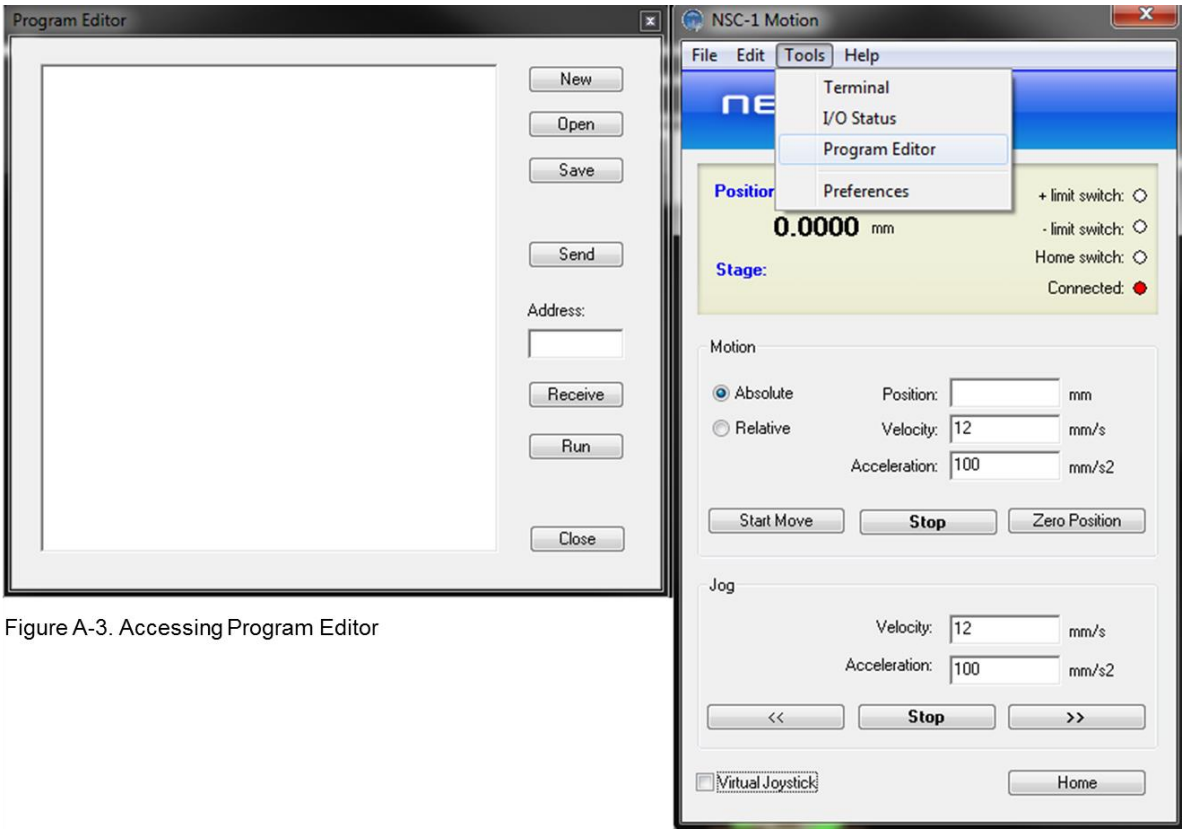

Figure A-3. Accessing Program Editor

a saved program click “Open” and select the program of interest. It will be displayed in the box on the left, as in Figure A-4. To program in a stretch protocol a particular sequence of buttons must be clicked, because I do not know how to do it any other way. First, the “Virtual Joystick” dialogue must be open. Then, click the “Record” button, then the “Stop” button. This will activate the “Send” and “Run” buttons. Copy the program of interest into the dialogue box as shown in figure A-5, then click “Send” and “Run.” The device should begin running the protocol.

The linear stage requires little maintenance, but some things are required to keep it functional. First, the screws are prone to rusting and

should be cleaned using a Dremel tool. This is required about once every 6 months. The Dremel tool has a wire brush head that is ideal for this. Wear safety goggles and perform cleaning far from other people to protect them from debris. Second, the lead screw in the stage requires greasing about once every 6 months. If a grinding noise is noticed, this indicates that it should be greased. Using the Allen wrenches in lab, take the device apart and apply the grease directly to the lead screw. Run the stage back and forth over the entire length of the screw to fully lubricate it. The grinding noise should disappear. Reassemble the stage and it will be ready for use.

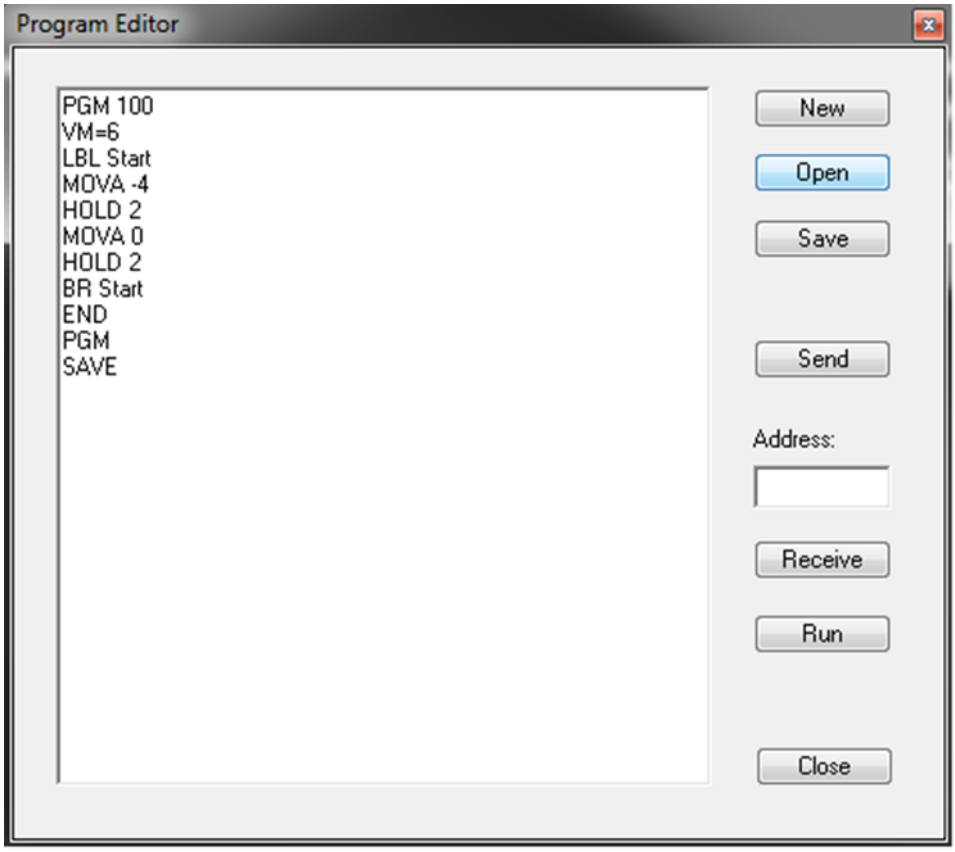

Figure A-4. Program Editor Dialogue

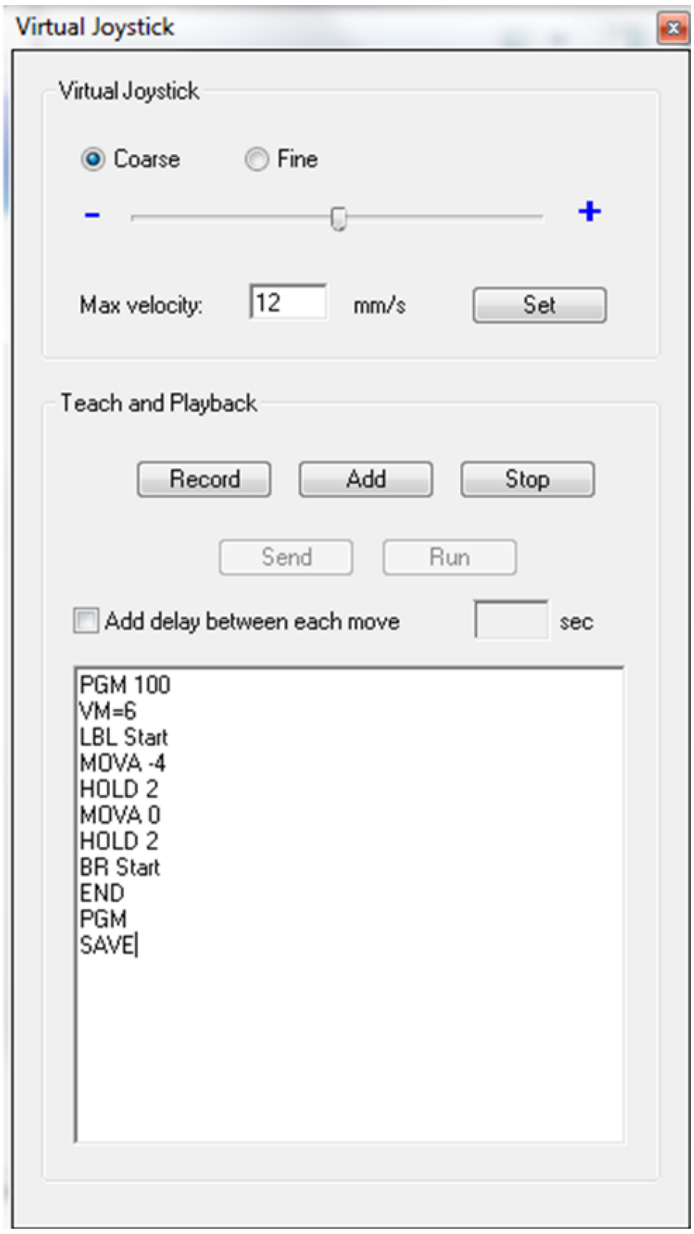

Figure A-5. Programming the stage.

Programming a Strain Protocol

As shown in Figure 5, Quickmotion uses a unique programming language. Some of the language is explained in the manual, so here I will explain the code as it relates to the stretch program that is shown in Figure 5. The code is as follows:

1. PGM 100
2. VM=6
3. LBL Start
4. MOVA -4
5. HOLD 2
6. MOVA 0
7. HOLD 2
8. BR Start
9. END
10. PGM
11. SAVE

The first line defines the program number and is arbitrary. The second line defines the maximum speed, in mm/s, that the linear stage will reach. This is the most important determinant of the frequency. Line 3 tells the controller to begin the program. Line 4 dines the distance, in mm, that the stage will move on an absolute scale relative to the current zero position. Line 5 tells the stage to pause (not for 2 seconds). The pause is very short. Line 6 tells the stage to move back to the zero position. Line 7 again tells it to hold. Line 8 tells the program that it should repeat indefinitely (the

program returns to the top and begins again). Lines 9 and 10 tell the controller that there are no more movement commands and line 11 saves the program in the controller.

To my knowledge, you cannot set a frequency directly using the Quickmotion software. To do so, you must measure the frequency based on the settings you provide and adjust accordingly. This can be cumbersome but it is the only way to reliably set the frequency. Relying on the “VM” value is not advised because the machine must accelerate, decelerate, pause, accelerate, and decelerate for a given cycle, and none of the accelerations are accounted for in the programming. Thus, measurements are required.

Appendix 3 : Performing the bead assay in a PDMS multi-well plate

Materials

- Coated beads (from previous protocol)
- Sterile Serum-free EGM-2
- Fully Supplemented EGM-2
- 0.05% trypsin
- PBS
- Bovine fibrinogen powder
- Medium for your interstitial cells (PBL, SHED, SMC, NHLF, etc.)
- 10ml syringe
- .22μm syringe filter
- FBS
- Thrombin stock solution (50U/ml)
- Microcentrifuge tubes
- PDMS multi-well paltes
- Linear stage
- Sterile DDH_2O
- Sterile, untreated deep petri dishes

Protocol

- The day before, autoclave all of the PDMS multi-well plates
- Warm all liquid reagents to 37°C
- Weigh out enough fibrinogen to make as many gels as you need at 2.5mg/ml final concentration
- Place as many PDMS multi-well plates into deep petri dishes as required
- Perform the rest of the protocol in a biosafety cabinet
- Dissolve fibrinogen in warm, sterile, serum-free EGM-2
- Filter through 0.22 micron filter into fresh, sterile tube

- Ready 1 microcentrifuge tube for each well that you plan to fill (for each 0.5 ml gel)
- Add sterile fibrinogen solution to each microcentrifuge tube
    - Add an amount pre-calculated to make a final concentration of 2.5mg/ml after the addition of any other reagents
- Remove coated beads from the incubator
- Shear off the beads from the bottom of the flask using P-1000 pipetter and leave flask in upright position
    - You will not get all of them, that is ok
    - This should only take 1-2 pipettes
- Add number of beads you want to each microcentrifuge tube
    - The volume of bead suspension should be accounted for in your calculations of the final concentration
- Add FBS to each microcentrifuge tube to make final FBS concentration 5%
- Add 10μl of thrombin stock solution into a microcentrifuge tube
- Add the 63μl cell suspension from 1 microcentrifuge tube into 1 well of the PDMS multi-well plate
    - A 63 μl gel will make the height of the fibrin equal to the height in a 24-well plate
    - 1 500 μl microcentrifuge tube will fill 7-8 wells of the PDMS plate
- Repeat until you have made all of the gels you want
- Allow the beads to settle to the bottom for 5 minutes
- Incubate at 37°C for 25 minutes to allow the gels to finish polymerizing
- If you are not adding interstitial cells, add 100 μl of medium after the gel polymerizes

- If you are adding interstitial cells:
- While the fibrin polymerizes, trypsinize the interstitial cells you want using your standard trypsiniziation protocol
- Count cells
- Once the incubation of the fibrin gel is complete, add 4,000 interstitial cells to the top of the fibrin gel
- Add 100 μl medium to feed
- Change medium daily

- Once the interstitial cells are plated, place the PDMS plates into the incubator and prepare the linear stage
- The basin in the linear stage should be filled with 50-70 ml sterile DDH_2O to maintain humidity in the semi-open chamber
    - This will need to be replenished every 4-6 days
- The clamps should be positioned such that they can grab enough PDMS surface without touching the liquid in the wells
- The distance between the clamps should be measured with calipers so that strain can be applied accurately
- Plug the device into the controller and the controller into a computer
- Using the protocol in Appendix 2, program a strain protocol
- Get the PDMS multi-well plate out of the incubator and clamp it in
    - Each linear stage has room for up to 2 PDMS plates
- Begin the protocol and make sure that the clamps are holding
- Place the lid on the device
- Place the entire device, PLUGGED IN, into the incubator
- ***In the event of a power outage the device must be re-started

Special Notes

The linear stage may generate enough heat to kill the cells in the PDMS plates if it is left on its default settings. This will happen regardless of whether the basin underneath the PDMS plate is filled or empty. The motor will become hot to the touch (not dangerously so, but uncomfortable to hold). This heating does not appear to damage the motor. If this occurs it means that the device is drawing more current than it should and it must be adjusted. To adjust the current settings, open the “Terminal” dialogue under the “Tools” menu (Figure A-6). In this dialogue enter the following commands and press “Send” after each:

1. MHC = 7
2. MRC = 12
3. MAC = 12
4. SAVE

This will tell the stage to draw significantly less current. If the settings are too low the stage will visibly decrease in speed when it is under load (when devices are clamped in). The default settings are MHC = 10, MRC = 20, MAC = 20. After the settings are applied, if the linear stage is stopped for any reason they must be re-entered.

The stage must remain plugged into the controller for the duration of its use, but the controller does not need to be attached to a computer. Attaching the controller to a computer will not disrupt the protocol that the stage is running without an input from the user.

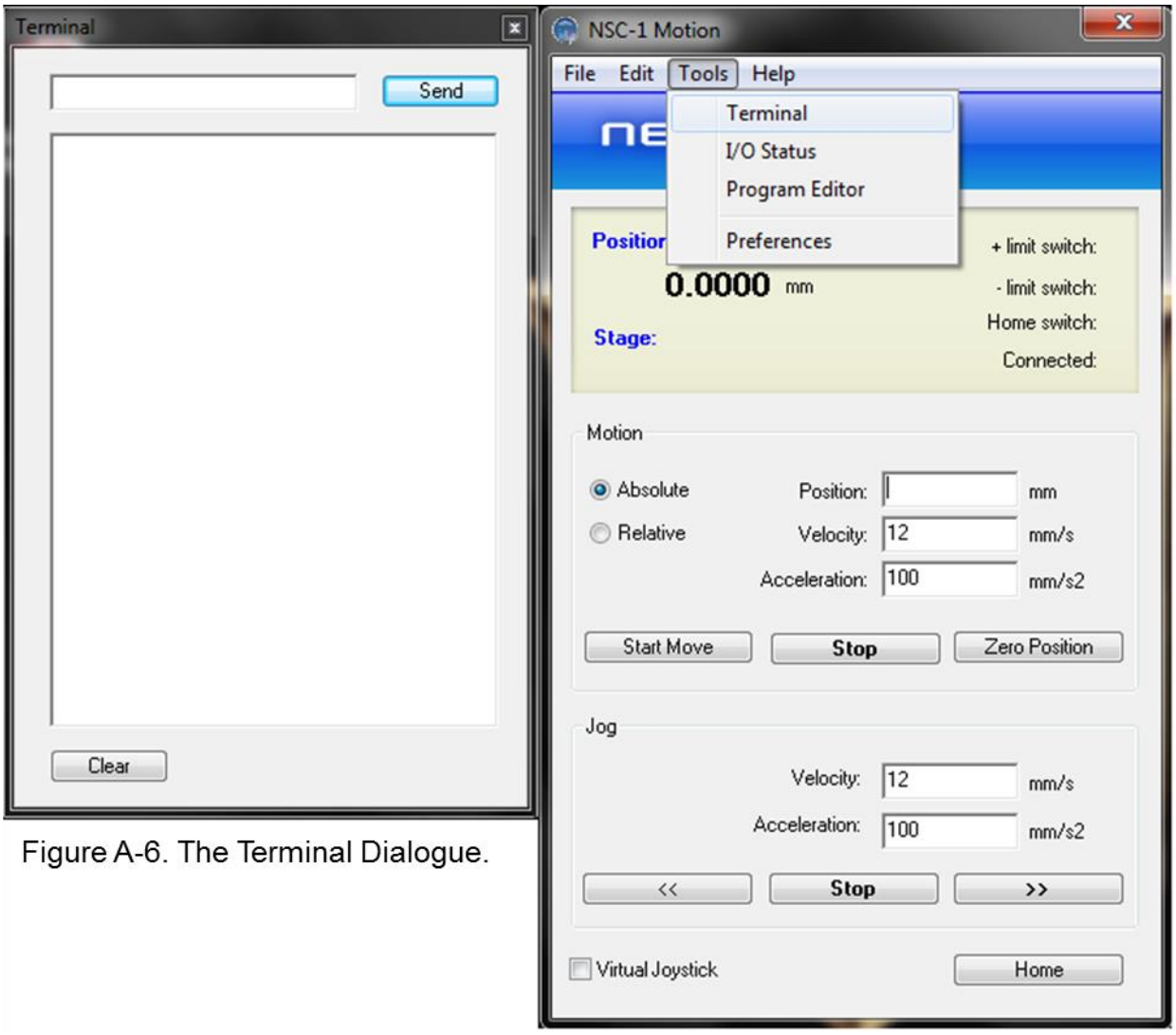

Figure A-6. The Terminal Dialogue.

Appendix 4 : Creating a PDMS multi-well plate with a thin bottom

This protocol is for the creation of a PDMS multi-well plate with wells having bottoms thin enough to perform high magnification (60x and higher) microscopy on the hydrogel within. It required the use of a spin coater (with David Lai's recipe) and a plasma bonder to bond the thin PDMS to the bottom of the multi-well plate. This protocol was performed using the Takayama lab's, and David Lai's personal equipment.

Materials

- PDMS multi-well plate
- X-Acto knife
- PDMS precursor
- PDMS cross-linker
- Disposable cup
- Plastic knife (or any stirring utensil)
- Spin Coater
- Plasma bonder
- Silane-coated glass

Protocol

- Using the X-Acto knife, carefully cut the bottoms of the wells out of the PDMS multi-well plate
- Discard the extra pieces
- Make PDMS as described above by mixing the components and de-gassing them in a desiccator

- Apply a small amount of PDMS to the silane-coated glass
- Place the glass on the spin coater
- Spin the PDMS to 100 μm thickness using
- Cure the PDMS at 120 °C for 2-5 minutes
- Place the PDMS multi-well plate in a plasma bonder face down
- Place the cured, thin PDMS (still on the glass) in the plasma bonder
- Treat them for 1 minute
- Very carefully, peel the thin PDMS off of the glass and place the treated side against the treated bottom of the PDMS multi-well plate
    - Be EXTREMELY careful to place the thin PDMS flat
- Place the thin-bottomed PDMS in a petri dish for storage

Once this protocol is complete the devices can be stored indefinitely just like normal multi-well plates. They can also be autoclaved. Keep in mind that the devices are now slightly deeper and may look different with gels in them. This does not affect their performance. Stretching them does not appear to damage the thin PDMS or cause it to delaminate from the multi-well plate.

Performing high-magnification microscopy on these is identical to performing it in any other culture system; however, I have not used an oil objective and do not know what it will do to the PDMS.

Appendix 5 : Comparison of network length using various stromal and endothelial cell types

A5.1 Introduction

While the above work has focused on a particular combination of endothelial and stromal cells, the bead assay has been used with many different stromal cell types [1, 2]. Understanding the pro-angiogenic characteristics of these cells is beneficial for choosing the proper supporting cells for tissue engineering applications and for finding more abundant, easier to access cell types for tissue engineering purposes.

Umbilical cords are a cheap and easily accessible source of endothelial cells, but not a likely candidate for tissue engineering purposes unless cord banking services become commonplace, and even in that case many people will not have a banked cord from which to draw these cells. Thus, alternative sources of endothelial cells must be found. Human microvascular endothelial cells (HMVEC) can be extracted from dermal biopsies, making them an ideal candidate for the creation of autologous, vascularized tissues, provided their ability to undergo angiogenesis is

robust. Unfortunately, we show here that their ability to undergo angiogenesis is markedly reduced in the presence of multiple stromal cell types which are capable of supporting robust angiogenesis when cultured with HUVECs, however, because passage known is known by our lab to be an important factor in capillary network length (anecdotally), these results warrant additional study.

A5.2 Methods

A5.2.1 Cell culture

HUVECs were isolated from freshly harvested umbilical cords as previously described [2]. HMVECs (Lonza), SHEDs, and PDLSCs were acquired from the laboratory of Dr. Darnell Kaigler [3]. Both cell types were cultured in Endothelial Growth Medium-2 (EGM-2, Lonza, Walkersville, MD). HUVECs were trypsinized and coated onto microcarrier beads at passage 2 and HMVECs at passage 6. Primary HASMCs (Cascade Biologics, Portland, Oregon) were cultured in Medium 231 supplemented with Smooth Muscle Growth Supplement (SMGS, both Life Technologies), NHLFs were cultured in Medium 199 containing 10% serum (Life Technologies), MSCs were cultured in DMEM containing 10% serum (Life Technologies), and both SHEDs and PDLSCs were cultured in Alpha MEM containing L-glutamine, ribonucleosides, deoxyribonucleosides, serum,

antibiotics, and ascorbic acid 2 phosphate (see [3] for more detail). HASMCs were used before passage 15, NHLFs before passage 10, and both stem cell types at passage 6. All cell culture was performed in a 37°C, 5.0% CO_2 incubator. Media was changed every other day.

A5.2.1 Creation of fibrin tissue co-cultures

To create fibrin tissues for 3D cell cultures, 490 μl of 2.5 mg/ml bovine fibrinogen (lot# 029K7636V, Sigma-Aldrich) solutions containing approximately 100 HUVEC or HMVEC-coated microcarrier beads were combined with 10 μl thrombin stock solution (50 U/ml, Sigma-Aldrich) and pipetted into 1 well of a 24-well culture plate. All gels were left at room temperature for 5 minutes to allow the beads to settle to the bottom then incubated for 25 minutes in a 37°C, 5.0% CO_2 incubator to allow gelation to complete. After incubation, 25,000 HASMCs, NHLFs, SHEDs, or PDLSCs, depending on condition, were plated on top of each fibrin gel. Tissues were cultured in a 37°C, 5.0% CO_2 incubator for the duration of the experiments. Media was changed every other day. Cells were imaged at day 7 and total network length was quantified.

A5.3 Results

A5.3.1 All stromal cell types equally support HUVEC angiogenesis

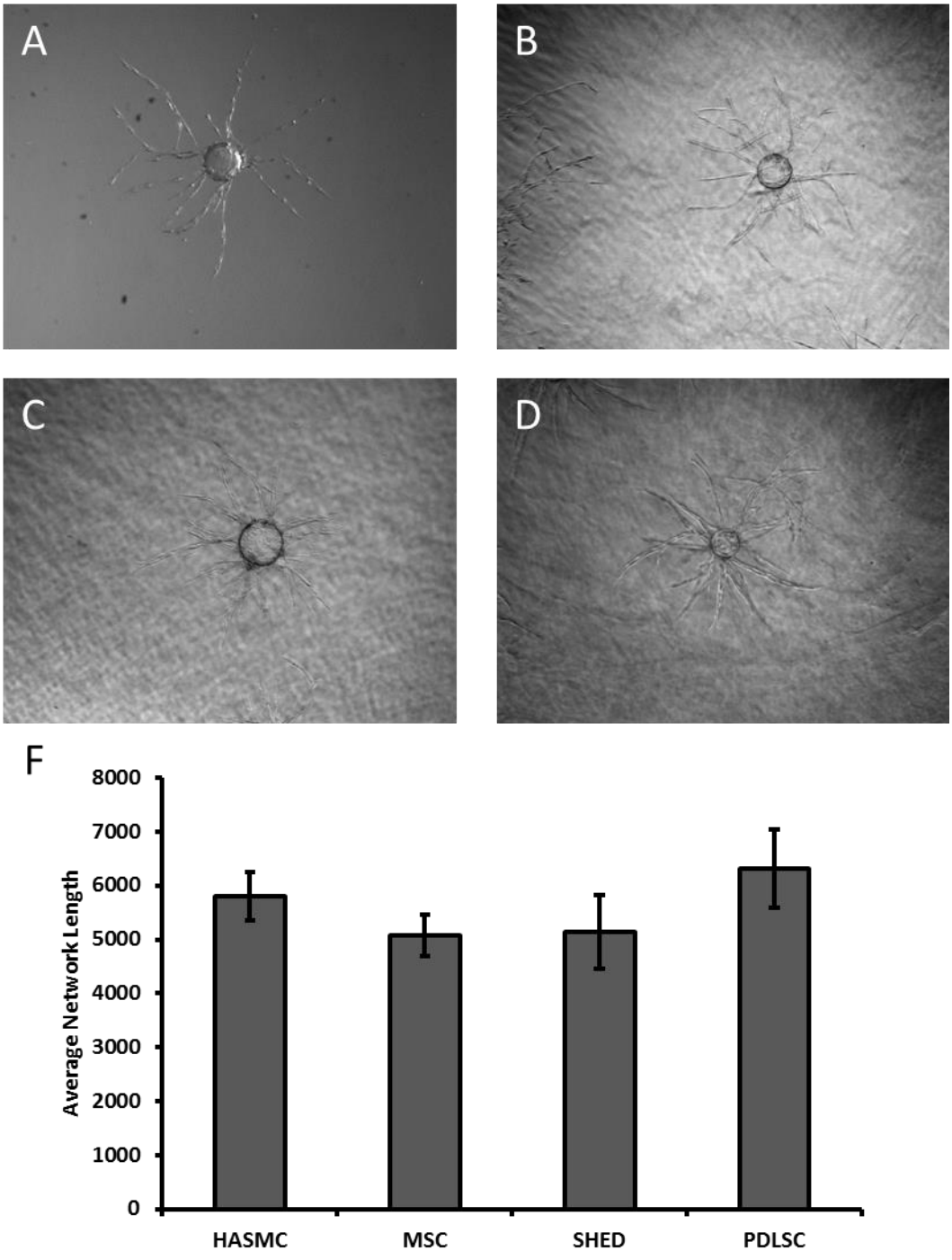

Figure A-7. Network length is independent of supporting cell type. HUVECs cultured in a 24-well plate microcarrier bead assay with HASMC (A), MSC (B), stem cells from human deciduous teeth (SHED) (C), and stem cells from human periodontal ligaments (PDLSC) (D) show robust capillary network growth. Quantification of total network length (F) reveals no differences between supporting stromal cell types.

HUVECs coated onto microcarrier beads and cultured in the presence of HASMCs, MSCs, SHEDs, and PDLSCs all generated capillary networks of equal length, supporting the hypothesis that all of these cell types support angiogenesis to an equal extent (Figure A-7).

A5.3.2 Capillary network length depends on endothelial cell type

HUVECs and HMVECs cultured with various stromal cell types show a marked difference in total network length, independent of the stromal cell type (Figure A-8). HUVECs cultured with NHLFs produce a network over 4 times longer than HMVECs cultured with NHLFs, SHEDs, and PDLSCs. Qualitatively, the quality of the vessels produced by HMVECs appears to be similar to those produced by HUVECs, with the HMVEC capillaries also possessing lumen-like structures and clear, albeit shorter, vessels penetrating the matrix.

A5.4 Discussion

Here it is shown that three novel stromal cell types, HASMCs, SHEDs and PDLSCs, support angiogenesis to an extent equal to a mainstay stromal cell type used in our lab – MSCs. This opens an avenue for angiogenesis research using an even wider variety of stromal cell types than before and provides a basis for comparison of new stromal cell types for tissue engineering purposes. Additionally, we have shown that the

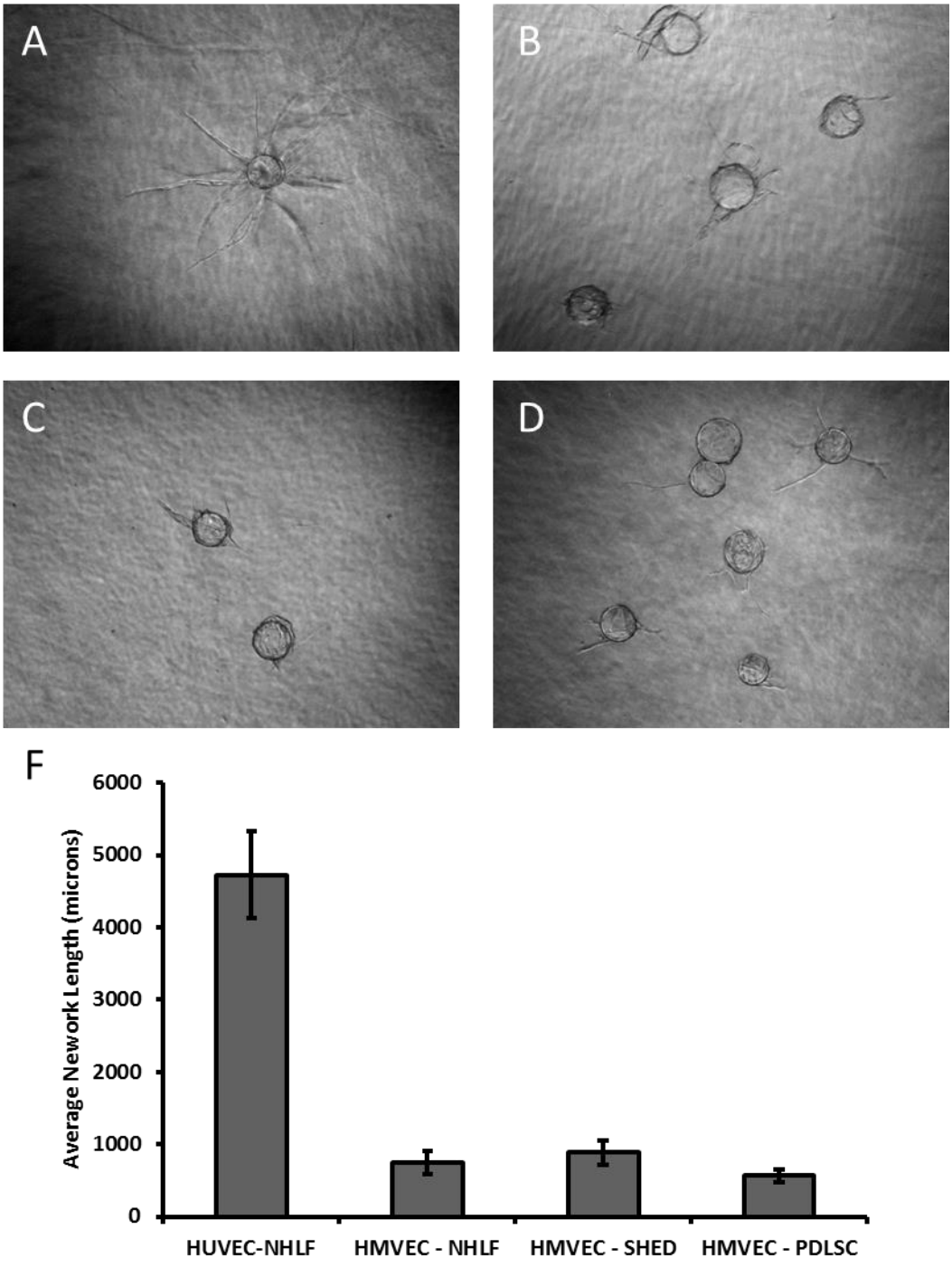

Figure A-8. Network length is dependent on endothelial cell type. HUVECs cultured in a 24-well plate microcarrier bead assay with normal human lung fibroblasts (NHLF) (A) show long capillary networks. Human microvascular endothelial cells co-cultured with NHLF (B), SHED (C), and PDLSC (D) display abbreviated capillary formation. Quantification of total network length (F) reveals that HUVECs produce much longer capillary networks than microvascular endothelial cells under similar conditions.

particular endothelial cell type used is important for the creation of large capillary networks and that HUVECs are an ideal endothelial cell source for this purpose.

Although it was shown that HUVECs out-perform HMVECs at producing large capillary networks, it should be noted that unpublished evidence from our laboratory has shown that the passage number of the endothelial cells is an important factor when considering network length and that higher passage HUVECs produce dramatically shorter networks. It is unknown whether the effect of endothelial cell type in this study is due solely to differences between HUVECs and HMVECs or due to the use of passage 6 HMVECs. Future research is necessary to parse out whether these effects are due to cell type, passage number, or if both have an effect on network length. Stromal cell passage number is not known to affect network length in our hands. NHLFs have been used up to passage 10 [4] and HASMCs have been used up to passage 15 [5] with no noticeable changes in network length. The effect of passage number on the effectiveness of SHEDs, PDLSCs, and other stromal cell types remains to be determined.

The hypothesis that the extent of angiogenesis is dependent on endothelial and not stromal cell type is also supported by Figure A-2, which

shows that each of the HMVEC conditions produced network length of equal extent, despite being much shorter than those produced by HUVECs. This implies a need for careful choice of endothelial as well as stromal cell types when designing an engineered tissue construct and that there are likely optimal choices of both cell types for particular tissue engineering applications. Future studies should examine the differences between various combinations of endothelial and stromal cells to determine if there are any synergistic or antagonistic interaction effects.

Finally, all of these experiments were carried out in fibrin matrices and the behavior of all of the cell types used in other ECM materials is not yet known. Particular ECMs may be more conducive to angiogenesis by certain endothelial cell types than others, and thus optimization of the ECM material used may be a factor that must be considered in future applications.

A5.5 References

[1] Kachgal S, Putnam AJ. Mesenchymal stem cells from adipose and bone marrow promote angiogenesis via distinct cytokine and protease expression mechanisms. Angiogenesis 2011;14:47-59.

[2] Ghajar CM, Blevins KS, Hughes CC, George SC, Putnam AJ. Mesenchymal stem cells enhance angiogenesis in mechanically viable

prevascularized tissues via early matrix metalloproteinase upregulation. Tissue Eng 2006;12:2875-88.

[3] Tarle SA, Shi S, Kaigler D. Development of a serum-free system to expand dental-derived stem cells: PDLSCs and SHEDs. J Cell Physiol 2011;226:66-73.

[4] Grainger SJ, Putnam AJ. Assessing the permeability of engineered capillary networks in a 3D culture. PLoS One 2011;6:e22086.

[5] Ceccarelli J, Cheng A, Putnam AJ. Mechanical Strain Controls Endothelial Patterning During Angiogenic Sprouting. Cellular and Molecular Bioengineering 2012;5:463-73.